Microgrid Operation under Various Types of Faults for the Assessment of Power Quality Parameters

A Dissertation submitted in fulfilment of the requirements for the Degree

of

MASTER OF ENGINEERING

in

Power Systems

Submitted by

Navneet Kaur

Roll No - 802042017

Under the Guidance of

Dr. Jitender Kaushal

Assistant Professor

&

Dr. Suman Bhullar

Assistant Professor

THAPAR INSTITUTE
OF ENGINEERING & TECHNOLOGY
(Deemed to be University)

2022

Electrical and Instrumentation Engineering Department
Thapar Institute of Engineering & Technology, Patiala
(Declared as Deemed-to-be-University u/s 3 of the UGC Act., 1956)
Post Bag No. 32, Patiala – 147004
Punjab (India)

DECLARATION

I hereby certify that the work which is presented in dissertation entitled, "**Microgrid Operation under Various Types of Faults for the Assessment of Power Quality Parameters**" in partial fulfillment of the requirements for the award of the degree of **Master of Engineering (Power Systems)**, submitted to Electrical & Instrumentation Engineering Department of Thapar Institute of Engineering & Technology (Deemed to be University) is as authentic record of my own work carried under the supervision of **Dr. Jitender Kaushal & Dr. Suman Bhullar.** It refers others researcher's work which are duly listed in the reference section. The matter contained in this dissertation has not been submitted, neither in part nor in full to any other degree to any other university or institute except as reported in text and references.

Navneet Kaur

Navneet Kaur

(Roll No.: 802042017)

Place: TIET, Patiala, Punjab

Date: 30 August 2022

It is certified that the above statement made by the student is correct to the best of my knowledge and belief.

Dr. Jitender Kaushal
Assistant Professor

Dr. Suman Bhullar
Assistant Professor

ACKNOWLEDGEMENT

To my supervisors, **Dr. Jitender Kaushal (Assistant Professor, EIED)** and **Dr. Suman Bhullar (Assistant Professor, EIED)**, I would like to convey my sincere thanks for your great advice, encouragement, support, and inspiration in helping me finish this dissertation work.

I want to express my gratitude to **Dr. R.S. Kaler, Professor, and head of the EIED**, as well as **Dr. Nitin Narang, Associate Professor and PG Coordinator**, for their assistance. Additionally, I want to thank all my friends who have supported me emotionally and offered advice, inspiration, and challenging questions.

I want to express my sincere gratitude to my parents for their unwavering support and acceptance of all my life's decisions. I am grateful to my brother for always appreciating me. Finally, I want to give God gratitude.

Navneet Kaur

(Roll. No. 802042017)

TABLE OF CONTENT

DECLARATION ..... ERROR! BOOKMARK NOT DEFINED.

ACKNOWLEDGEMENT ..... **II**

TABLE OF CONTENT ..... **IV**

LIST OF FIGURES ..... **VI**

LIST OF TABLES ..... **X**

LIST OF ABBREVIATIONS ..... **XI**

ABSTRACT ..... **XIII**

CHAPTER 1 INTRODUCTION **1**

1.1 OVERVIEW 1
1.2 LITERATURE REVIEW 2
1.3 RESEARCH GAPS 6
1.4 OBJECTIVES OF THESIS 7
1.5 ORGANIZATION OF THE DISSERTATION 7

CHAPTER 2 DESCRIPTION OF SCHEMATIC DIAGRAM AND MEASURING PROCESS **8**

2.1 DESCRIPTION OF SCHEMATIC DIAGRAM 8
2.1.1 PWM GENERATION SUBSYSTEM 9
2.1.2 CONVERTER INTERFACED BATTERY ENERGY STORAGE SUBSYSTEM 9
2.1.3 POWER QUALITY PARAMETERS SUBSYSTEM 10
2.2 DESCRIPTION OF COMPONENTS USED 11
2.2.1 PV ARRAY BLOCK 11
2.2.2 BATTERY BLOCK 13
2.2.3 TWO LEVEL THREE PHASE IGBT INVERTER BLOCK 14
2.2.4 PWM GENERATOR BLOCK 15
2.2.5 DISTRIBUTION LINE BLOCK 16
2.2.6 THREE PHASE PARALLEL RL LOAD 16
2.2.7 NON LINEAR LOAD 16

CHAPTER 3 EFFECT OF VARIOUS TYPES OF FAULTS ON MICROGRID OPERATION **18**

3.1 SHUNT FAULTS 18
3.2 LIGHTNING STRIKE/ HIGH IMPULSE VOLTAGE 19

CHAPTER 4 RESULTS AND DISCUSSIONS..... 22

4.1 SHUNT FAULTS..... 22

4.1.1 PARALLEL RL LOAD..... 22

4.1.2 NON-LINEAR LOAD..... 34

4.2 LIGHTNING STRIKE/ HIGH IMPULSE VOLTAGE..... 50

4.2.1 1.2/50 µs WAVEFORM..... 50

4.2.2 1.2/4 µs WAVEFORM..... 51

4.2.3 1.2/10 µs WAVEFORM..... 52

4.2.4 3/10 µs WAVEFORM..... 53

4.2.5 7.5/30 µs WAVEFORM..... 54

CHAPTER 5 CONCLUSIONS AND FUTURE SCOPE..... 56

5.1 CONCLUSIONS..... 56

5.2 FUTURE SCOPE..... 56

REFERENCES..... 57

LIST OF PUBLICATIONS..... 61

PLAGIARISM REPORT.....ERROR! BOOKMARK NOT DEFINED.

LIST OF FIGURES

Figure 2.1: Schematic Diagram 8
Figure 2.2: Simulink diagram of PWM generation subsystem 9
Figure 2.3: Simulink diagram of Converter-based battery energy storage subsystem 10
Figure 2.4: Simulink diagram of power quality parameters subsystem 10
Figure 2.5: PV array block 11
Figure 2.6: Equivalent circuit diagram of PV array 11
Figure 2.7: VI and PV characteristics with specified temperature 12
Figure 2.8: VI and PV plot with specified irradiances 13
Figure 2.9: Battery block 13
Figure 2.10: Typical discharge curve for Li-ion battery 14
Figure 2.11: IGBT block 14
Figure 2.12: Circuit diagram of IGBT diode inverter 15
Figure 2.13: PWM generator block 15
Figure 2.14: Distribution line block 16
Figure 2.15: Parallel RL load block 16
Figure 2.16: Non-Linear load 17
Figure 3.1: Three phase fault block 18
Figure 3.2: Simulink diagram for impulse fault 19
Figure 3.3: Impulse fault 21
Figure 4.1: Waveforms for voltage, current, power factor and frequency under normal conditions 23
Figure 4.2: Waveforms for active power, reactive power, voltage THD and current THD under normal conditions 23
Figure 4.3: Waveforms for voltage, current, power factor and frequency under LG fault 24
Figure 4.4: Waveforms for active power, reactive power, voltage THD and current THD under LG fault 24
Figure 4.5: Waveforms for voltage, current, power factor and frequency under LL Fault 25
Figure 4.6: Waveforms for active power, reactive power, voltage THD and current THD under LL fault 25
Figure 4.7: Waveforms for voltage, current, power factor and frequency under LLG Fault 26
Figure 4.8: Waveforms for active power, reactive power, voltage THD and current THD under LLG fault 26

Figure 4.9: Waveforms for voltage, current, power factor and frequency under normal conditions 27
Figure 4.10: Waveforms for active power, reactive power, voltage THD and current THD under normal conditions 27
Figure 4.11: Waveforms for voltage, current, power factor and frequency under LG fault ... 28
Figure 4.12: Waveforms for active power, reactive power, voltage THD and current THD under LG fault 28
Figure 4.13: Waveforms for voltage, current, power factor and frequency under LL Fault ... 29
Figure 4.14: Waveforms for active power, reactive power, voltage THD and current THD under LL fault 29
Figure 4.15: Waveforms for voltage, current, power factor and frequency under LLG Fault 30
Figure 4.16: Waveforms for active power, reactive power, voltage THD and current THD under LLG fault 30
Figure 4.17: Waveforms for voltage, current, power factor and frequency under normal conditions 31
Figure 4.18: Waveforms for active power, reactive power, voltage THD and current THD under normal conditions 31
Figure 4.19: Waveforms for voltage, current, power factor and frequency under LG Fault .. 32
Figure 4.20: Waveforms for active power, reactive power, voltage THD and current THD under LG fault 32
Figure 4.21: Waveforms for voltage, current, power factor and frequency under LL Fault ... 33
Figure 4.22: Waveforms for active power, reactive power, voltage THD and current THD under LL fault 33
Figure 4.23: Waveforms for voltage, current, power factor and frequency under LLG Fault 34
Figure 4.24: Waveforms for active power, reactive power, voltage THD and current THD under LLG fault 34
Figure 4.25: Waveforms for voltage, current, power factor and frequency under normal conditions 35
Figure 4.26: Waveforms for active power, reactive power, voltage THD and current THD under normal conditions 35
Figure 4.27: Waveforms for voltage, current, power factor and frequency under LG Fault .. 36
Figure 4.28: Waveforms for active power, reactive power, voltage THD and current THD under LG fault 36
Figure 4.29: Waveforms for voltage, current, power factor and frequency under LL Fault ... 37

Figure 4.30: Waveforms for active power, reactive power, voltage THD and current THD under LL fault 37
Figure 4.31: Waveforms for voltage, current, power factor and frequency under LLG Fault 38
Figure 4.32: Waveforms for active power, reactive power, voltage THD and current THD under LLG fault 38
Figure 4.33: Waveforms for voltage, current, power factor and frequency under normal conditions 39
Figure 4.34: Waveforms for active power, reactive power, voltage THD and current THD under normal conditions 39
Figure 4.35: Waveforms for voltage, current, power factor and frequency under LG Fault .. 40
Figure 4.36: Waveforms for active power, reactive power, voltage THD and current THD under LG fault 40
Figure 4.37: Waveforms for voltage, current, power factor and frequency under LL Fault ... 41
Figure 4.38: Waveforms for active power, reactive power, voltage THD and current THD under LL fault 41
Figure 4.39: Waveforms for voltage, current, power factor and frequency under LLG Fault 42
Figure 4.40: Waveforms for active power, reactive power, voltage THD and current THD under LLG fault 42
Figure 4.41: Waveforms for voltage, current, power factor and frequency under normal conditions 43
Figure 4.42: Waveforms for active power, reactive power, voltage THD and current THD under normal conditions 43
Figure 4.43: Waveforms for voltage, current, power factor and frequency under LG Fault .. 44
Figure 4.44: Waveforms for active power, reactive power, voltage THD and current THD under LG fault 44
Figure 4.45: Waveforms for voltage, current, power factor and frequency under LL Fault ... 45
Figure 4.46: Waveforms for active power, reactive power, voltage THD and current THD under LL fault 45
Figure 4.47: Waveforms for voltage, current, power factor and frequency under LLG Fault 46
Figure 4.48: Waveforms for active power, reactive power, voltage THD and current THD under LLG fault 46
Figure 4.49: Voltage and current impulse waveforms 50
Figure 4.50: Voltage and current THD waveforms 51
Figure 4.51: Voltage and current impulse waveforms 51

Figure 4.52: Voltage and current THD waveforms 52
Figure 4.53: Voltage and current impulse waveforms 52
Figure 4.54: Voltage and current THD waveforms 53
Figure 4.55: Voltage and current impulse waveforms 53
Figure 4.56: Voltage and current THD waveforms 54
Figure 4.57: Voltage and current impulse waveforms 54
Figure 4.58: Voltage and current THD waveforms 55

LIST OF TABLES

Table 2.1 Main operation events 9
Table 2.2 Specifications of PV array 11
Table 2.3. Specifications of converter based BES system 13
Table 2.4. Specifications of loads 17
Table 3.1 Specifications of fault block 18
Table 3.2: Different impulse waveshapes with Damping Factor 20
Table 4.1 Microgrid operation under different types of modes and faults 22
Table 4.2 Comparison between the modes of operation under different types of faults for RL load 46
Table 4.3 Comparison between the modes of operation under different types of faults for Non linear load 48
Table 4.4 Microgrid operation under different waveforms with parameters to be calculated 50

LIST OF ABBREVIATIONS

AC	Alternating Current
APF	Active Power Filter
AGC	Automatic Gain Control
BES	Battery Energy System
DC	Direct Current
DRES	Distributed Renewable Energy Resources
D-STATCOM	Distribution Synchronous Compensator
EMTDC	Electromagnetic Transients Including DC
FET	Field Effect Transistor
GTO	Gate Turn Off Thyristor
IEEE	Institute of Electrical and Electronics Engineers Standard
IGBT	Insulated Gate Bipolar Transistor
IVTG	Identity Vector Template Generation
LG	Line to Ground
LL	Line to Line
LLG	Double Line to Ground
LV	Low Voltage
MATLAB	MATRIX Laboratory
M & V	Measuring and Verification
MOSFET	Metal Oxide Semiconductor Field Effect Transistor
MPPT	Maximum Power Point Tracking
MV	Medium Voltage

NREL	National Renewable Energy Laboratory
PCC	Point of Common Coupling
PLL	Phase Locked Loop
PQ	Power Quality
PSCAD	Power System Computer Aided Design
PV	Photovoltaic
PWM	Pulse Width Modulation
RES	Renewable Energy Sources
SAPF	Shunt Active Power Filter
STC	Standard Test Conditions
SVC	Static VAR Compensator
TCDIC	Transformer Coupled Dual Input Converter
THD	Total Harmonic Distortion

ABSTRACT

The effectiveness and cost of a power system can be significantly impacted by power quality. Therefore, it is crucial to ensure that the electric power which any system consumes is of the proper quality and that the system can operate with the designated power. This dissertation presents a comparison of different faults for analyzing the various power quality parameters in the mid of the distribution line. The microgrid is operating in both islanded mode and grid connected mode which is fed from solar based energy sources. A battery bank is connected to the common bus of solar energy sources and a three-phase two level IGBT-based inverter. The connecting wire from inverter to load is assumed to be an overhead distribution line with a length of 1 km which is a class of short-length distribution line. Various MATLAB/Simulink blocks are used for the calculation of power quality parameters connected to microgrid for the parallel RL load and non-linear load. The system is also put to the test without the availability of solar irradiance. A simulation diagram of the proposed model is developed in MATLAB-Simulink_R2020a software version. The results are presented for various conditions such as unavailability of solar irradiance, different categories of faults like Line to ground, line to line, double line to ground, impulse fault and low state-of-charge of the battery unit. In this dissertation work, the introduction of high impulse fault/lightning strike providing the comparison of standard and non-standard waveforms gives a different aspect of analyzing the power quality parameters.

Chapter 1

INTRODUCTION

This chapter covers the overview of the power quality parameters along with the IEEE standard definitions, detailed literature review, research gaps, objectives of thesis and organization of the thesis.

1.1 OVERVIEW

An electrical power system is a group of electrical parts that deliver energy to consumers including homes, companies, and industries. Generators that produce energy, transmission networks that move electricity from producing centres to load centres, and distribution systems that provide electricity to local clients make up the three components of the power system. Electricity must be sent from the generator to the consumer via an interconnection system, which joins transmission lines to nearby utilities, or a distribution system, which transfers power to customers who could be linked to equipment via underground or overhead cables. Alternating current (AC) energy, which is used in most power systems, makes switching from one point of generation to another more challenging, especially when combined with fluctuations in the generation, loads, weather, and other factors. Electric power sources and consumer loads are connected through a network called the grid. The grid oversees supplying the customers who have made requests with the various types of generated energy. Transmission cables are linked to the national electrical grid to supply power to the various state loads. A distribution system with a tiny grid is known as a microgrid. Microgrids are viewed as workable electrification options for military installations, rural communities, and college campuses [1], where main grid expansion is either impractical or makes no financial sense. According to some researchers, the microgrid is a distribution system with a distributed generation that may run in either grid-connected or islanded (stand-alone) mode [2]. Microgrids have their own structure, despite certain commonalities between distribution systems and them, such as voltage levels and client types. A microgrid is made up of several energy sources, including renewable energy, backup generators, energy storage, unequal load demand on each phase, and multiphase lines.

According to Institute of Electrical and Electronics Engineers Standard, power quality is "the notion of powering and grounding sensitive electronic equipment in a way suited for the equipment" (IEEE Std 1100) [3]. A simpler and concise definition is “Power Quality is a set of electrical boundaries that allows a piece of equipment to function in its intended manner

without significant loss of performance or life expectancy" [4]. At the level of transmission and distribution, power quality mostly refers to the voltage remaining within the range of ±5% [5]. It is advised that the voltage violation should be corrected within 2 s of occurrence [6]. An electrical device's performance and lifespan are impacted by poor power quality. The frequency, voltage, and currents that are applied to the electrical device are directly connected to both [4].

In a perfect distribution system, pure sinusoidal current and voltage waveforms with the voltage magnitude keeping within pre-specified bounds, with the expected fundamental frequency. Many PQ problems occur in the distribution network, especially when subterranean cables are outnumbered by overhead lines in the system. The interruption may be brought on by the lines coming into touch with one another, particularly on windy days or because of birds, the lines meeting tree branches, the lines being cut by falling trees or branches, illumination, or other natural factors. These issues affect the power quality of the network. Power electronic equipment which is used in electronic devices, transformers, the switching and operation of capacitor or inductor banks, and other man-made causes are instances of switching off/on of large loads. Voltage quality is typically meant when we discuss power quality because the voltage is typically what is regulated. The ability of the electrical utilities to sustain system reliability is referred to as "power quality". Maintaining electrical power quality to keep it within acceptable bounds is the most difficult element. Low power quality has several downsides. There are several potential results, including increased power losses, strange and unexpected behaviour of electrical equipment, interference with nearby communication lines, a poor voltage profile, harmonics, voltage sags and swells, poor and low distortion, and displacement factor.

1.2 LITERATURE REVIEW

Active power is balanced through the supply by grid connection during normal operation to produce a stable dc voltage while the system is linked to the grid [7]. By synchronizing the grid converter and battery energy storage system, electricity is automatically balanced during an AC grid fault. It is advised to develop an integrated strategy for the wind turbine, battery system, and load management, including power shedding, to guarantee that the system can function in islanded circumstances. The proposed control system is validated and shown to operate robustly under a variety of operating conditions, including grid ac faults, wind power generation, load variations, and islanding, using PSCAD/EMTDC simulations. According to [8], some microgrids may function as islands permanently, while others may function normally as a component of the macro-grid and only become islands when service is interrupted.

However, harmonics, voltage imbalance, and voltage fluctuation are some of the negative effects of their installation and operation. The on-off switching of distributed generating resources can result in voltage quality disruptions due to variations in power, which harm the connected power system. This study looks at microgrids, as well as the problems with power quality they cause and how to fix them.

[9] asserts that the creation of a microgrid, whether intentional or unintentional, introduces several control issues related to power quality, microgrid stability, and harmonics. Controlling an island microgrid becomes progressively more difficult as the use of erratic Distributed Renewable Energy Sources (DRES) like solar and wind increases. To eliminate voltage sag utilizing a Distribution Static Compensator, this work offers a regulating technique for enhancing power quality by infusing reactive power into more of an isolated microgrid (D-STATCOM). The MATLAB/Simulink environment was used to execute the simulation model. The results of the simulation demonstrate that the suggested control approach delivers the necessary voltage stability under voltage sag, improving power quality in an islanded power system. The random nature of current Power Electronics Converter (PEC)-equipped Renewable Energy Sources (RES) creates a problem for Power Quality (PQ) [10]. Additionally, the presence of unbalanced and non-linear loads in microgrids appears to have an impact on the distribution network's power quality. In this study, the Low Voltage (LV) distribution network of a typical microgrid power system model was used to investigate the effects of power quality factors such as voltage variations, power variations, unbalanced voltage levels, and Total Harmonic Distortion (THD). This study constructed a microgrid model and used simulation in the PSS-Sincal software environment to analyze the influence of power quality. The analytical results of the study can be utilized to build a real, independent microgrid power system with better power quality conditions.

[11] uses an experimental inquiry to look at the intricate consequences of power quality in a genuine microgrid network. Under various generation and demand situations, voltage and frequency variations are investigated in both islanded and grid modes of microgrid operation. Unbalanced PV generation and unequal load distribution cause imbalanced voltage and current levels in the microgrid network. Various PV power levels also allow for the measurement of voltage and current THD. The outcomes of the discovery are then contrasted with the Australian network standard level. For planned recurring transitions between islanded modes and, grid-connected this paper provides a unique PQ restricted optimization approach for smart microgrids with nonlinear loads in [12]. To optimize the microgrid's overall profit from sending electricity to the grid while also fulfilling network and PQ limits, generation, loads, and energy

storage are all scheduled precisely. The measuring and verification (M&V) methods for estimating, comparing, and measuring building energy efficiency are developed in this study [13]. To assess a building's overall efficiency, this article discusses the measurement-informed modelling approach, which is a way for creating and changing an energy model for a building using metered data. This study offers a brand-new voltage quality index that may be used to rate the electrical quality of AC and DC buildings. The apparatus, machinery, and processes described in this article are necessary to compute power quality and efficiency.

[14] suggests a brand-new method for identifying faults by extracting current fault features. The first and second derivatives of current, overcurrent, and signal processing techniques are used in the proposed fault detection system. A sliding window is used to separate a time-domain current signal into three discrete properties. The root squared- zero, second, and fourth-order moments are used to extract the features. The features are then subjected to individual criteria to distinguish between defects with low, high, and extremely high resistance. The suggested method is put to the test with a MATLAB/Simulink implementation of a modified IEEE 13 node distribution network.

At the point of common coupling (PCC) close to the load bus in the microgrid, series active power filter (APF) is included in [15] as a compensating device for harmonic reduction and reactive power compensation. Using a prototype model and a novel control strategy called Identity Vector Template Generation (IVTG), which is contrasted with a typical controller in terms of voltage profile consistency and harmonic filtering, the compensation offered by APF is studied. According to [16], the goal of the study addressed is to carry out the best reconfiguration on an off-grid system. The view of the distributed generator's power is taken for granted in terms of location and ideal sizing. The available power in a generator or inverter for RES, however, is less than the visible power. The capacity curve is utilized in this study to examine microgrid reconfiguration. A synchronous generator's limit is imposed by a modified D curve, whereas an inverter's limit is enforced by four distinct curves. On a modified IEEE 33 bus system, the impact of reconfiguration on radiality, reactive power, system loss, and voltage profile reserves is investigated.

To predict the possibility of low impedance failures in low voltage AC microgrids that are dominated by inverters, a guarding method based on voltage sags, current magnitude, and active power flow direction is presented in [17]. Several fault scenarios are assessed for each microgrid component (node, load, line section, and energy sources). The MATLAB/Simulink program was used to run the simulation. According to [18], active and reactive power control is necessary for grid-connected microgrid mode. Power quality may be impacted by the various

types of loads connected to the power distribution network. This research analyses power quality problems with shifting loads and provides a 14-bus IEEE distribution system. The MATLAB/Simulink environment is utilized to construct the proposed hybrid microgrid.

According to [19], raising the amplitude of the positive and negative sequence current supplied to the grid will increase the line-to-line PCC voltage for a certain inverter rating. Four-leg inverters can supply both positive and negative sequence currents to the grid, in contrast to three-leg inverters, which can only deliver positive and negative sequence current to the grid. When operating with low voltage, this additional level of control is not used. To reduce the peak current amplitude of a four-leg inverter, this study suggests a unique approach for determining the amplitude and phase angle of the zero-sequence current. A combined SVC and SAPF system are used in [20] to improve the power quality of a microgrid, using harmonic currents near the load to reduce voltage volatility and regulate reactive power and SAPF near the micro source to restrict SVC. Simulated outcomes demonstrate the integrated system's effectiveness.

[21] provides a DC-DC boost converter with three inputs. The suggested converter links a storage element's bidirectional port and two unidirectional input power ports in a unitary manner. PV and FC power sources alone or together may use to deliver the output load, charge, or discharge the battery. The proposed configuration only uses four power switches, each of which is individually controlled by four different duty ratios. The two-stage stand-alone method described in this study [22] new transformer-coupled dual input converter (TCDIC) followed by a conventional full-bridge inverter is a two-stage stand-alone approach. The suggested TCDIC may offer maximum power point tracking (MPPT) and battery charge management while preserving the right voltage level at the load terminal.

A technique for calculating the annual energy savings achieved by paralleled dc/dc converters worldwide is presented in [23] and is based on numerous algorithms. The smallest, most inexpensive PV system with dc/dc converter paralleling may also be chosen using this strategy. The focus of the research in [24] is to show how utility infrastructure development patterns and the characteristics of the available distribution equipment impact the circumstances that lead to continued arc generation from a lightning-induced fault. This will be accomplished by analyzing data from high-voltage laboratory testing and a genuine monitored distribution system. For the estimate of different types and locations of impulsive fault current, a trained wavelet network is employed in [25]. The second stage of the network may categories the fault kind and its position along the winding by examining the retrieved weight parameters of the optimally trained wavelet network. According to [26], for a variety of applied waves (both

standard and non-standard) and various winding connections, the insulation properties under non-standard lightning impulse voltage waveforms, which correspond to actual surge waveforms experienced in the field, can be mathematically compared to the properties under the standard lightning impulse waveform.

In [27], the electrical performance of a 10 kV polymer insulator under various impulse, insulator angle, and weather conditions about a cross-arm was examined (both experimentally and theoretically), and the results were analyzed in accordance with the findings. Results reveal that leakage current and breakdown voltage levels for both positive and negative impulses are surprisingly impacted by the insulator angle (with respect to the cross-arm) and weather. Therefore, while selecting an appropriate protection system for MV lines against lightning generated voltage, taking into account the insulator angles about the cross-arm as well as the local weather parameters is extremely beneficial for performance and line stability. In [28], during inquiry, several switching and lightning impulse waveforms were applied to a high-frequency transformer model created in MATLAB/Simulink. Because input impulse waveforms, kinds of fault, and placement along the windings might vary, the transformer response is examined.

1.3 RESEARCH GAPS

Based on the literature review some gaps have been identified and discussed as follows:

- According to the different research papers, less focus has been provided on the low voltage distribution network side for assessing the various fault effects.
- Various discussions have been done on the standard IEEE models regardless of using some software.
- As per the literature reviewed, maximum of four parameters can be found which is quite a small number.
- Effect of lightning strike/ high impulse voltage has been discussed on high voltage or medium voltage side so far along with high rating of power transformers (MVA). No focus has been given to the distribution network side.
- For creating impulse fault different methods like an ideal switch, Marx circuit which is used for transformer and DC circuit only have been used. For analyzing the real lightning effects, the online transient overvoltage monitoring system has been used. Less focus has been provided on creating fault on the transmission line with a low voltage distribution network.

1.4 OBJECTIVES OF THESIS

- Modelling and simulation of an LV microgrid system based on PV, BES, and utility grid.
- Analyze the power quality-related parameters under various types of shunt faults along with R-L and non-linear loads.
- Assessment of the on-grid microgrid system operation under the effect of impulse fault.

In this chapter, the overview and different literature surveys have been done in support of the proposed title of the dissertation. As per the research findings (gaps), the above three objectives have been formulated which will be discussed in detail from Chapter 2 to Chapter 4.

1.5 ORGANIZATION OF THE DISSERTATION

A brief description of the organization of the dissertation work is in the following format.

Chapter 1 provides information about power quality parameters. Along with that, great emphasis has been given to the work that has already been done in this field highlighting the effectiveness and deficiency in the works.

Chapter 2 has been divided into two subparts. The first subpart gives the description of the model which has been run under the MATLAB/Simulink environment providing brief information about the various subsystems used in the model. The second subpart gives a brief outline of the different blocks used in the model. The specification table of the blocks has also been discussed.

Chapter 3 presents the theory about the shunt faults and impulse fault on the low voltage microgrid. Theory about implementing the lightning block or impulse fault block in MATLAB/Simulink environment is discussed in depth.

Chapter 4 covers the simulation of the model under the MATLAB/Simulink environment under various load conditions. This chapter also covers the influence of different fault conditions on the power quality parameters. Comparison has been done with isolated mode without battery connection, isolated mode with battery connection and grid-connected mode. Various results for impulse fault conditions have been discussed.

Chapter 5 gives a conclusion to the work carried out in the thesis. The chapter also presents the scope for the future research based on the work carried out in dissertation.

Chapter 2

DESCRIPTION OF SCHEMATIC DIAGRAM AND MEASURING PROCESS

In this chapter, the schematic diagram and proposed methodology have been discussed along with various subsystems used. The details of the modelling work for PV, various blocks used in the Simulink diagram, nonlinear loads, energy storage system are shown in this chapter. The performances of each component are also shown along with the modelling method to demonstrate the viability.

2.1 DESCRIPTION OF SCHEMATIC DIAGRAM

In figure 2.1, a photovoltaic (PV) array is used with irradiance and temperature at standard test conditions (STC, I_{rr} = 1000 W/m^2, Temp = 25˚C). The output of the PV array which is a DC signal is further provided to the 2-level three-phase IGBT converter. A Battery Energy Storage (BES) system is used after the PV array through a bidirectional DC-DC converter. This BES system is acting as a storage device till the irradiance is maximum i.e., 1000W/m^2 and acts as a source when irradiance is reduced to zero i.e., 0 W/m^2. The irradiance is changed at 0.3s of the simulation time via a stair generator in MATLAB. The IGBT inverter converts the DC voltage to the corresponding three-phase AC. This voltage is transmitted through a distribution line of 1 km and is fed to the load. The type of load here is parallel RL load with the active power (P) provided as 100 kW and inductive reactive power (Q_L) is taken as 100 kVar. The simulation run time is 2s. The whole system is operating at 50 Hz frequency.

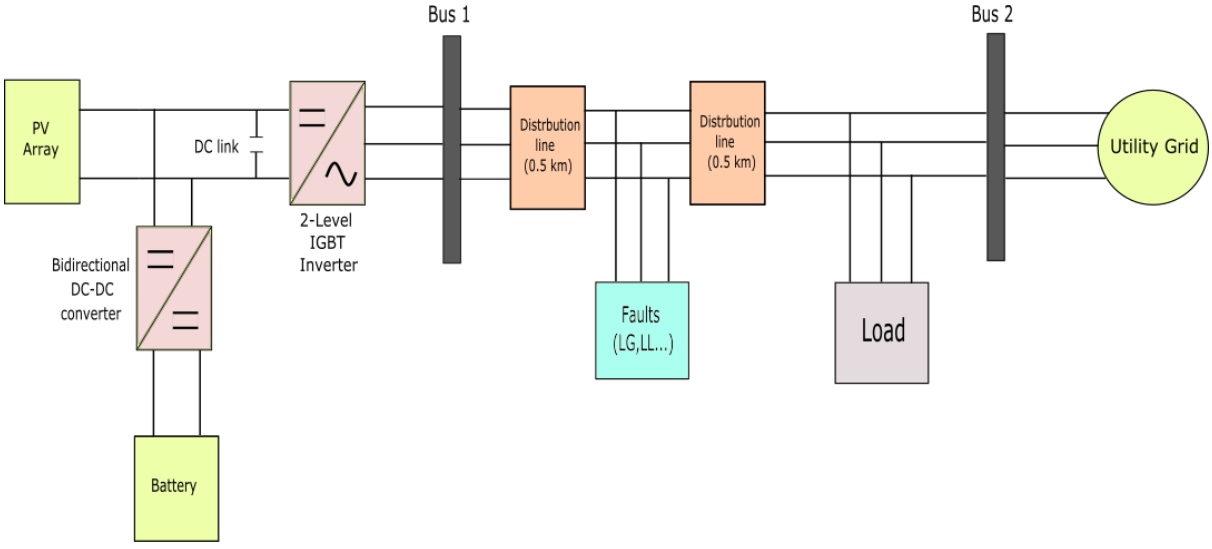

Figure 2.1: Schematic Diagram

The main operation events for the proposed scheme are given in Table 2.1.

Table 2.1 Main operation events

Events	Operation conditions	Time (s)
1.	Simulation Run time	1.2
2.	Irradiance becomes zero	0.3
3.	Fault switching time	(0.1,0.2)
4.	Battery response time	30
5.	Impulse fault occurrence time	0.15
6.	Simulation run time for impulse fault	0.25

In the Simulink diagram, there are 3 subsystems whose description is as follows.

2.1.1 PWM GENERATION SUBSYSTEM

The modulation index (m) of 0.95 is multiplied by a sine wave with a frequency of 50 Hz in this subsystem. The PWM generating block receives this output. Using the carrier-based two-level PWM approach, the PWM generator block creates pulses for PWM-controlled 2-Level converters. The block can control single-phase half-bridge, full-bridge (unipolar or bipolar modulation), or three-phase bridge switching devices. Figure 2.2 depicts the simulink diagram PWM generator subsystem.

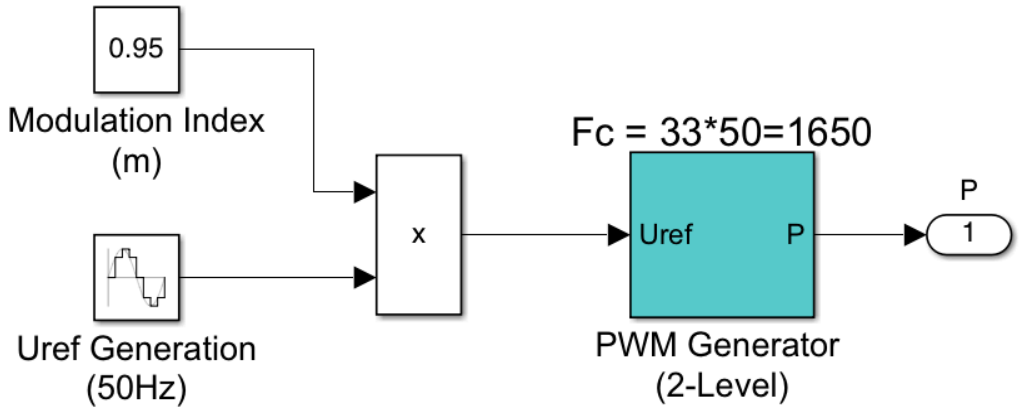

Figure 2.2: Simulink diagram of PWM generation subsystem

2.1.2 CONVERTER INTERFACED BATTERY ENERGY STORAGE SUBSYSTEM

This subsystem essentially functions as a BES system. As the name implies, a bidirectional DC-DC converter is used to flow power in both directions. A traditional buck-boost converter can only handle one-way power flow. Bidirectional DC-DC converters are the devices for serving the purpose of stepping up or stepping down the voltage with the capability of power flow in either forward direction or in the backward direction. Figure 2.3 depicts the simulink diagram of converter-based BES subsystem.

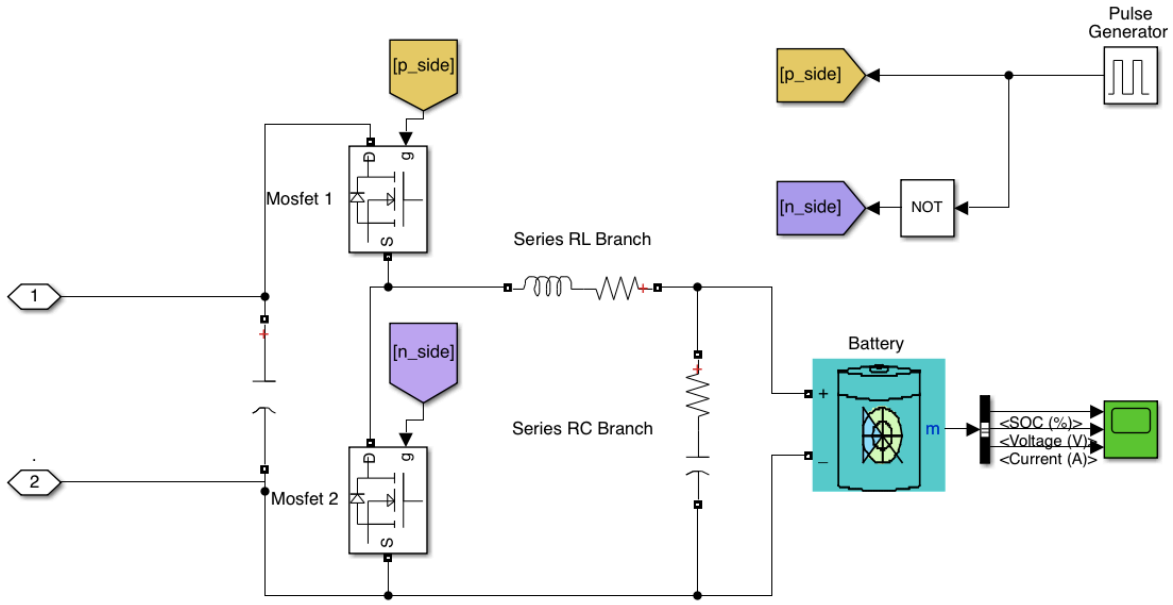

Figure 2.3: Simulink diagram of Converter-based battery energy storage subsystem

2.1.3 POWER QUALITY PARAMETERS SUBSYSTEM

The three phase voltage and current from the voltage current measuring block are distributed to other blocks in this subsystem. Power measurement, PLL, and THD are the three blocks used in this subsystem. Three-phase voltage and current are converted into three-phase real power (P) and reactive power (Q) using the power measurement block. The PLL block is used to synchronise on a series of three-phase, variable-frequency sinusoidal signals. If Automatic Gain Control (AGC) is enabled, the PLL regulator's input (phase error) is scaled according to the amplitude of the input signals. The THD block is used to compute the total harmonic distortion of signal. In Figure 2.4, power quality parameter subsystem is depicted.

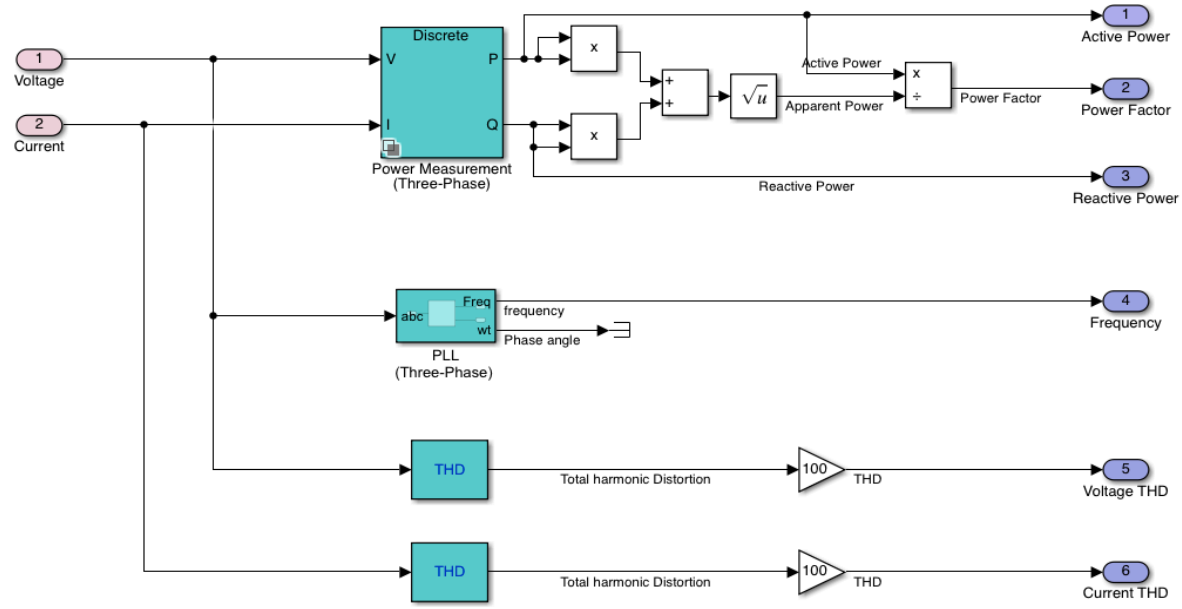

Figure 2.4: Simulink diagram of power quality parameters subsystem

2.2 DESCRIPTION OF COMPONENTS USED

2.2.1 PV ARRAY BLOCK

The PV array block represents a PV module array. An array is made up of strings of modules which are connected in series that are further connected in parallel. This block simulate preset PV modules from the National Renewable Energy Laboratory's (NREL) System Advisor Model (2018) as well as custom PV modules. It consists of a five-parameter model which represents the irradiance of module and temperature-dependent I-V characteristics by adding a diode, series resistance (R_s), shunt resistance (R_{sh}), and light-generated current source. Table 2.2 gives the information about the specifications of PV array. The simulink block for PV array block is shown in Figure 2.5. Figure 2.6 depicts an equivalent circuit design for a PV array, while Figures 2.7 and 2.8 depicts the PV and VI properties respectively.

Table 2.2 Specifications of PV array

Sr. No.	Parameters	Values used
1.	Number of parallel strings	40
2.	Number of series modules	10
3.	Max Power of modules	213.15 W

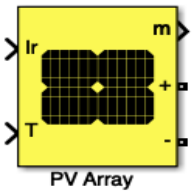

Figure 2.5: PV array block

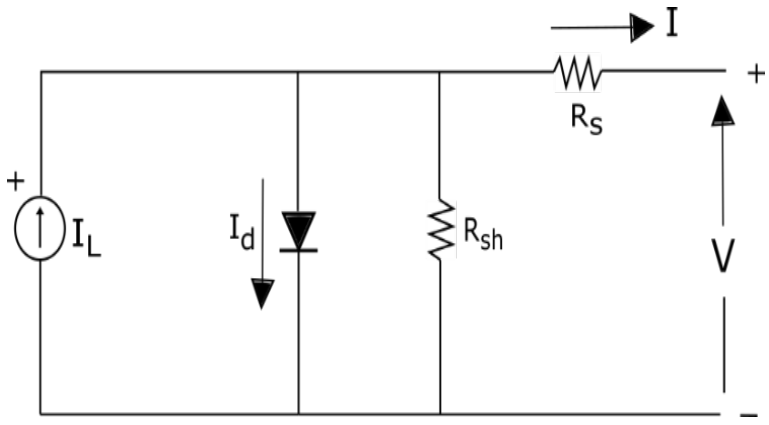

Figure 2.6: Equivalent circuit diagram of PV array

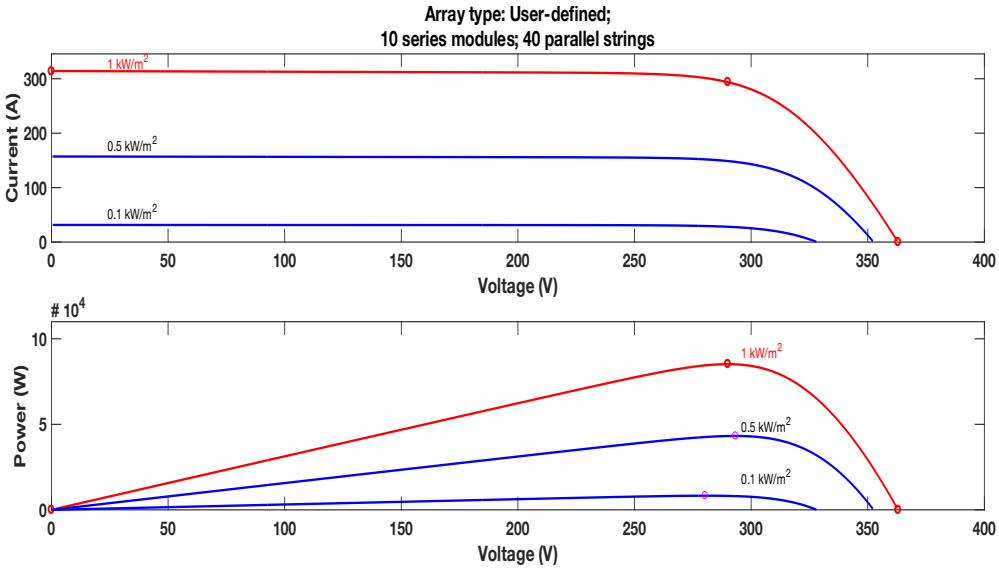

Figure 2.7: VI and PV characteristics with specified temperature

Equations (2.1) and (2.2) define the I-V characteristics of a single diode for a single module:

$$I_d = I_0 \left[exp\left(\frac{V_d}{V_0}\right) - 1 \right] \quad 2.1$$

$$V_T = \frac{kT}{q} \times nI \times N_{cell} \quad 2.2$$

where, I_d = Diode Current (A)

V_d = Diode Voltage (V)

I_0 = Diode Saturation Current (A)

nI = Diode Ideality factor, a number close to 1.

k = Boltzmann constant = 1.3806×10^{-23} JK^{-1}

q = Electron charge = 1.6022×10^{-19} C

T = Cell Temperature (K)

N_{cell} = number of cells in a module that are linked in series.

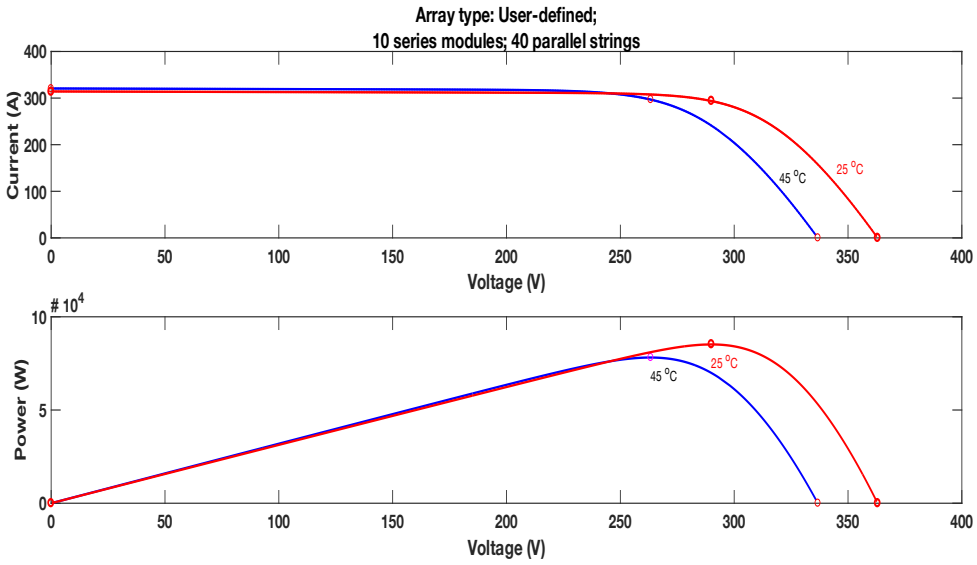

Figure 2.8: VI and PV plot with specified irradiances

2.2.2 BATTERY BLOCK

The battery block illustrates the most common types of rechargeable batteries using a general dynamic model. The circuit parameters may be changed to reflect a certain type of battery and its discharge characteristics. Table 2.3 shows the specifications of converter based BES system. Figures 2.9 and 2.10 depict the simulink battery block and a typical discharge curve with three portions respectively.

Table 2.3. Specifications of converter-based BES system

Sr. No.	Parameters	Values used
1.	Nominal voltage of battery	400 V
2.	Resistance	1 Ω
3.	Inductance	1 mH
4.	Capacitance	1 µF
5.	Rated Capacity	5.4 Ah
6.	Initial state of charge	50 %
7.	Battery Response time	30 s

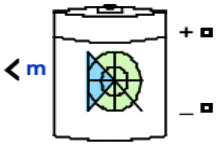

Figure 2.9: Battery block

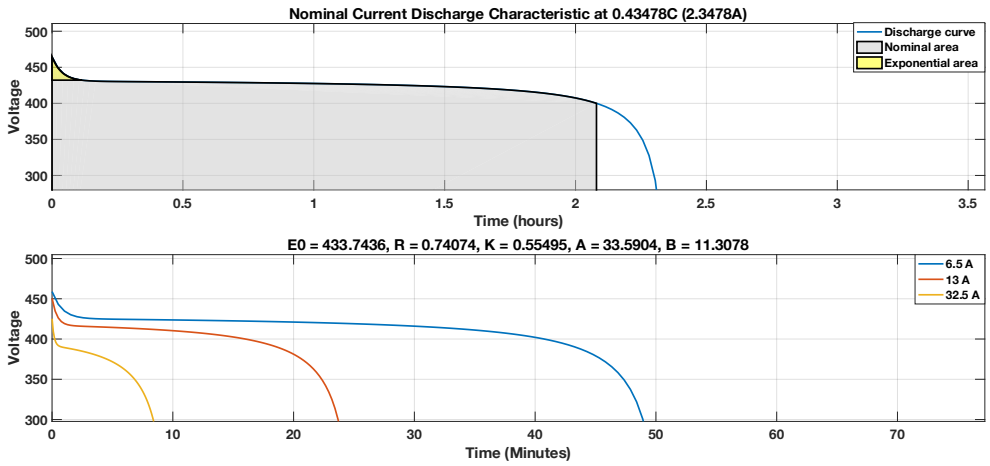

Figure 2.10: Typical discharge curve for Li-ion battery

The first segment depicts the exponential voltage decrease caused by charging the battery. The breadth of the decline is determined on the type of battery used. The charge that can be retrieved from the battery before the voltage falls below the battery's nominal voltage is represented in the second part. Finally, the third segment illustrates the whole drain of the battery, when the voltage drops fast.

When the battery current is negative, it recharges in accordance with the charge characteristic. The discharge characteristics are used to calculate the model parameters. It is believed that the discharging and charging behaviours are same.

2.2.3 TWO LEVEL THREE PHASE IGBT INVERTER BLOCK

The universal bridge block creates a universal three-phase power converter from up to six power switches coupled in a bridge arrangement. Figure 2.11 represents the MATLAB simulink block for IGBT inverter. The dialogue box allows the user to choose the type of power switch and converter setup. The universal bridge block enables the modelling of converters utilising both naturally commutated (diodes or thyristors) and forced-commutated power electronic devices (GTO, IGBT, MOSFET). Figure 2.12 (a) and (b) represents the connection diagram and switch arrangement for IGBT inverter block respectively.

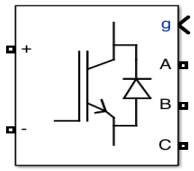

Figure 2.11: IGBT block

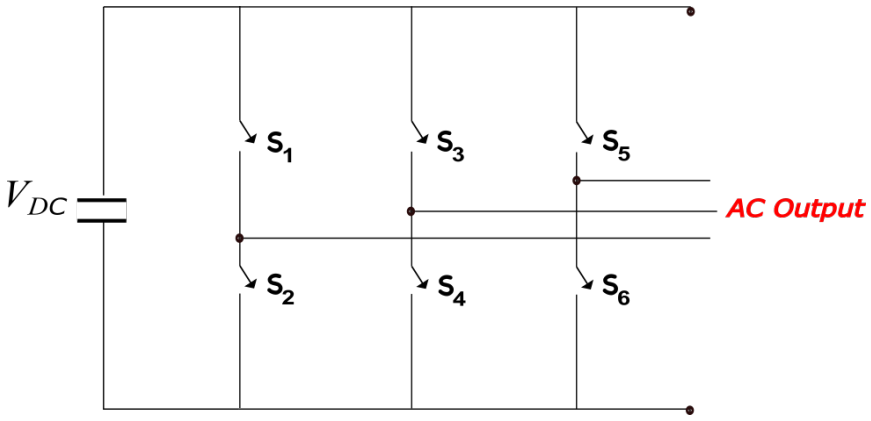

(a)

where S_1, $S_{2....}$ S_6 are the switches with IGBT connected antiparallel with diodes.

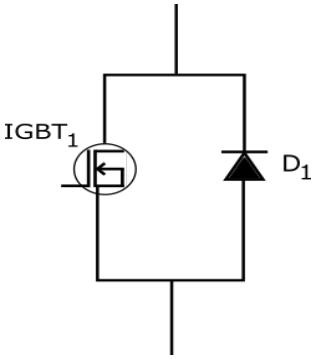

(b)

Figure 2.12: Circuit diagram of IGBT diode inverter

2.2.4 PWM GENERATOR BLOCK

The PWM generator (2-Level) block creates pulses for two level carrier based PWM converters. The block may control switching devices like FETs, IGBTs, or GTOs by using three types of converters: single phase half bridge (1 arm), single phase full bridge (2 arms), or three phase bridge (3 arms). Figure 2.13 shows the PWM generator block.

Figure 2.13: PWM generator block

A symmetrical triangular carrier is used to compare the reference signal, also known as the modulating signal. To compare the reference signal, also known as the modulating signal, a symmetrical triangular carrier wave is employed. Unipolar or bipolar PWM modulation may be used to operate a single phase full-bridge device. Each arm is controlled individually using unipolar modulation. Internally, a second reference signal is formed via 180˚ phase shift of the original reference signal.

2.2.5 DISTRIBUTION LINE BLOCK

The three-phase series RLC branch block implements three phase balanced branches made up of a resistor, an inductor, a capacitor, or a series mix of all of them. Select the components to include in each branch using the branch type option. Resistance, inductance, and capacitance can all have negative values. The block used for the distribution line is a series RLC block in which capacitance value is neglected as it is a very short transmission line of length 1 km only as shown in Figure 2.14. For this model, the resistance value is assumed to be 0.642 Ω and the inductance value is 0.264×10^{-3} H [29]. These values are multiplied by the half-length of the distribution line.

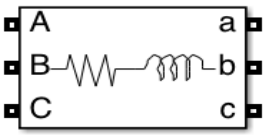

Figure 2.14: Distribution line block

2.2.6 THREE PHASE PARALLEL RL LOAD

The three-phase parallel RLC load block provides a three-phase balanced load as a parallel collection of RLC components as shown in Figure 2.15. At the indicated frequency, the impedance of load is constant. The ratio between the active and reactive powers of the load and the square of the applied voltage. The block icon only displays components with nonzero powers.

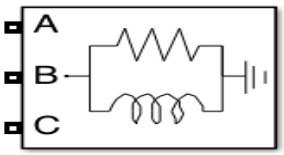

Figure 2.15: Parallel RL load block

2.2.7 NON LINEAR LOAD

The non linear load block consists of a three phase diode rectifier with a resistive load of value 0.5 Ω. A rectifier is a device that transforms alternating current (AC) in two directions that is oscillating into direct current in just one direction (DC). The non linear load block used in this work is shown in Figure 2.16. The specifications of loads are shown in Table 2.4.

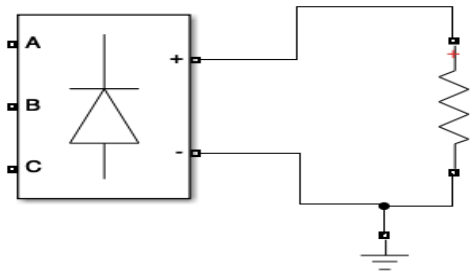

Figure 2.16: Non-Linear load

Table 2.4. Specifications of loads

Sr. No.	Parameters	Values used
1.	**Three phase parallel RL load (Yg)**	
(i)	Phase to Phase voltage (V_{RMS})	415 V
(ii)	Active Power	100 KW
(iii)	Reactive Power	75 kVar
2.	**Non-Linear load**	
(i)	Rectifier with resistive load	0.5 Ω

The chapter provides a brief information about the proposed methodology with various subsystem used in the simulink model. The specification table for each block has been highlighted in this chapter.

Chapter 3

EFFECT OF VARIOUS TYPES OF FAULTS ON MICROGRID OPERATION

This chapter gives brief description about the different faults like shunt and impulse fault implemented in the thesis work. The Simulink diagram for creating impulse fault has been discussed briefly. Three phase fault block has been discussed with its specifications.

3.1 SHUNT FAULTS

The type of shunt faults used in this thesis work are as follows:

1. Line to ground fault
2. Line to line fault
3. Double line to ground fault

The three-phase fault block from MATLAB/Simulink is used to give the above faults, as shown in Figure 3.1. This block enables the creation of a short circuit between any phase and the ground, or fault. This block makes use of three breaker blocks that may be turned on and off in accordance with the necessity to produce a problem. Switching time, fault resistances (R_{on}), ground resistances (R_g), snubber resistances (R_s), and snubber capacitances (C_s) are some of the parameter possibilities.

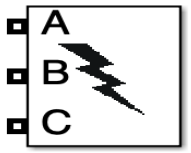

Figure 3.1: Three phase fault block

Table 3.1 contains all the parameters along with their values which are being used in the thesis work.

Table 3.1 Specifications of fault block

Sr. No.	Parameters	Values
1.	Switching Time	[5/50,10/50]
2.	Fault Resistance (R_{on})	0.001 Ω
3.	Ground Resistance (R_g)	0.01 Ω
4.	Snubber Resistance (R_s)	10^6 Ω
5.	Snubber Capacitance (C_s)	inf

3.2 LIGHTNING STRIKE/ HIGH IMPULSE VOLTAGE

The Simulink diagram used in this dissertation work for the lightning block is shown in the Figure 3.2. It simulates an impulsive transient carried on by lightning striking a distribution line. The Simulink model is already described in Chapter 2. The fault is the main change. To create an impulsive transient, the lightning block is connected to the mid of the distribution line. Since the MATLAB/Simulink blockset library does not have a lightning block, one may be created using already-existing Simulink blocks.

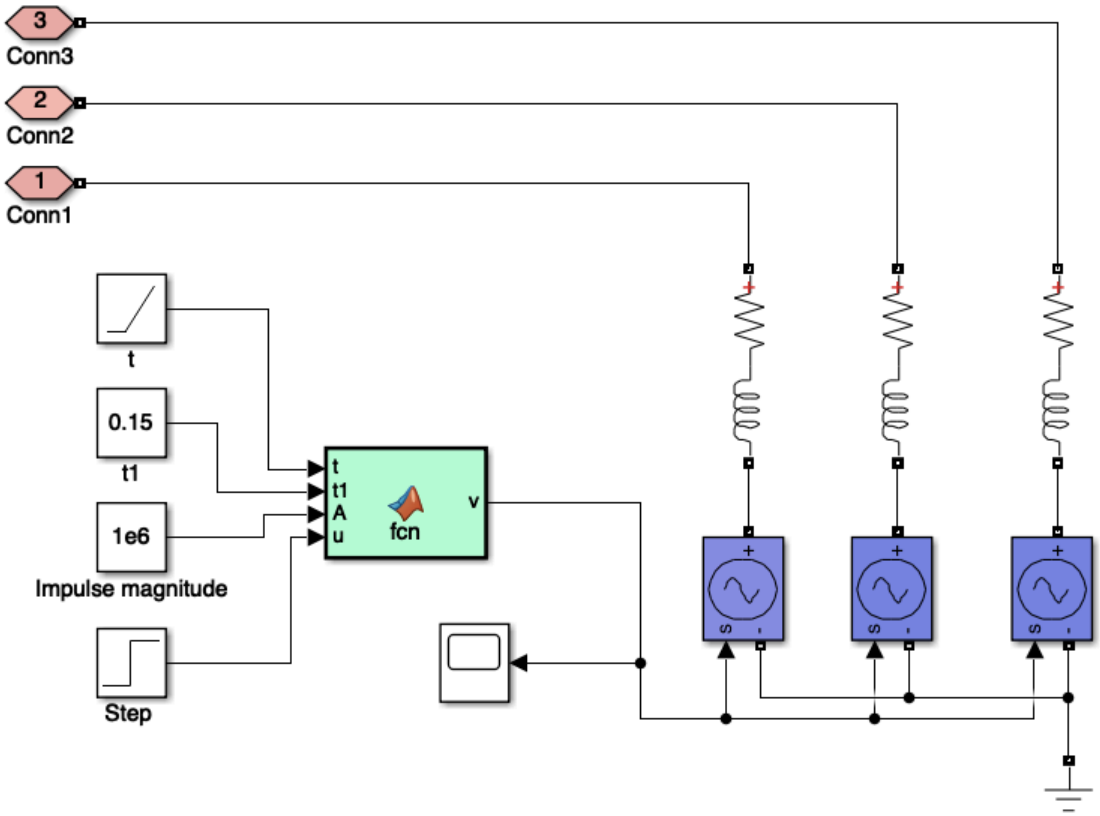

Figure 3.2: Simulink diagram for impulse fault

To connect the produced lightning impulse to a particular phase of the power system line, a controlled voltage source with a resistive and inductive network is employed. A three phase system needs three sets of resistive networks, regulated voltage sources, and inductive networks. Equation (3.1), [30] calculates the lightning impulse that is sent to the voltage controlled source input.

$$V(t) = Ae^{(-\alpha(t-t_1))} \times u(t-t_1) \qquad 3.1$$

where, A is the impulse magnitude,

t is the time function,

α is the damping factor,

t_1 is the time at which the impulse starts,

u is the impulse rising step

As illustrated in Figure 3.2, the lightning impulse fault may be implemented using the MATLAB Function block, Constant block, Ramp block, and Step function block. For the time function t, the ramp block is utilized, followed by the constant block for the impulse start time t_1 and impulse magnitude A, and finally, the step function block u for step rising. Equation (3.1) is coded in the MATLAB function block in the manner seen in Figure 3.3. According to IEEE C62-41.2 2002 and IEEE 1159.1 2009 standards [31], the typical lightning impulse characteristic is 1.2/50 μs, where the amplitude of impulse increases to a peak at 1.2 μs and decays to 50% at 50 μs time. The 1.2/50 μs lightning impulse waveform model, calculated using Equation (3.1) and a damping factor of alpha = 14,000 in a MATLAB function block, is shown in Figure 3.3. The impulse rises to its greatest magnitude of 10 at sample 10,000, or 0.01μs, and then declines to 5.036 by sample 10,050, or 50 μs later. The command given to the MATLAB function block for the generation of impulse fault is as follows:

```
Function v = fcn(t,t1,A,u)
alpha = 14000;
v = A*exp(-alpha*abs(t-t1))*u;
```

The coupling network is set to 10 Ω and 1 μH, and the impulse magnitude is set to 1 MV. The standard impulse waveform is compared with other four non-standard waveforms for assessing the different results under these conditions. The comparison table with the waveshape and different damping factor is shown in the Table 3.2.

Table 3.2: Different impulse waveshapes with Damping Factor

Sr No.	Type of waveshape	Type of impulse	Damping factor value
1.	Standard	1.2/50μs	14000
2.	Non-Standard	1.2/4μs	240000
3.	Non-Standard	1.2/10μs	78000
4.	Non-Standard	3/10μs	100000
5.	Non-Standard	7.5/50μs	31000

The coupling network impedance, which measures the closeness of the lightning discharge to the distribution line, determines the magnitude of the impulsive transient induced in the waveform. The coupling network impedance decreases as lightning distance to the transmission line increases.

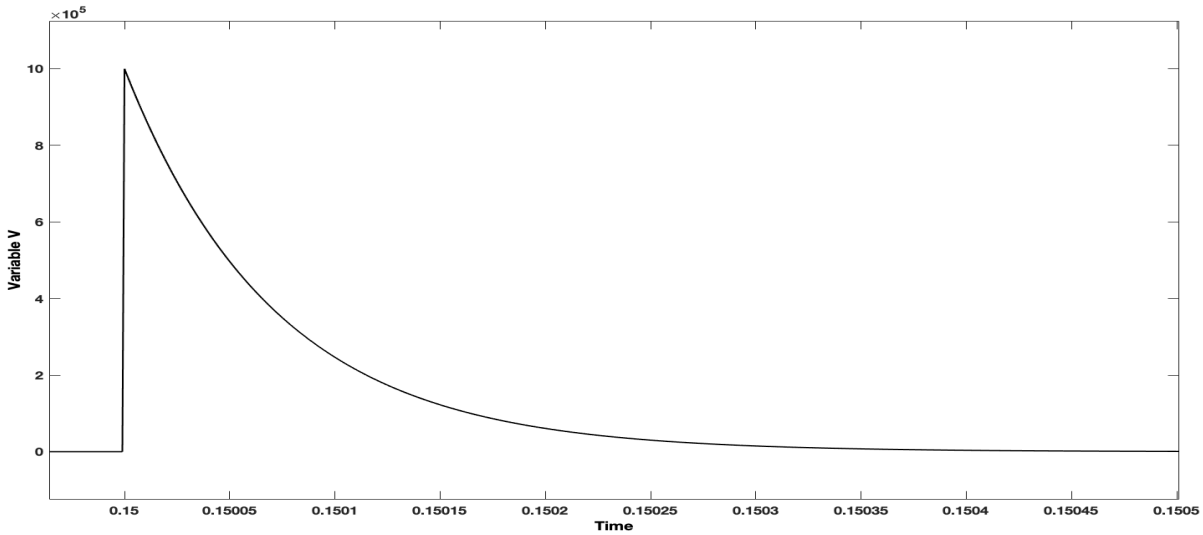

Figure 3.3: Impulse fault

Different kind of faults based on which all the results are taken, discussed in this Chapter.

Chapter 4

RESULTS AND DISCUSSIONS

This chapter provides an analysis of the major power quality parameters under MATLAB Simulink environment with various loads and under different fault conditions which affects the performance of the distribution line.

4.1 SHUNT FAULTS

The shunt faults discussed in the Chapter 3 are implemented in the MATLAB/Simulink model one by one to get the results. The complete layout for discussing the results further in this subsection are discussed in the Table 4.1.

Table 4.1 Microgrid operation under different types of modes and faults

Type of Load	Mode of operation	Types of faults
RL load, Non-linear load	Isolated mode without BES	Normal conditions, LG, LL, LLG
	Isolated mode with BES	Normal conditions, LG, LL, LLG
	Grid-connected mode	Normal conditions, LG, LL, LLG

4.1.1 PARALLEL RL LOAD

The three phase RL load is connected across the Bus-2 as per Figure 2.1 with the rated capacity of 100 kW and 75 kVar.

ISOLATED MODE WITHOUT BES SYSTEM

In first case, the source used is PV array which is providing DC voltage. This case is working under isolated microgrid without any battery backup.

Under Normal conditions: In these conditions all the eight parameters which are considered in these studies of power quality are analyzed. There are two stages of providing irradiances to the PV array. First case is at STC i.e., irradiances at 1000 W/m^2 and temperature at 25˚ C. Second case is when there is no availability of source. This case is attained by making irradiance zero. At 0.3 s irradiance is made zero so are results as shown in Figures 4.1 and 4.2. The active power (P) in the parallel RL load is 100 kW and the inductive reactive power (Q_L) is 75% of the active power i.e., 75 kVar. With the help of P and Q_L, the power factor is given by Equations (3.1) and (3.2).

$$\cos \emptyset = \tan^{-1} \frac{Q_L}{P} \qquad 3.1$$

$$\cos \emptyset = \frac{P}{\sqrt{(P^2 + Q_L^2)}} \qquad 3.2$$

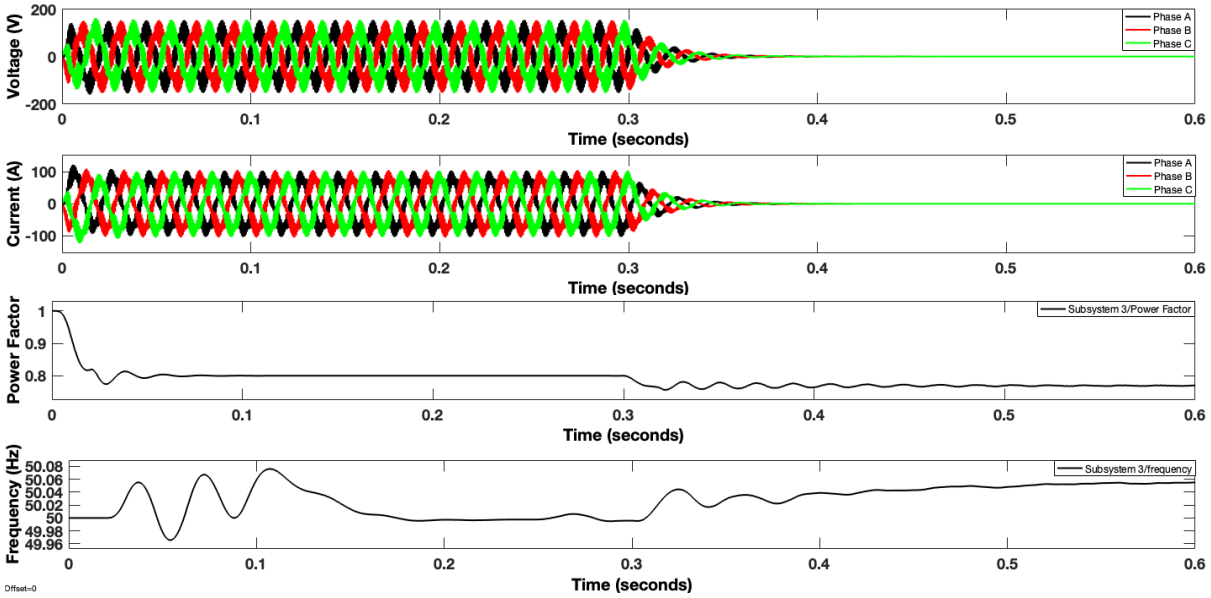

Figure 4.1: Waveforms for voltage, current, power factor and frequency under normal conditions

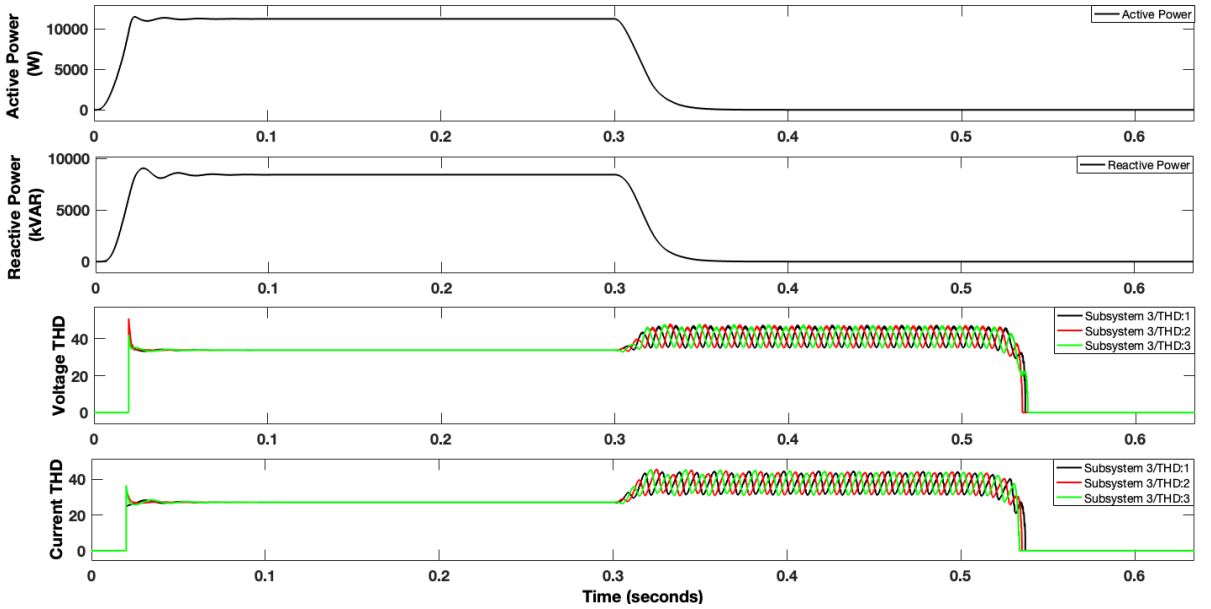

Figure 4.2: Waveforms for active power, reactive power, voltage THD and current THD under normal conditions

LG fault: The switching time for the fault is from 0.1s to 0.2s. The phase to ground fault occur at the mid of the distribution line due to which the voltage and current become zero in one of the phases and increase in the rest of two phases. Reactive and active power decrease due to fault incidence which can be seen in Figure 4.3. The high spikes occur in the current and voltage THD due to fault occurrence as shown in Figure 4.4.

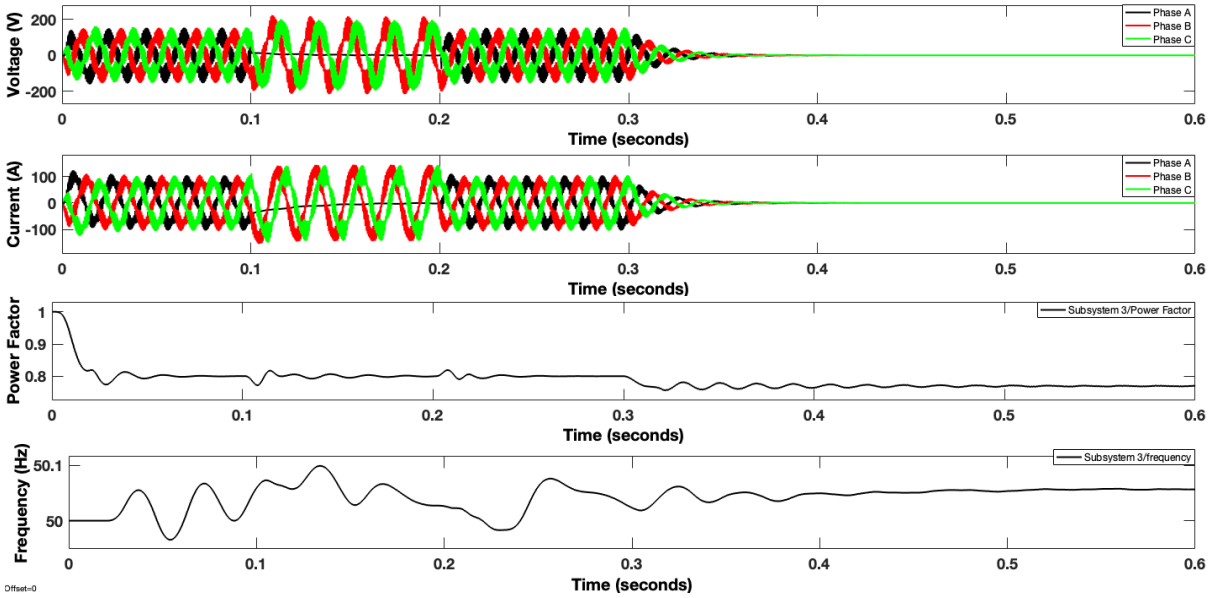

Figure 4.3: Waveforms for voltage, current, power factor and frequency under LG fault

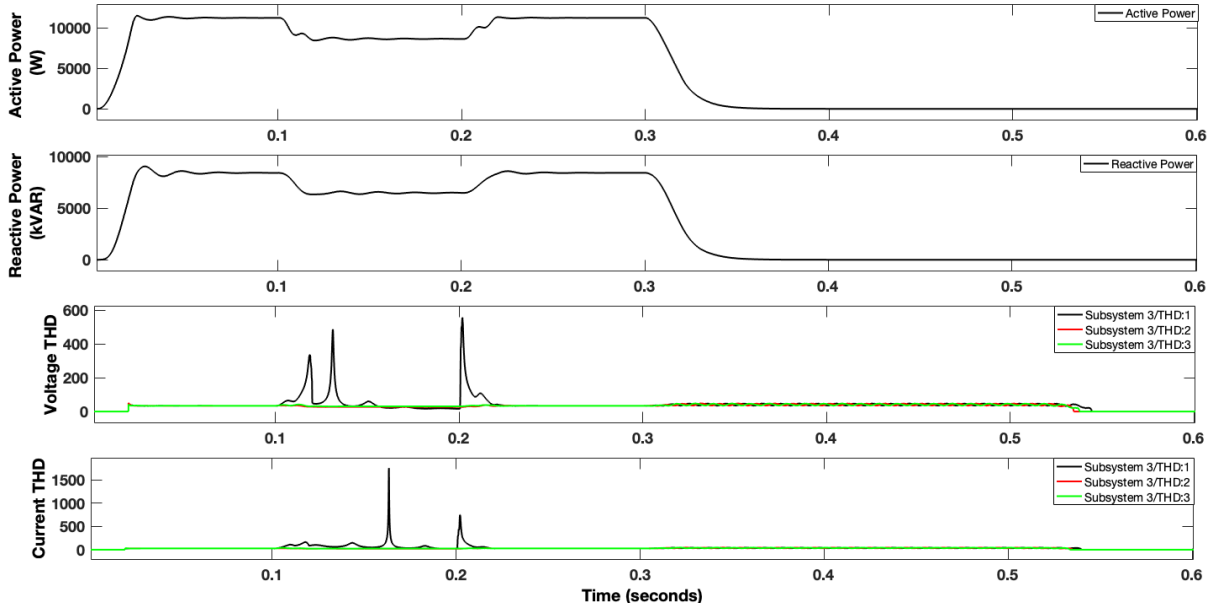

Figure 4.4: Waveforms for active power, reactive power, voltage THD and current THD under LG fault

LL fault: During line-to-line fault voltage and current decrease instead of becoming zero at 0.1 s and 0.2 s. When there is the unavailability of PV source i.e., irradiance becomes zero at 0.3 s, all the power quality parameters become zero except frequency and power factor as in Figures 4.5 and 4.6.

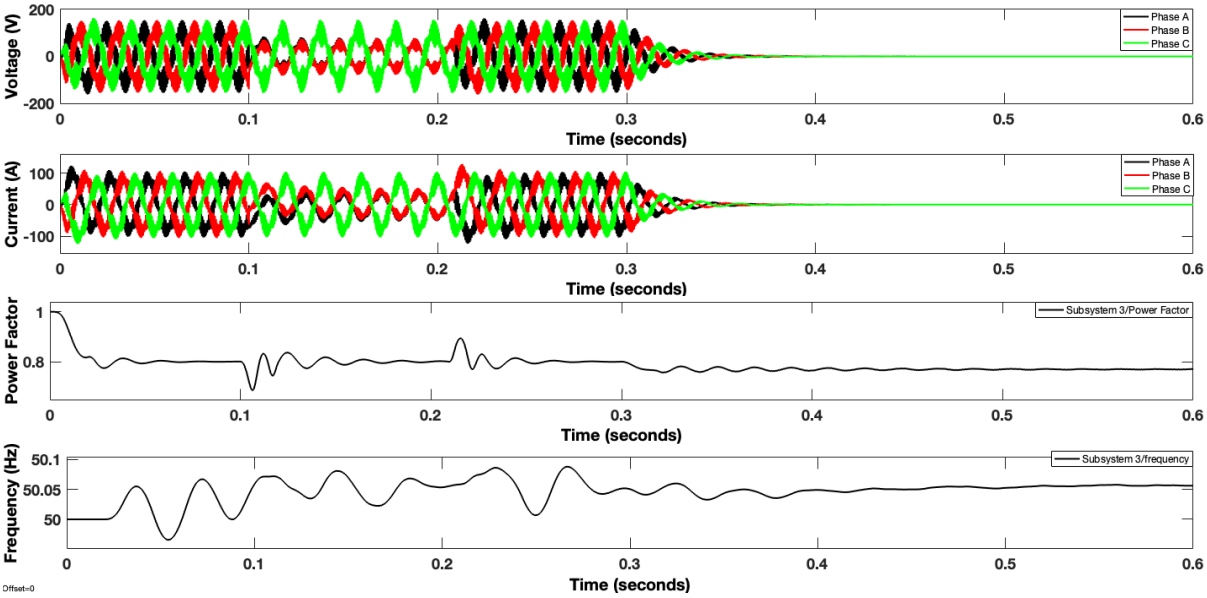

Figure 4.5: Waveforms for voltage, current, power factor and frequency under LL Fault

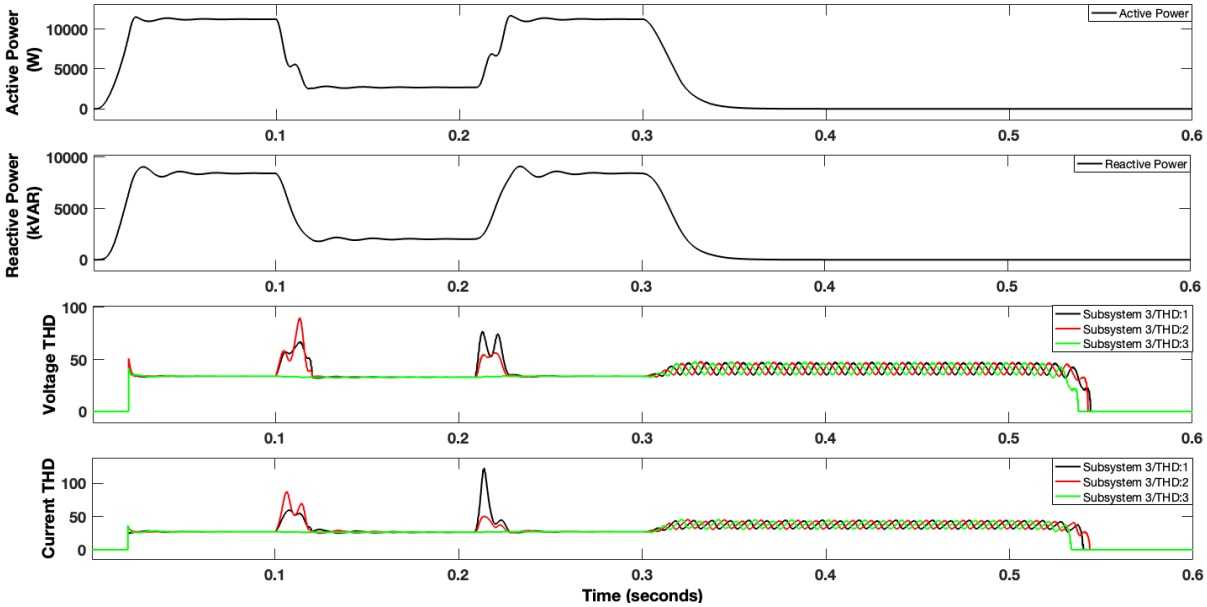

Figure 4.6: Waveforms for active power, reactive power, voltage THD and current THD under LL fault

LLG fault: Due to double line to ground fault the voltage and current become zero in the faulted section while increase in the remaining phase for maintaining a balance. All the power quality parameters become zero except frequency and power factor figure as in Figure 4.7. The results for power and THD are shown in Figure 4.8.

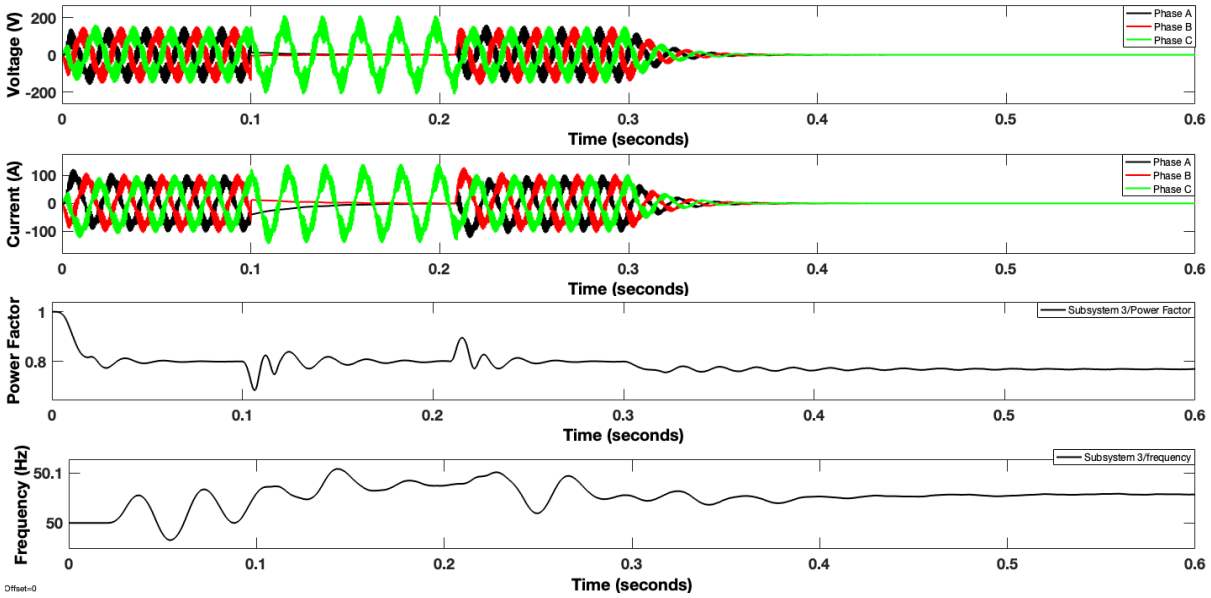

Figure 4.7: Waveforms for voltage, current, power factor and frequency under LLG Fault

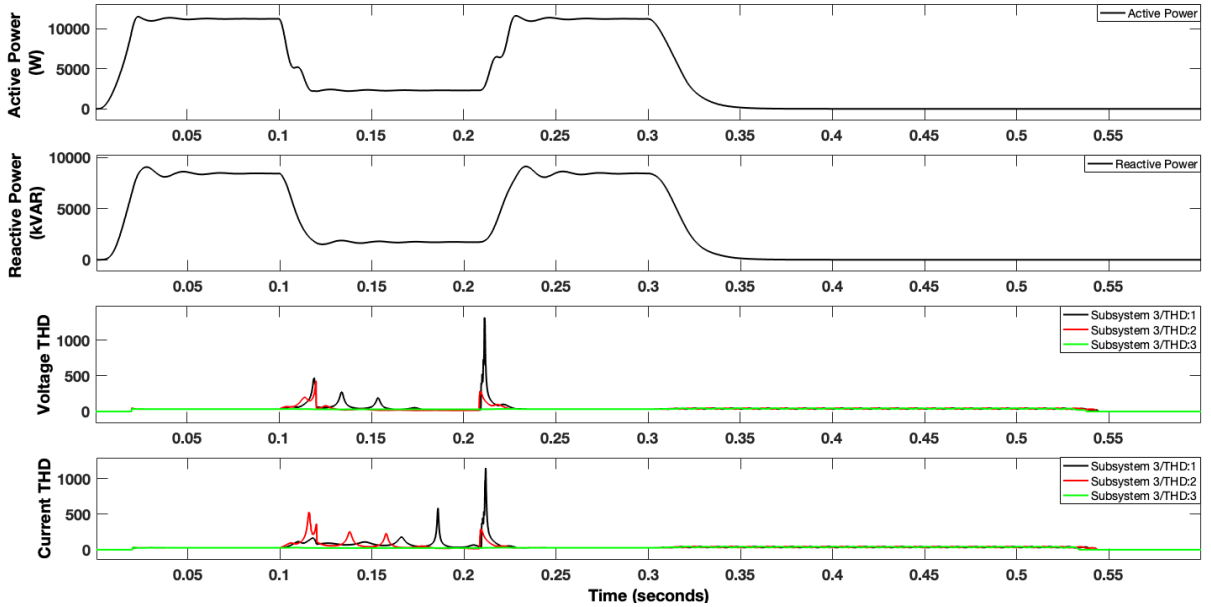

Figure 4.8: Waveforms for active power, reactive power, voltage THD and current THD under LLG fault

ISOLATED MODE WITH BES SYSTEM

In this case we are providing a battery system with bidirectional dc-dc converter. During normal operation, battery is charging through solar system. When there is no availability of solar system, then battery will act as a source.

Under Normal Conditions: In this case, when irradiance becomes zero the system is provided supply by battery system, hence the power quality parameters don't become zero. The power factor becomes 0.8 according to the equation (3.1) and (3.2). The frequency waveform becomes stable after 1 s as shown in Figure 4.9. Active and reactive power decreases after irradiance becomes zero as in Figure 4.10. Transients occur after 0.3 s but become stable within 0.1 s.

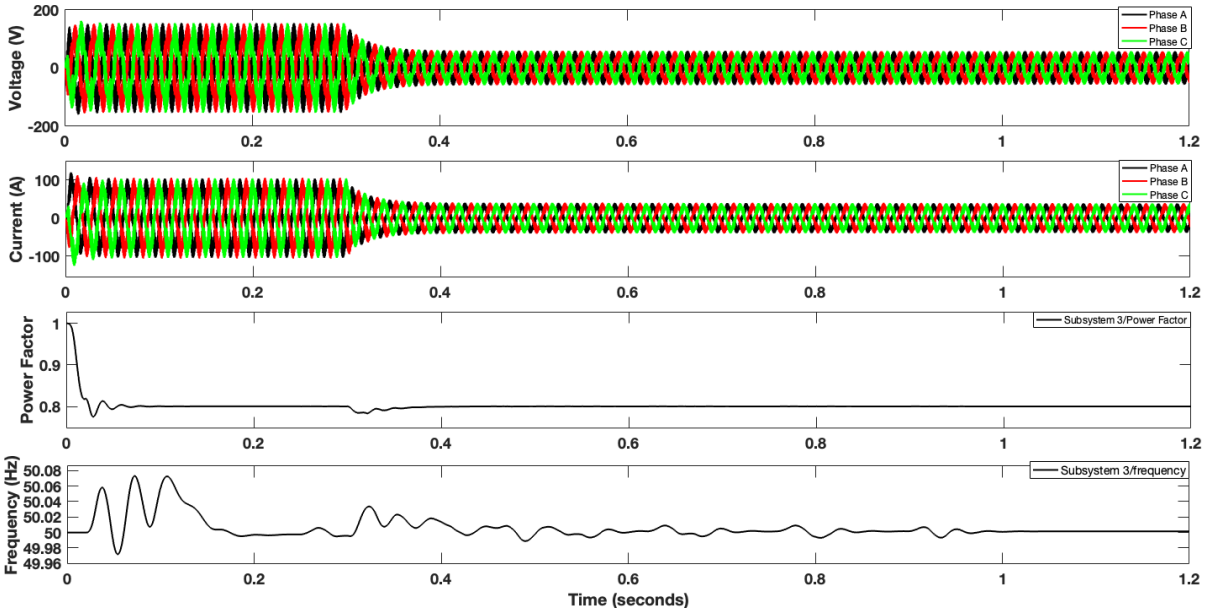

Figure 4.9: Waveforms for voltage, current, power factor and frequency under normal conditions

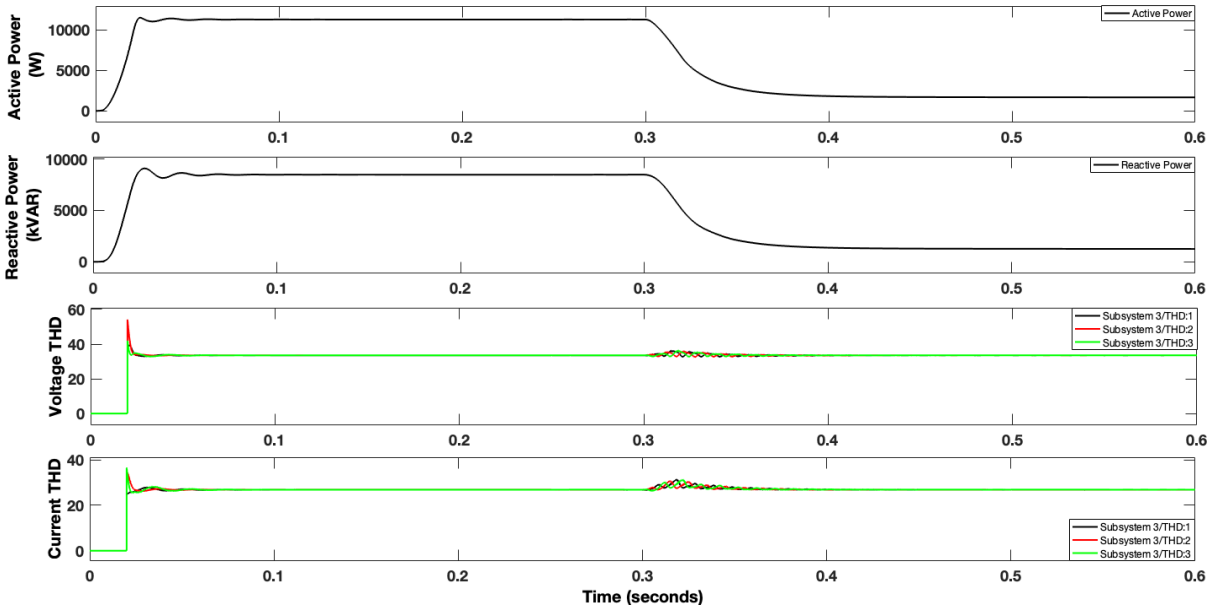

Figure 4.10: Waveforms for active power, reactive power, voltage THD and current THD under normal conditions

LG Fault: The switching time for the fault is from 0.1s to 0.2s. The phase to ground fault occur at the mid of the distribution line due to which the voltage and current become zero in one of the phases and increase in the rest of two phases as shown in Figure 4.11. Active and reactive power decrease due to fault incidence. The high spikes occur can be seen in the voltage and current THD due to fault occurrence in Figure 4.12. After unavailability of source, no parameter decreases to zero due to battery system.

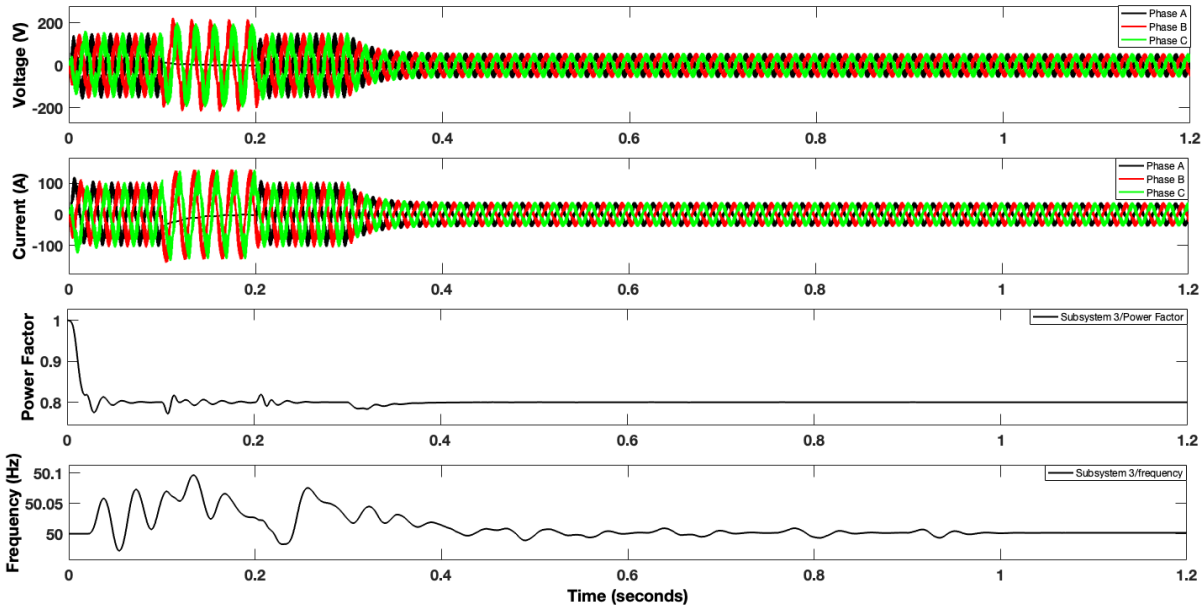

Figure 4.11: Waveforms for voltage, current, power factor and frequency under LG fault

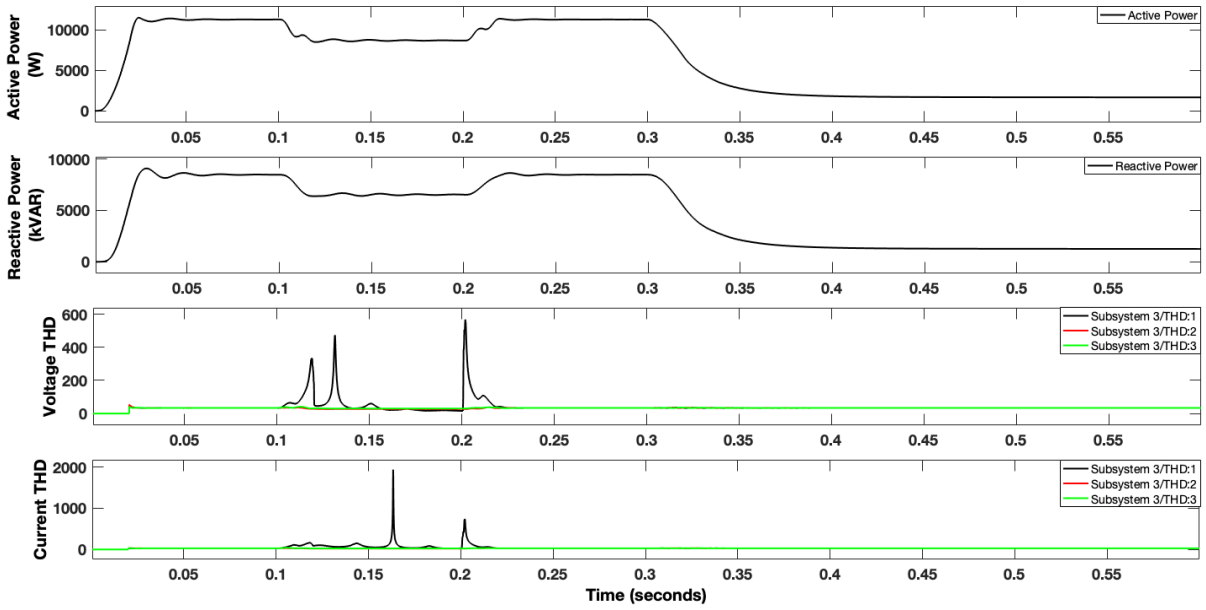

Figure 4.12: Waveforms for active power, reactive power, voltage THD and current THD under LG fault

LL Fault: During line-to-line fault voltage and current decrease instead of becoming zero at 0.1 s and 0.2 s. When there is unavailability of PV source i.e., irradiance becomes zero at 0.3 s, all the power quality parameters are supported by BES which helps in keeping system working as shown in Figures 4.13 and 4.14. Frequency becomes stable after 1 s.

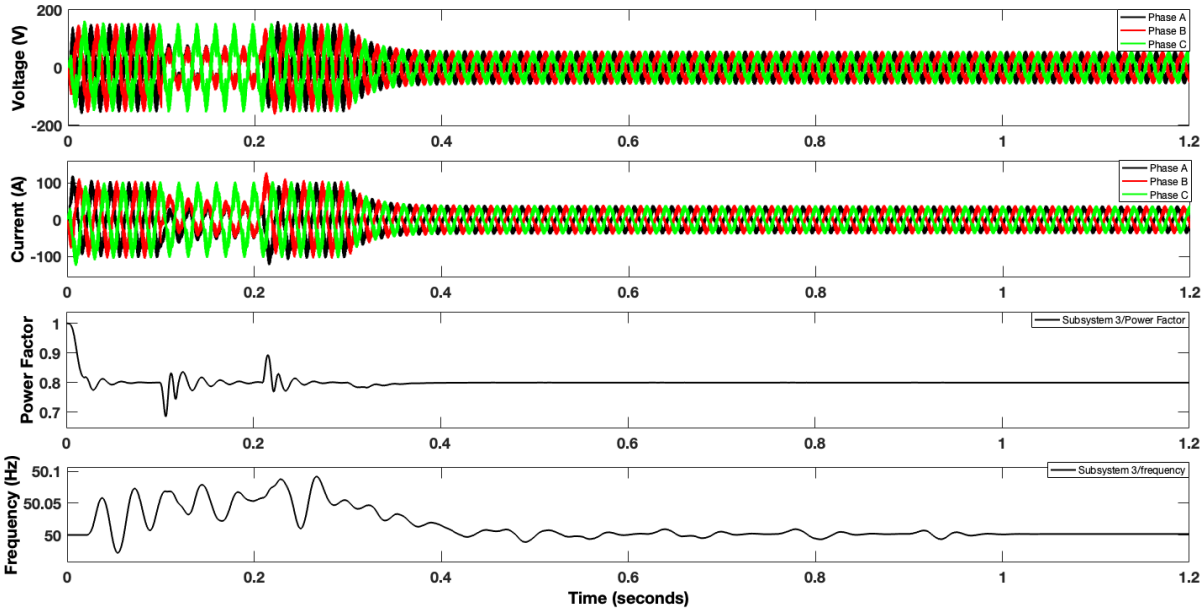

Figure 4.13: Waveforms for voltage, current, power factor and frequency under LL Fault

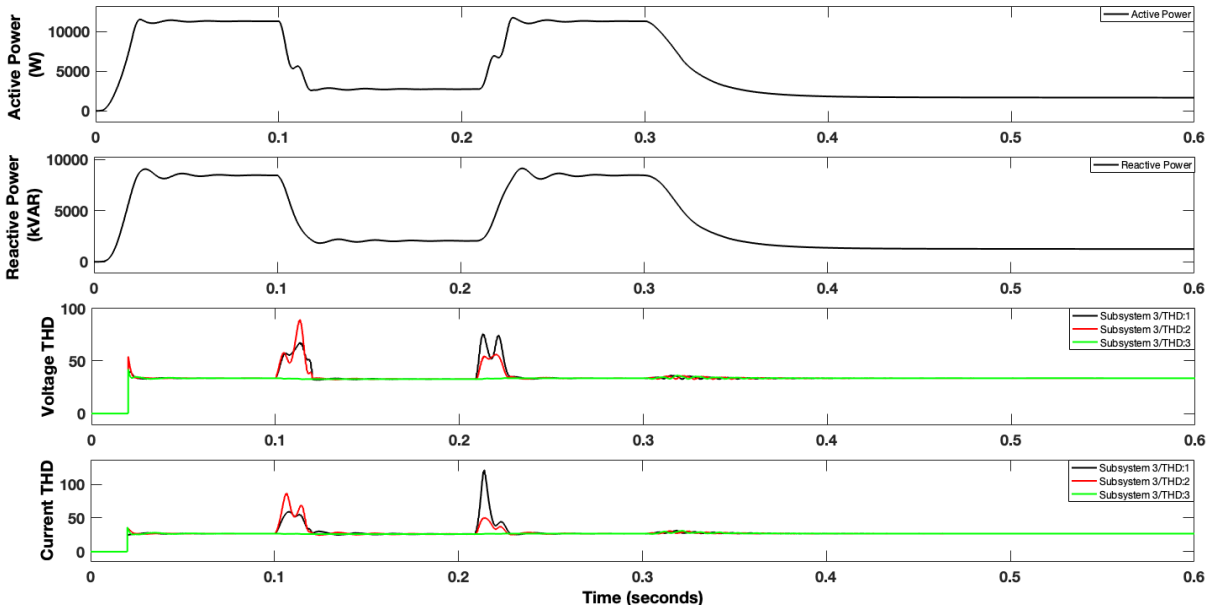

Figure 4.14: Waveforms for active power, reactive power, voltage THD and current THD under LL fault

LLG Fault: Due to double line to ground fault, the voltage and current become zero in the faulted section while increase in the remaining phase for maintaining a balance. Power factor become 0.8 because of the applied active and reactive power of the parallel RL load. All the parameters have some values because of the battery system as shown in Figures 4.15 and 4.16.

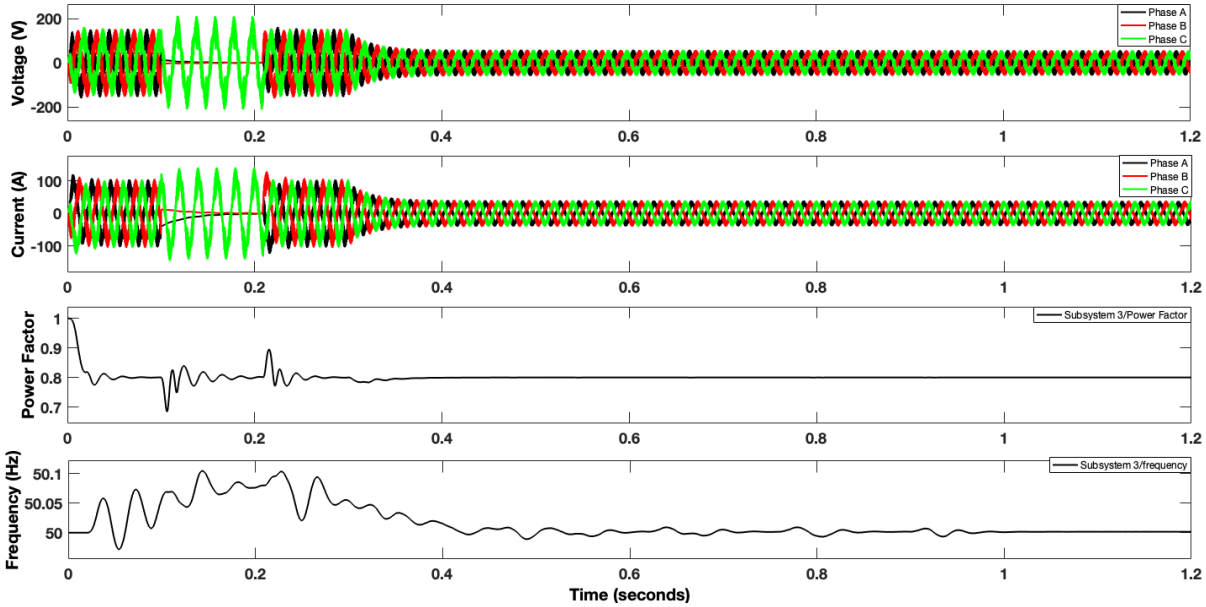

Figure 4.15: Waveforms for voltage, current, power factor and frequency under LLG Fault

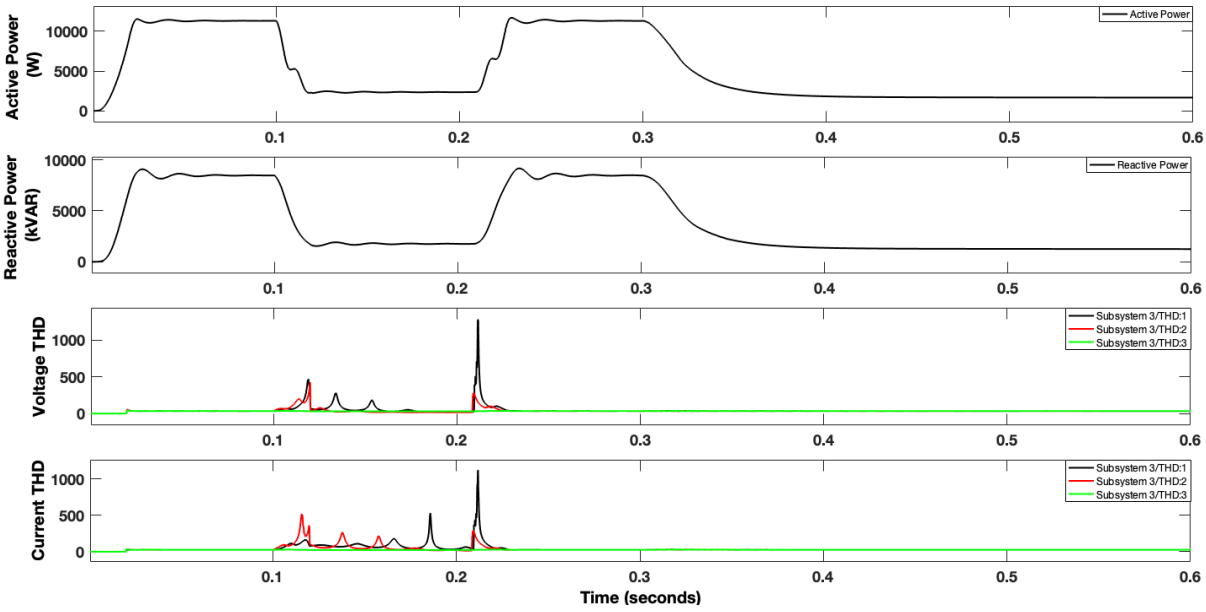

Figure 4.16: Waveforms for active power, reactive power, voltage THD and current THD under LLG fault

GRID CONNECTED MODE

Under Normal conditions: In these conditions, all the eight parameters which are considered in these studies of power quality are analyzed. There are two stages of providing irradiances to the PV array. First case is at STC i.e., irradiances at 1000 W/m^2 and temperature at 25˚ C. Second case is when there is no availability of source. This case is attained by making irradiance zero. At 0.3 s irradiance is made zero so are results as shown in Figures 4.17 and 4.18. The active power (P) in the parallel RL load is 100 kW and the inductive reactive power (Q_L) is 75% of the active power i.e., 75 kVAr. The utility grid-connected provides the complete supply after unavailability of source.

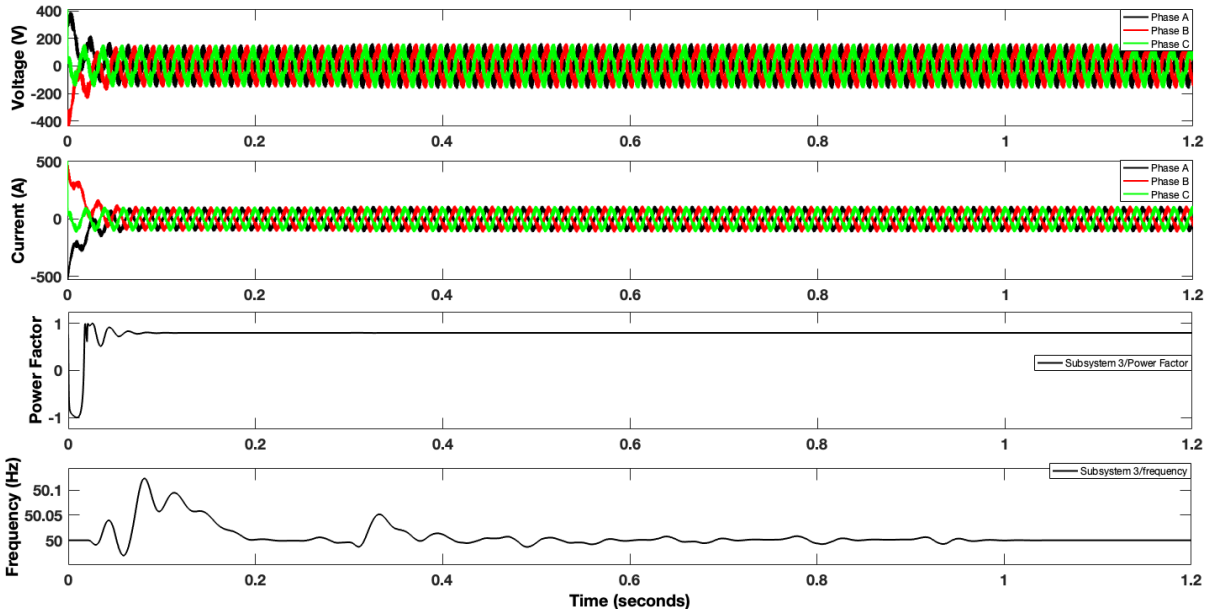

Figure 4.17: Waveforms for voltage, current, power factor and frequency under normal conditions

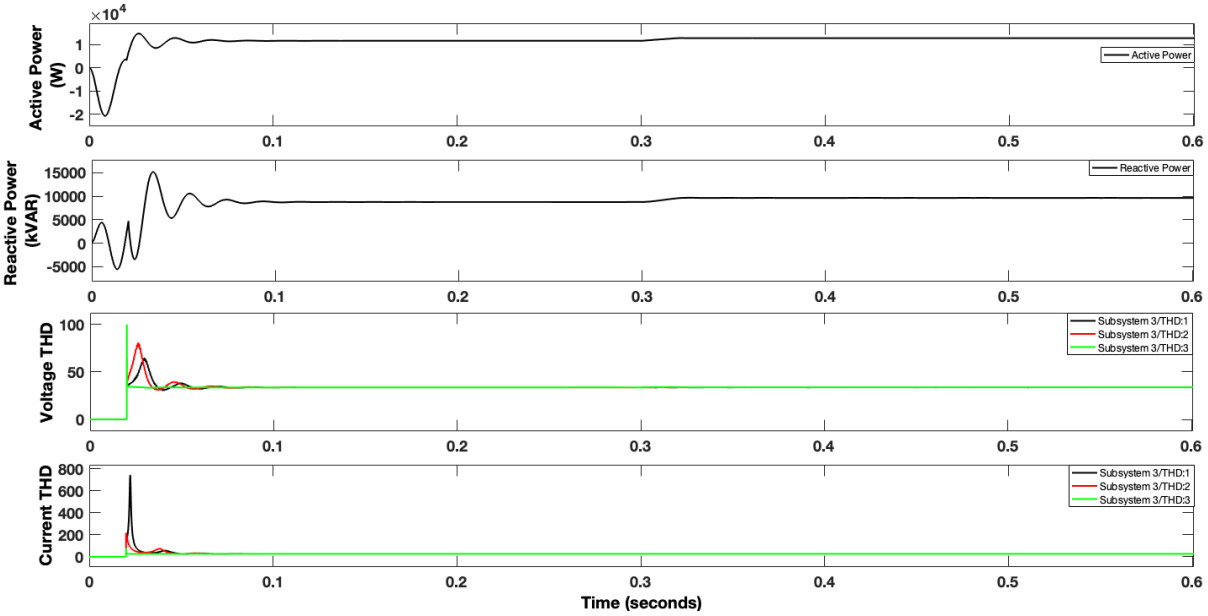

Figure 4.18: Waveforms for active power, reactive power, voltage THD and current THD under normal conditions

LG fault: The switching time for the fault is from 0.1s to 0.2s. The phase to ground fault occur at the mid of the distribution line due to which the voltage and current become zero in one of the phases and increase in the rest of two phases shown in Figure 4.19. Active and reactive power decrease due to fault incidence shown in Figure 4.20. The high spikes occur in the voltage and current THD due to fault occurrence. Due to the utility grid, no parameter falls to zero when the source is unavailable.

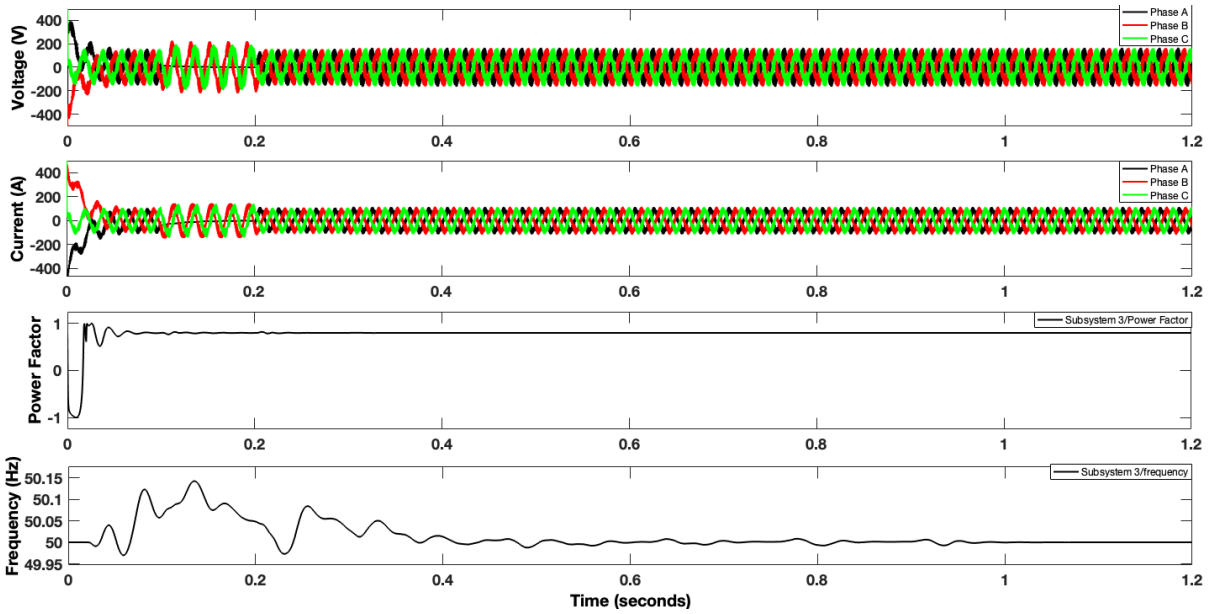

Figure 4.19: Waveforms for voltage, current, power factor and frequency under LG Fault

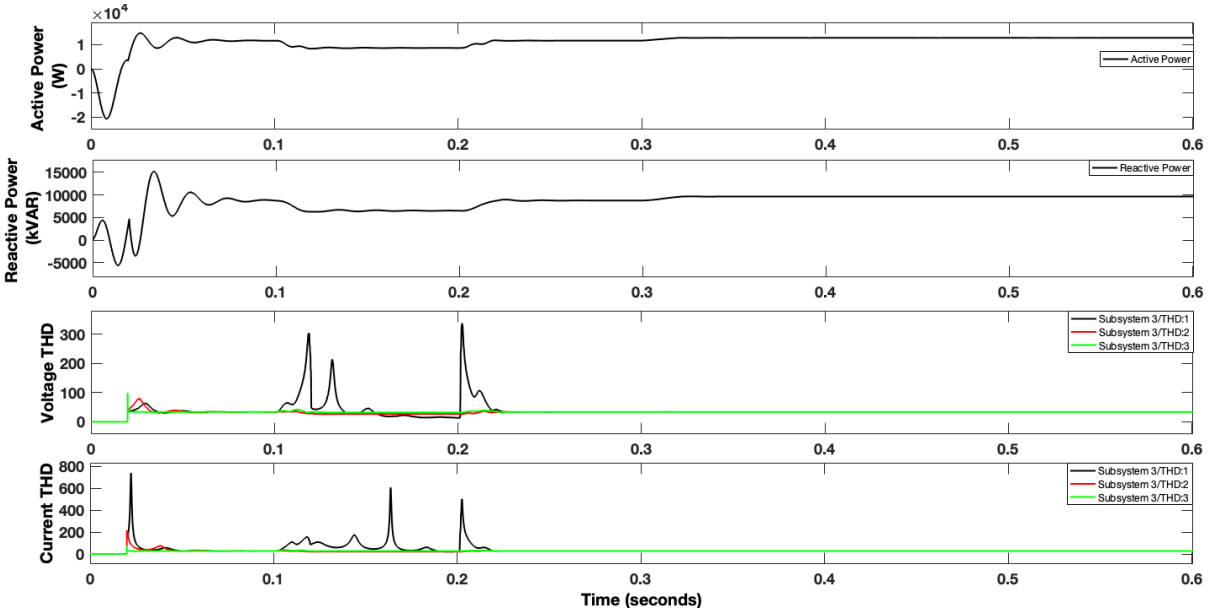

Figure 4.20: Waveforms for active power, reactive power, voltage THD and current THD under LG fault

LL Fault: During line-to-line fault, voltage, and current decrease instead of becoming zero at 0.1 s and 0.2 s. When there is unavailability of PV source i.e., irradiance becomes zero at 0.3 s, all the power quality parameters are supported by BES which helps in keeping system working as shown in Figure 4.21 and 4.22. Frequency becomes stable after 1 s.

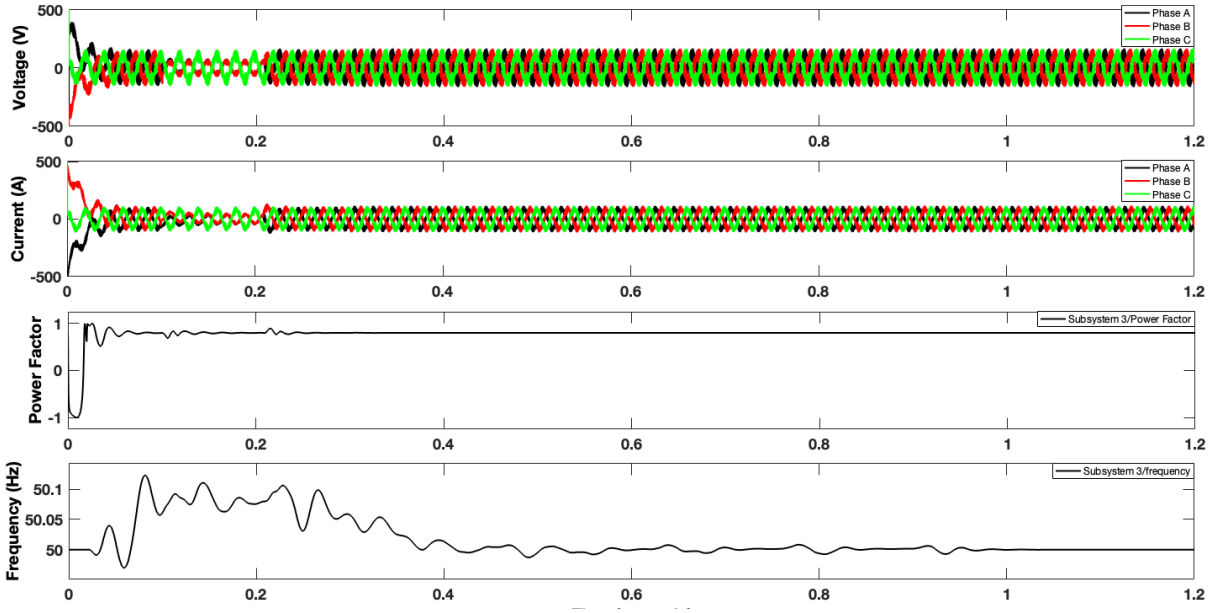

Figure 4.21: Waveforms for voltage, current, power factor and frequency under LL Fault

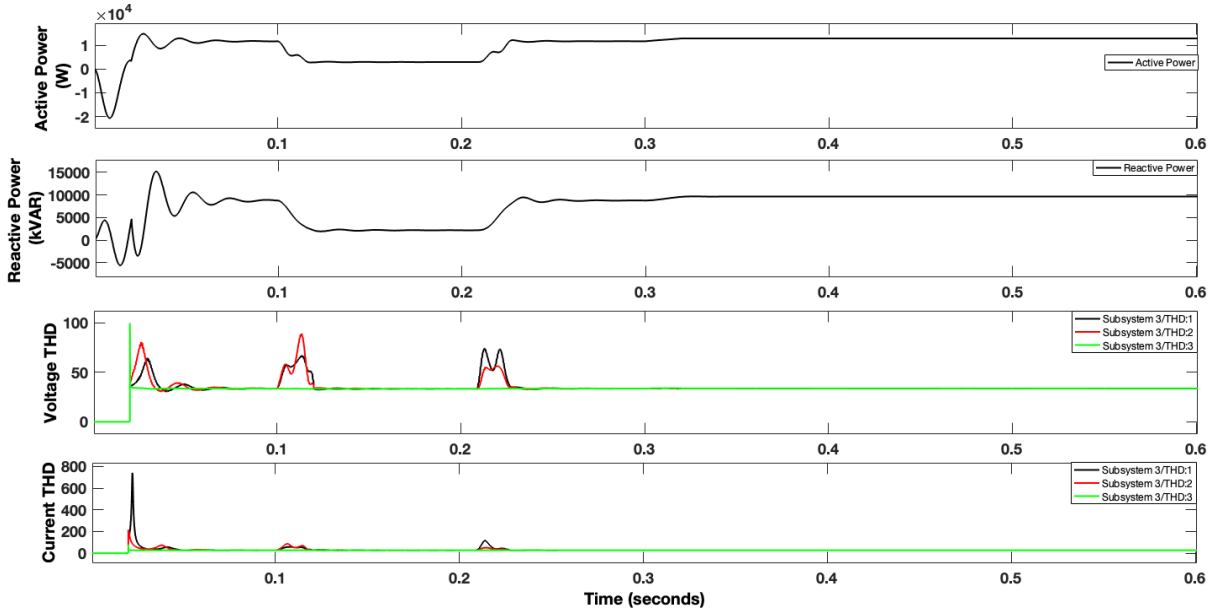

Figure 4.22: Waveforms for active power, reactive power, voltage THD and current THD under LL fault

LLG fault: Due to double line to ground fault the voltage and current become zero in the faulted section while increase in the remaining phase for maintaining a balance. Power factor become 0.8 because of the applied active and reactive power of the parallel RL load. All the parameters have some values because of the utility grid which can be clearly seen in Figures 4.23 and 4.24.

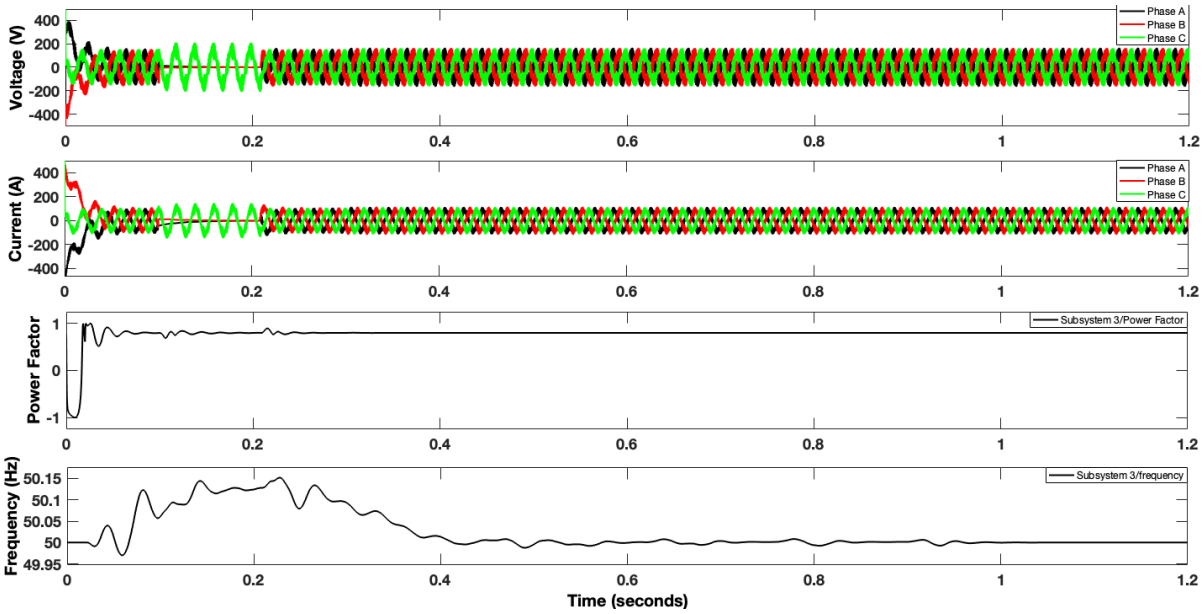

Figure 4.23: Waveforms for voltage, current, power factor and frequency under LLG Fault

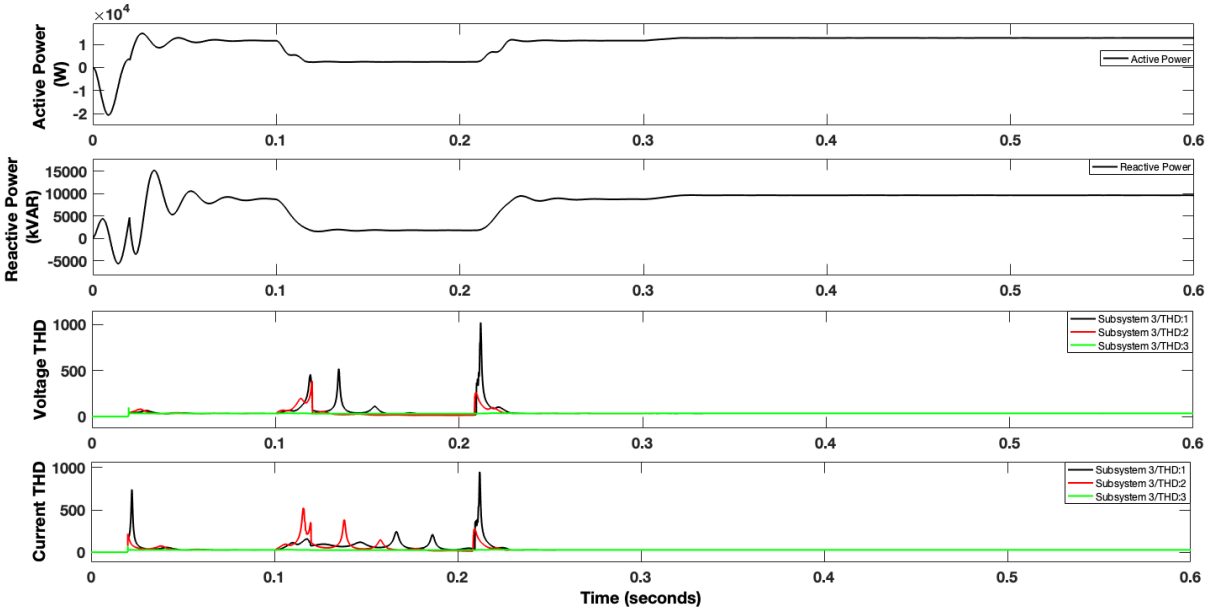

Figure 4.24: Waveforms for active power, reactive power, voltage THD and current THD under LLG fault

4.1.2 NON-LINEAR LOAD

The three-phase rectifier uses six diodes with resistive load having value of 0.5Ω which is connected across the Bus-2 to measure the PQ parameters. The complete layout for discussing the results further is discussed in the Table 4.1.

ISOLATED MODE WITHOUT BES SYSTEM

Under Normal conditions: In these conditions all the eight parameters which are considered in these studies of power quality are analyzed. Due to rectifier with resistive load, the AC voltage is converted into DC voltage while the current remains the AC. When irradiance

become zero all the parameters become zero except power factor and frequency as in Figures 4.25 and 4.26.

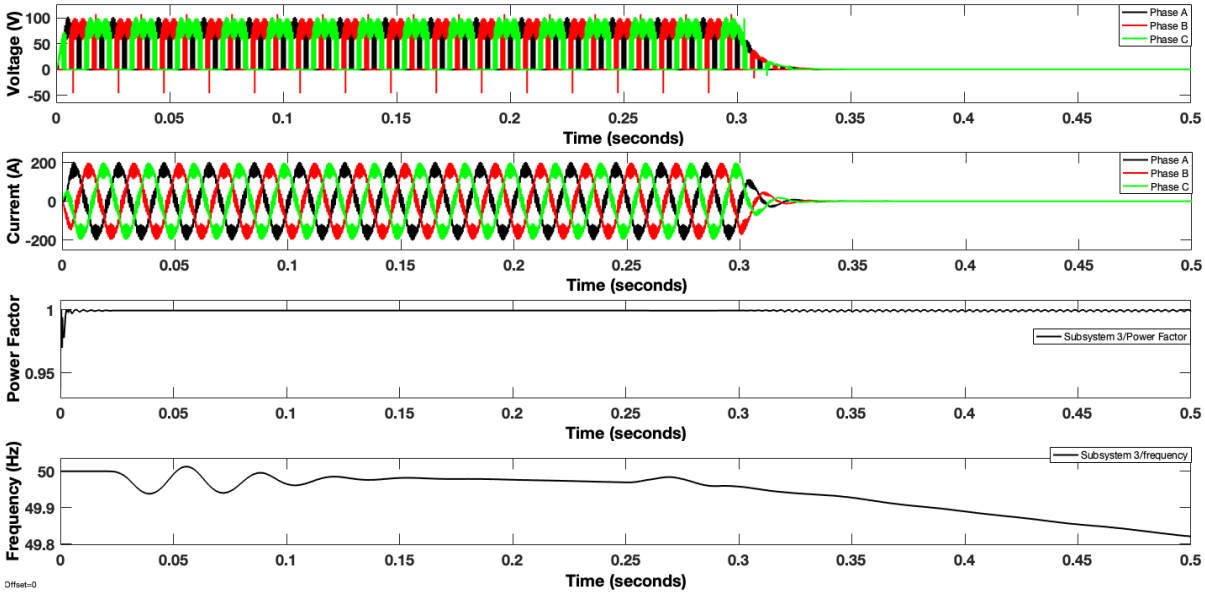

Figure 4.25: Waveforms for voltage, current, power factor and frequency under normal conditions

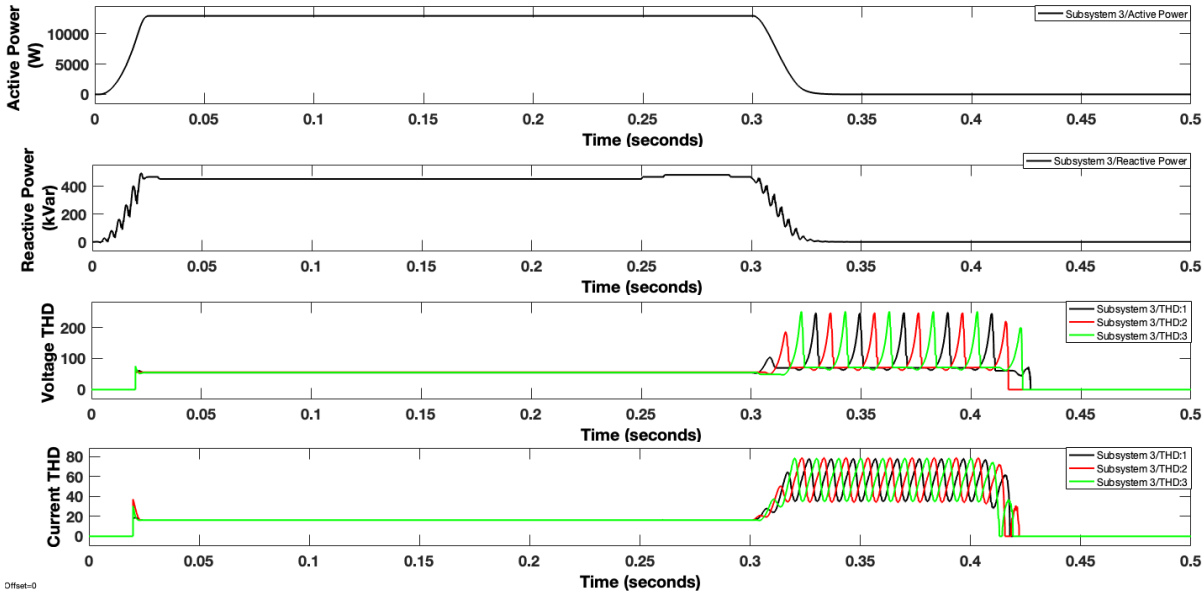

Figure 4.26: Waveforms for active power, reactive power, voltage THD and current THD under normal conditions

LG Fault: The switching time for the fault is from 0.1s to 0.2s. The phase to ground fault occur at the mid of the distribution line due to which the voltage and current become zero in one of the phases and increase in the rest of two phases in Figure 4.27. Active and reactive power decrease due to fault incidence. The high spikes occur in the voltage and current THD due to fault occurrence in Figure 4.28.

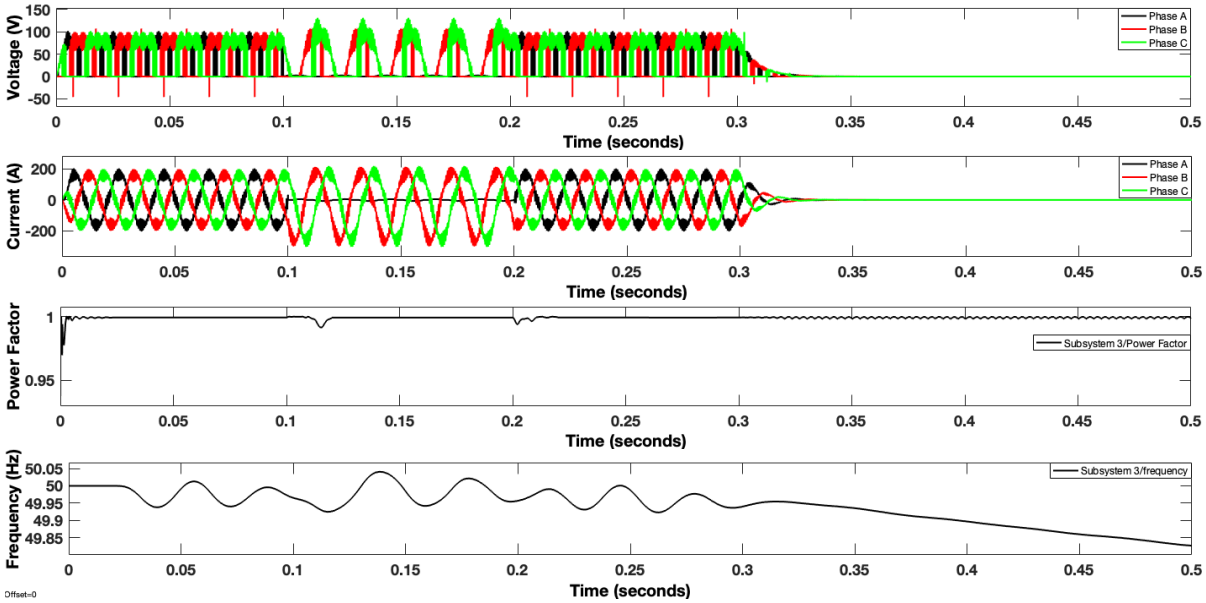

Figure 4.27: Waveforms for voltage, current, power factor and frequency under LG Fault

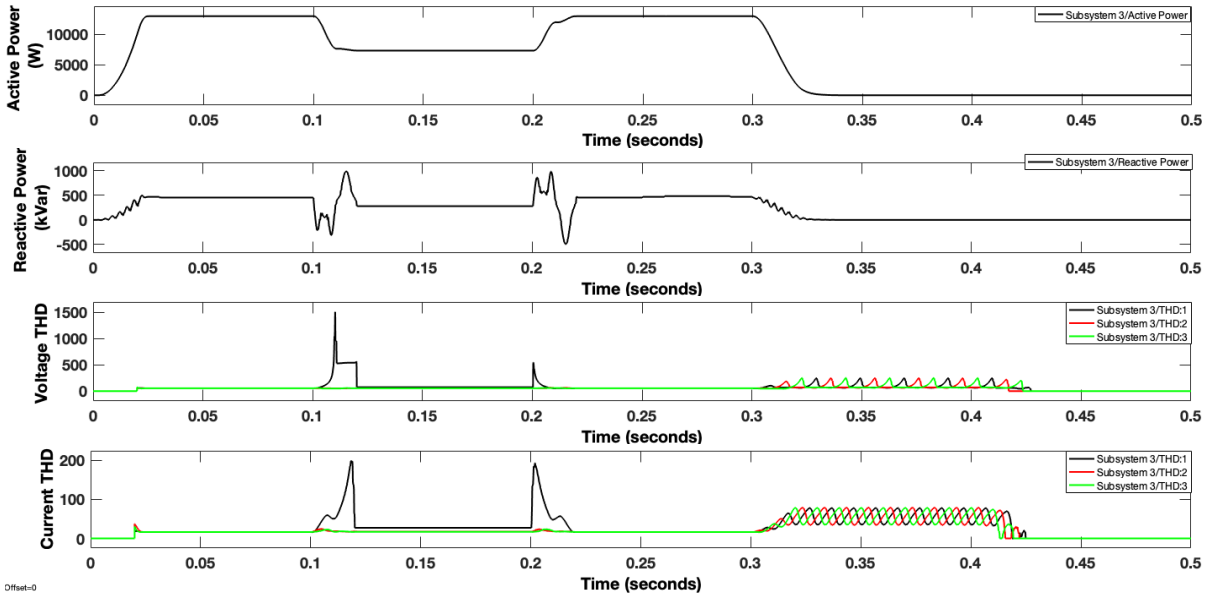

Figure 4.28: Waveforms for active power, reactive power, voltage THD and current THD under LG fault

LL Fault: During line-to-line fault voltage and current decrease instead of becoming zero at 0.1 s and 0.2 s. When there is unavailability of PV source i.e., irradiance becomes zero at 0.3 s, all the power quality parameters become zero except frequency as frequency doesn't depend on source availability along with power factor as in Figures 4.29 and 4.30.

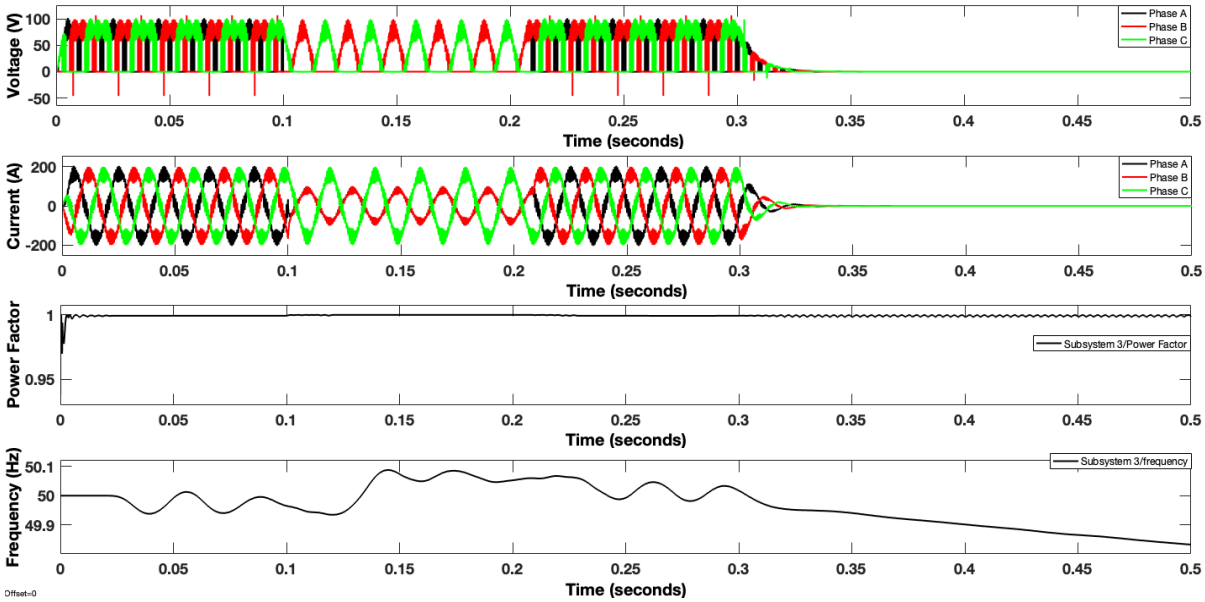

Figure 4.29: Waveforms for voltage, current, power factor and frequency under LL Fault

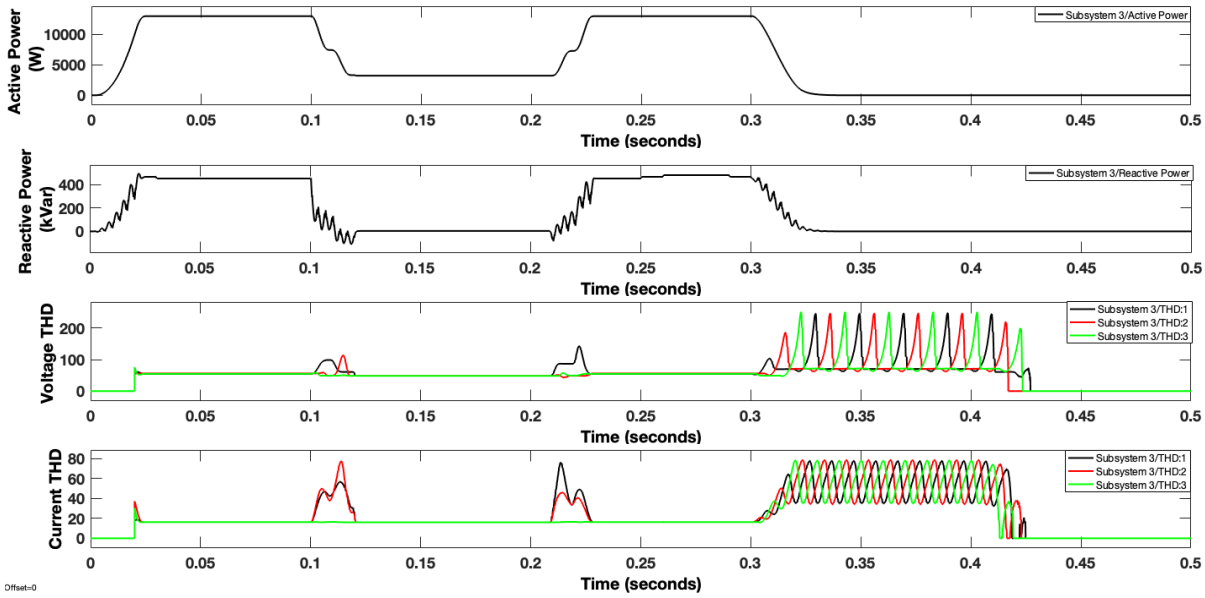

Figure 4.30: Waveforms for active power, reactive power, voltage THD and current THD under LL fault

LLG fault: Due to double line to ground fault the voltage and current become zero in the faulted section while increase in the remaining phase for maintaining a balance. Power factor become 0.8 because of the applied active and reactive power of the nonlinear load. All the parameters become zero due to unavailability of any source except frequency and power factor which can be seen in Figures 4.31 and 4.32.

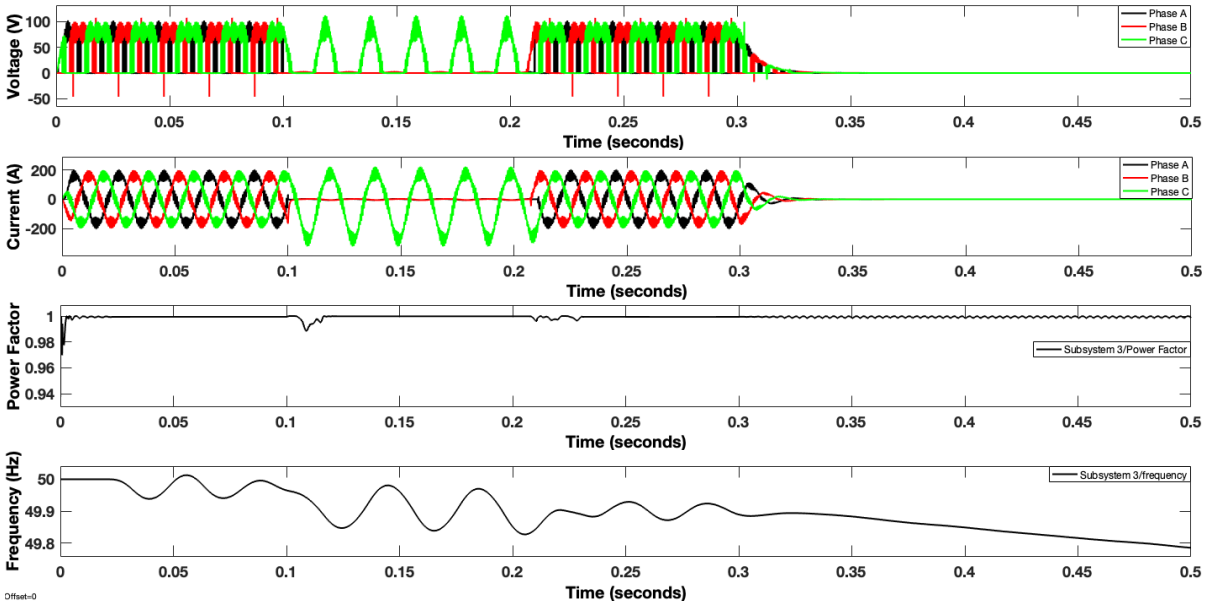

Figure 4.31: Waveforms for voltage, current, power factor and frequency under LLG Fault

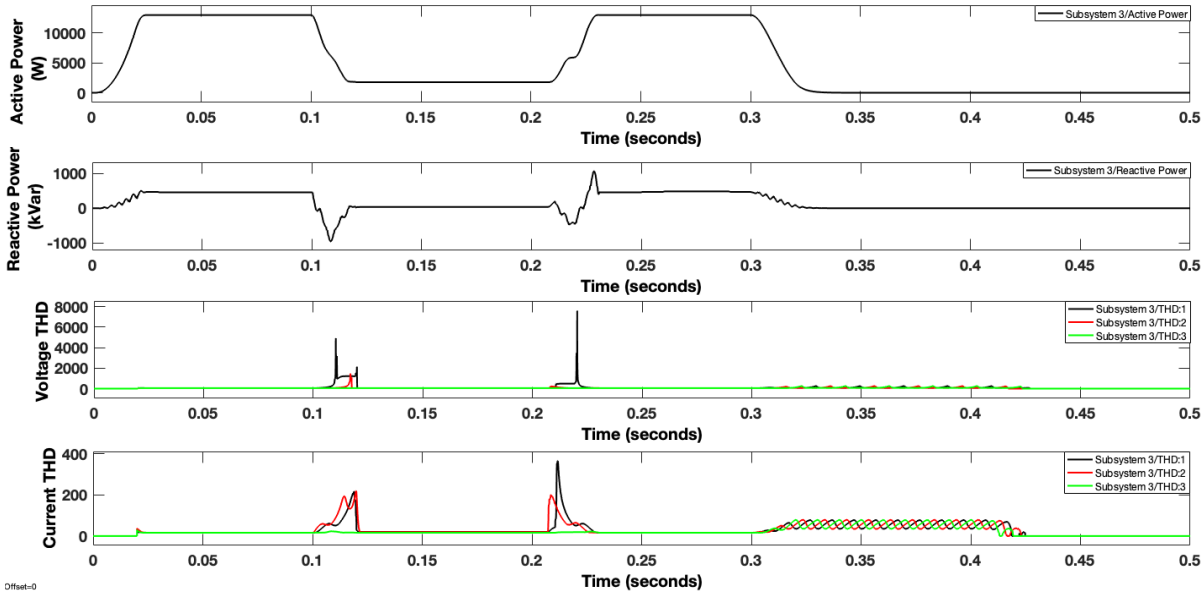

Figure 4.32: Waveforms for active power, reactive power, voltage THD and current THD under LLG fault

ISOLATED MODE WITH BES SYSTEM

Under Normal conditions: In these conditions, all the eight parameters which are considered in these studies of power quality are analyzed. There are two stages of providing irradiances to the PV array. The first case is at STC i.e., irradiances at 1000 W/m^2 and temperature at 25˚ C. Second case is when there is no availability of source. This case is attained by making irradiance zero. At 0.3 s irradiance is made zero so are the results as shown in Figures 4.33 and 4.34. The power factor is unity because of the resistive load in the rectifier acting as a nonlinear load.

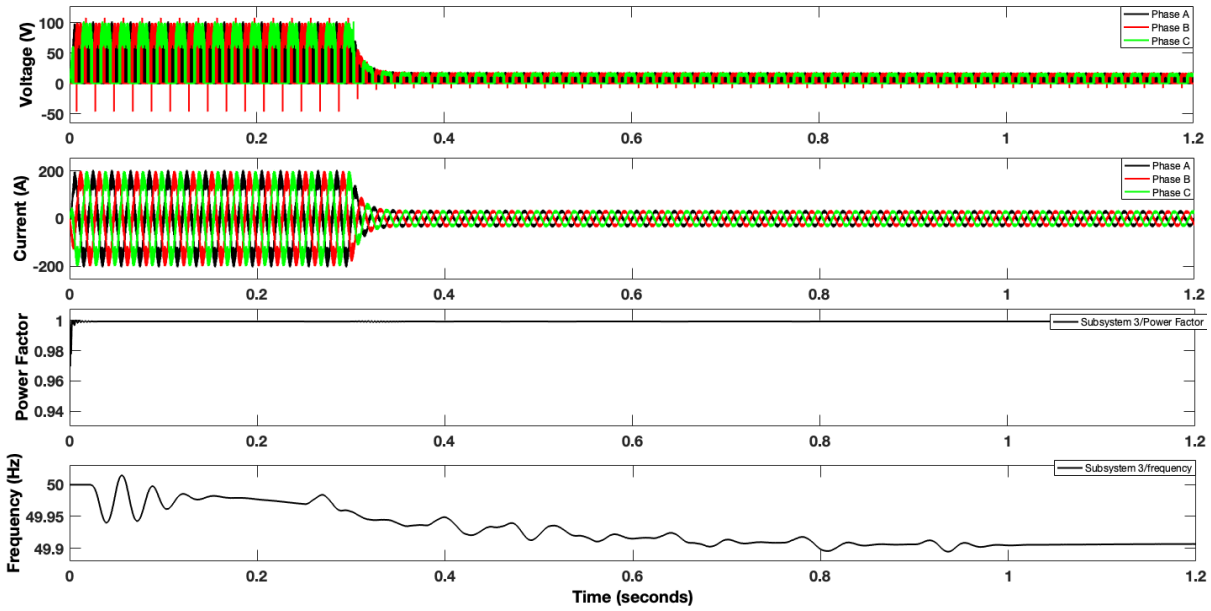

Figure 4.33: Waveforms for voltage, current, power factor and frequency under normal conditions

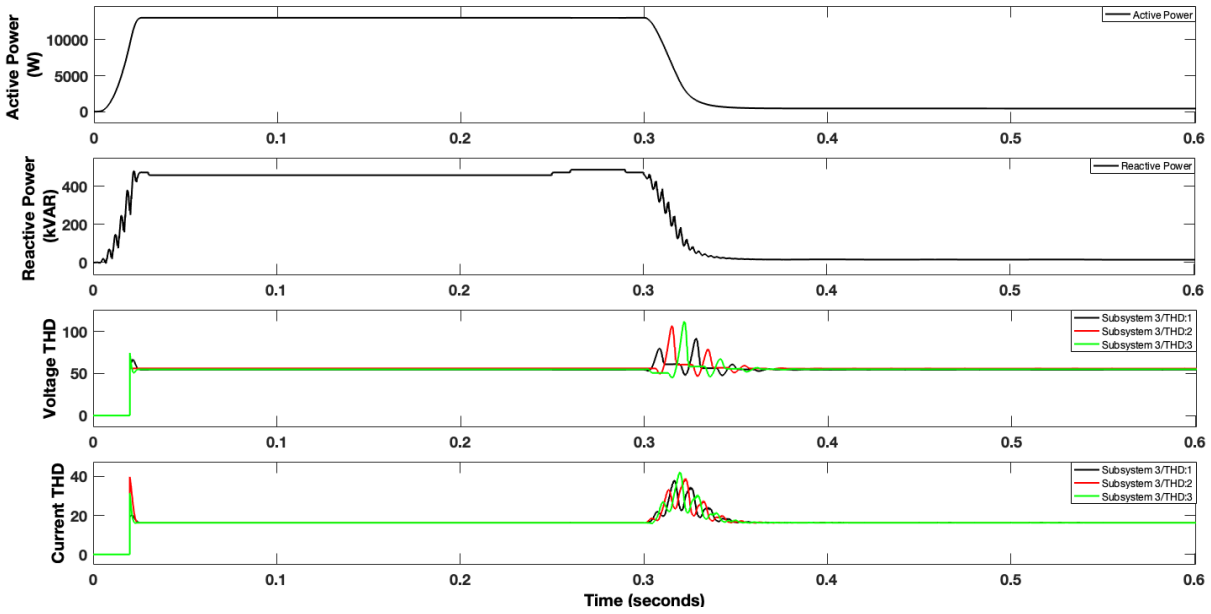

Figure 4.34: Waveforms for active power, reactive power, voltage THD and current THD under normal conditions

LG Fault: The switching time for the fault is from 0.1s to 0.2s. The phase to ground fault occur at the mid of the distribution line due to which the voltage and current become zero in one of the faults and increase in the rest of two phases. Active and reactive power decrease due to fault incidence as shown in Figure 4.35. The high spikes occur in the voltage and current THD due to fault occurrence as shown in Figure 4.36. After unavailability of source, no parameter decreases to zero due to battery system.

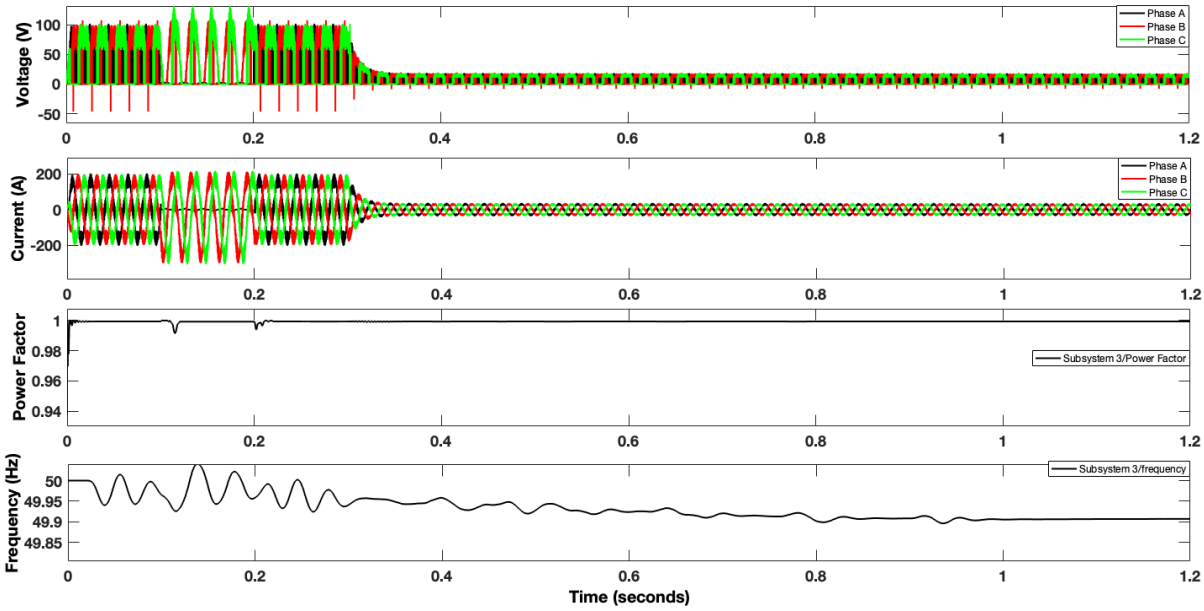

Figure 4.35: Waveforms for voltage, current, power factor and frequency under LG Fault

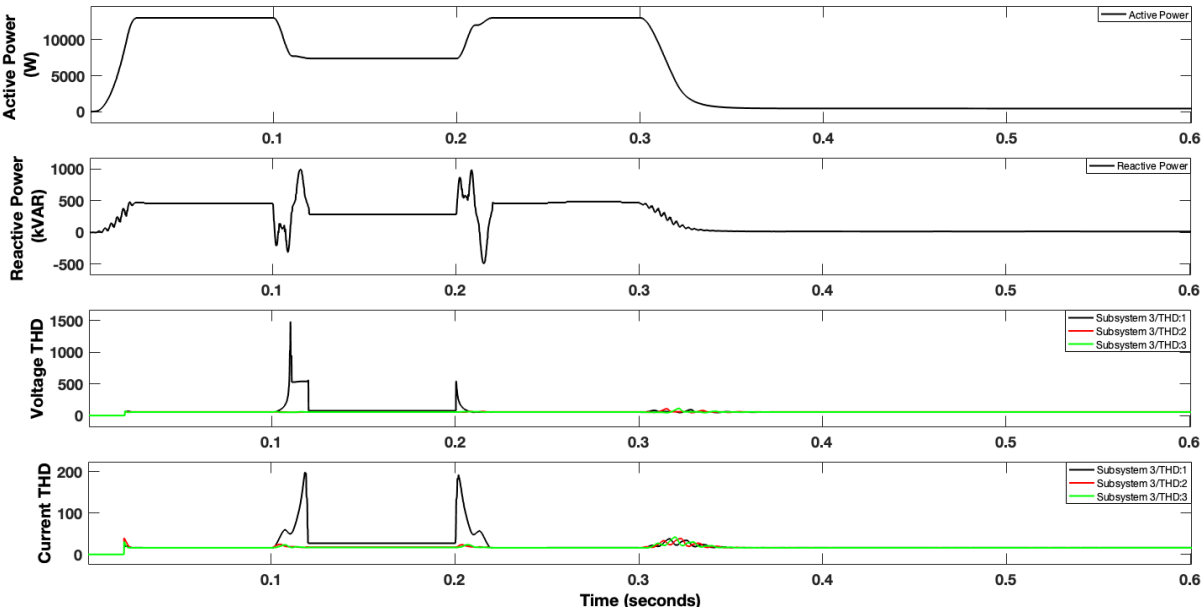

Figure 4.36: Waveforms for active power, reactive power, voltage THD and current THD under LG fault

LL Fault: During line-to-line fault, voltage, and current decrease instead of becoming zero at 0.1 s and 0.2 s. When there is unavailability of PV source i.e., irradiance becomes zero at 0.3 s, all the power quality parameters are supported by BES which helps in keeping system working as shown in Figures 4.37 and 4.38.

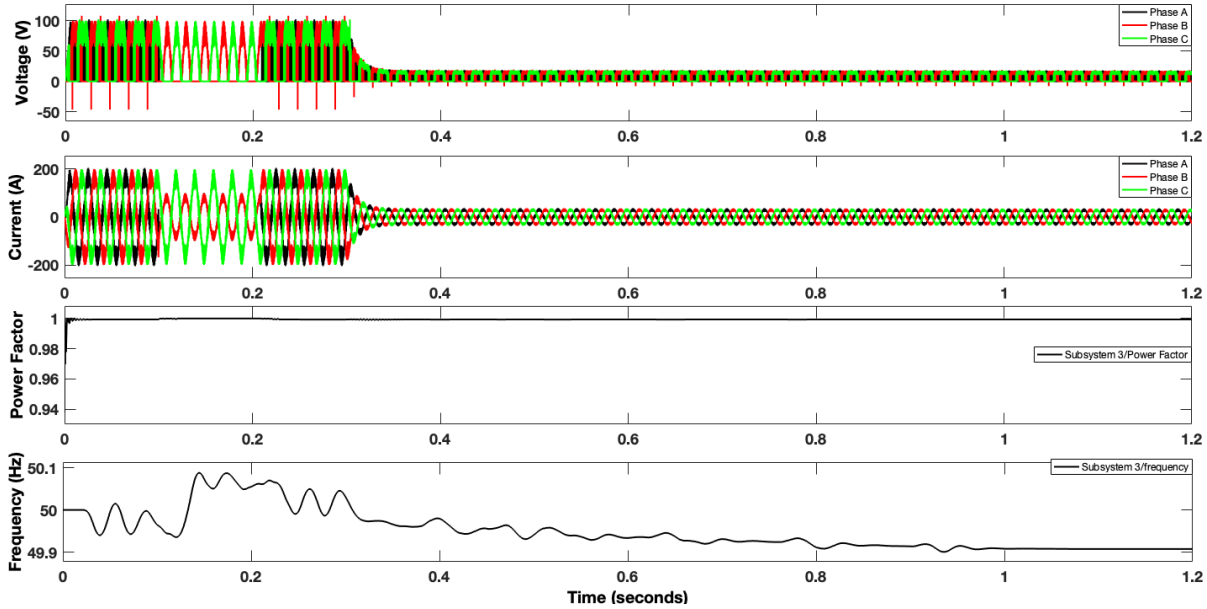

Figure 4.37: Waveforms for voltage, current, power factor and frequency under LL Fault

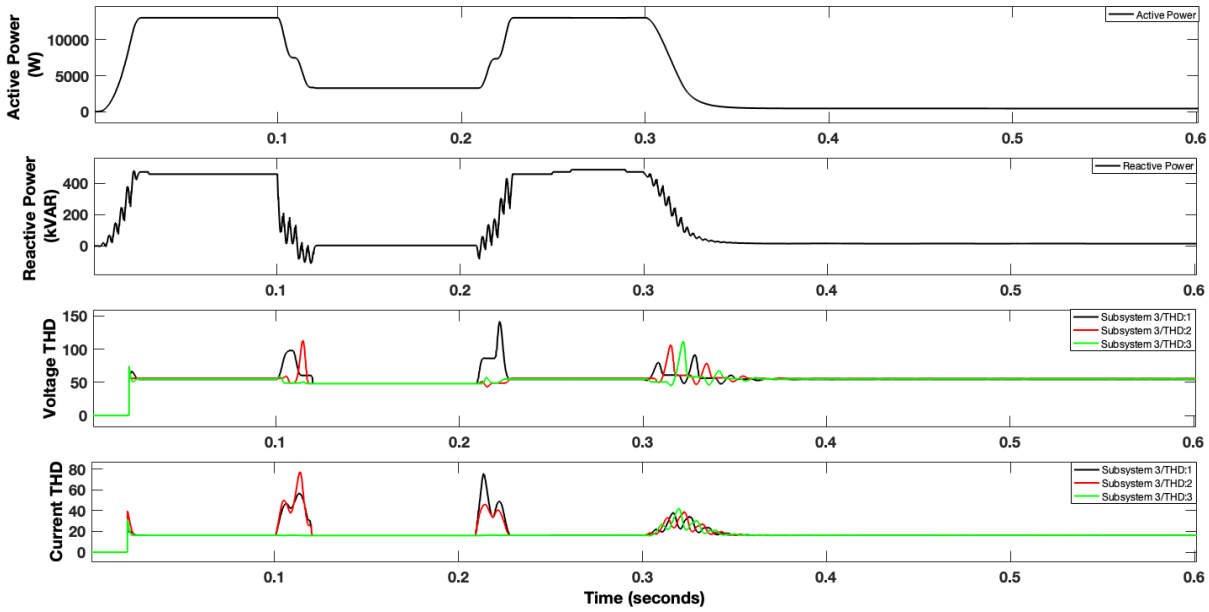

Figure 4.38: Waveforms for active power, reactive power, voltage THD and current THD under LL fault

LLG fault: Due to double line to ground fault the voltage and current become zero in the faulted section while increase in the remaining phase for maintaining a balance. Power factor become 0.8 because of the applied active and reactive power of the parallel RL load. All the parameters have some values because of the battery system which can be seen in Figures 4.39 and 4.40.

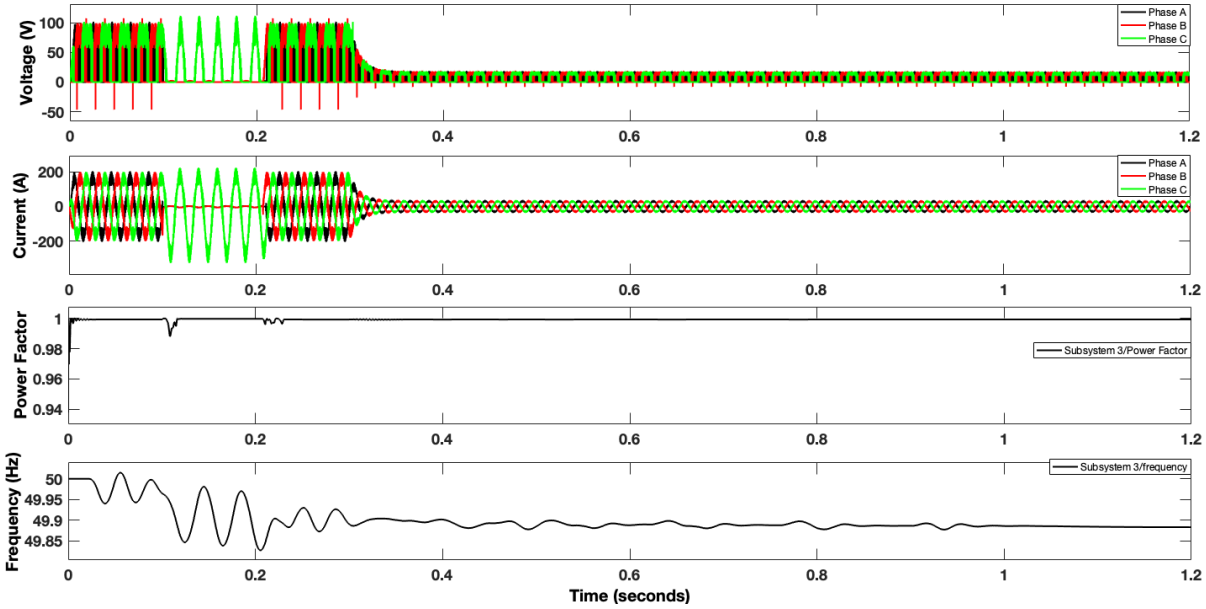

Figure 4.39: Waveforms for voltage, current, power factor and frequency under LLG Fault

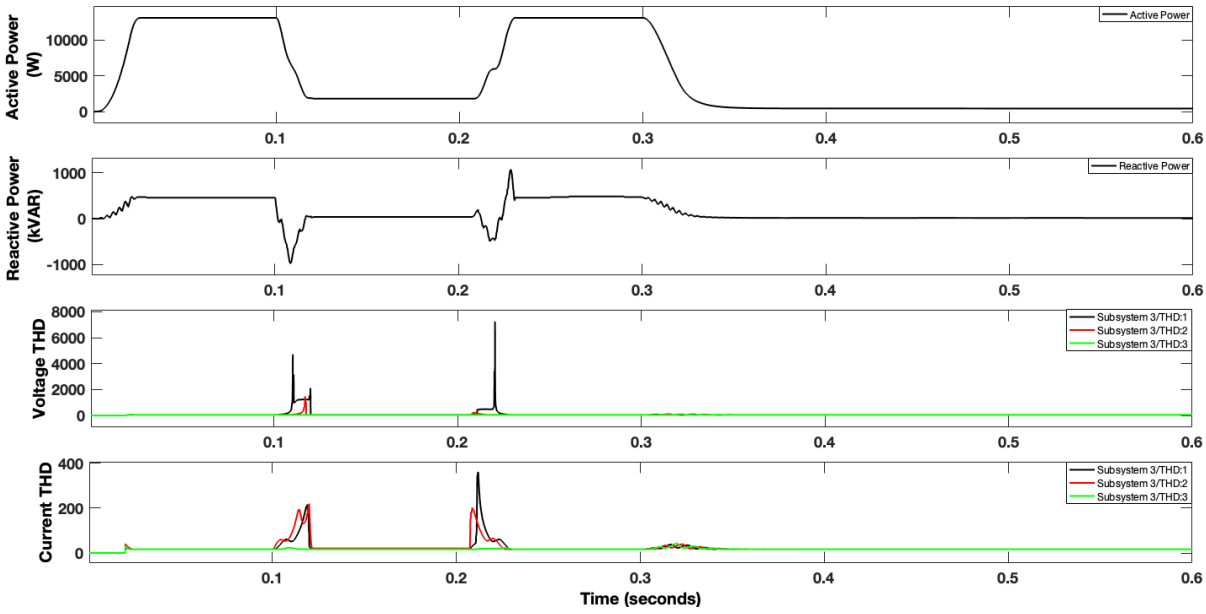

Figure 4.40: Waveforms for active power, reactive power, voltage THD and current THD under LLG fault

GRID CONNECTED SYSTEM

Under Normal conditions: In these conditions all the eight parameters which are considered in these studies of power quality are analyzed. There are two stages of providing irradiances to the PV array. First case is at STC i.e., irradiances at 1000 W/m^2 and temperature at 25° C. Second case is when there is no availability of source. This case is attained by making irradiance zero. At 0.3 s irradiance is made zero so are results as shown in Figures 4.41 and 4.42.

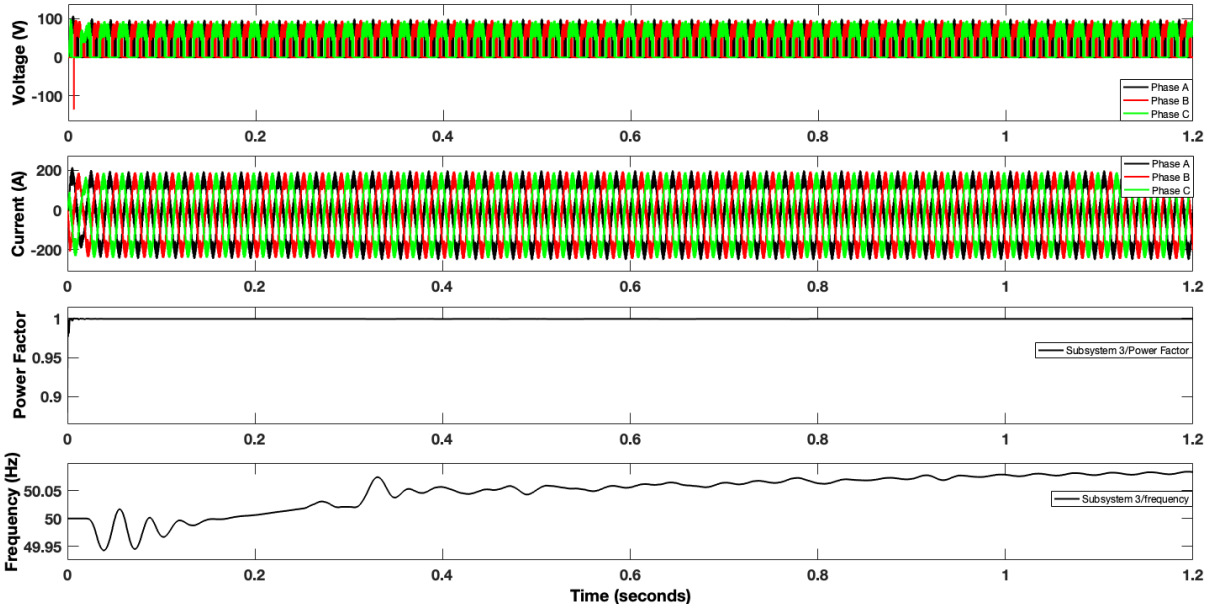

Figure 4.41: Waveforms for voltage, current, power factor and frequency under normal conditions

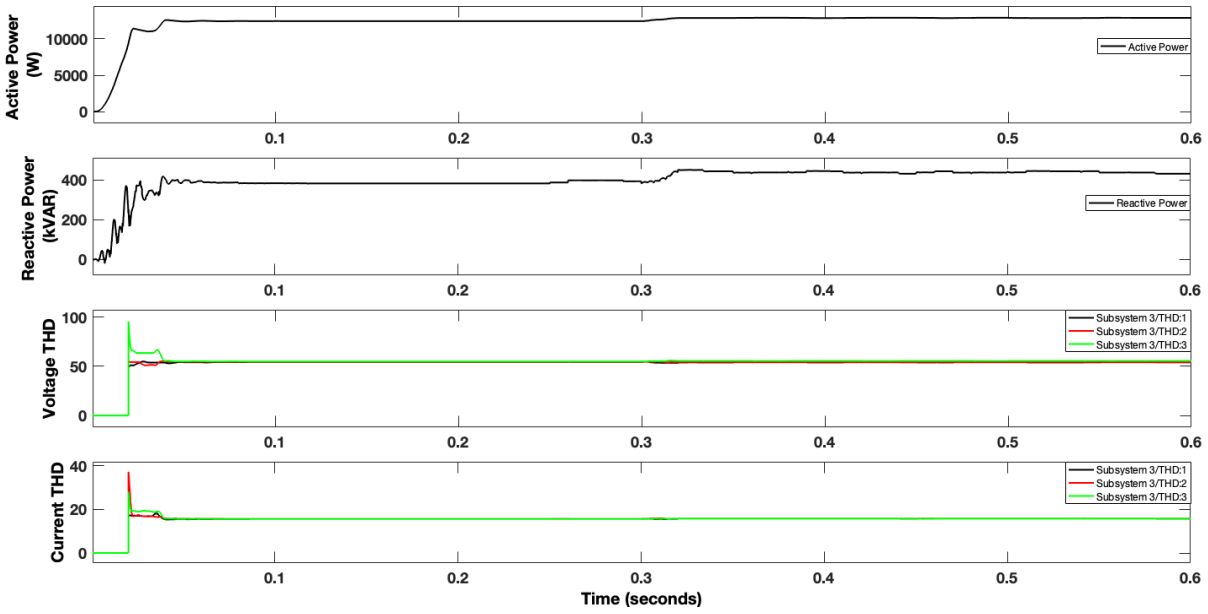

Figure 4.42: Waveforms for active power, reactive power, voltage THD and current THD under normal conditions

LG Fault: The switching time for the fault is from 0.1s to 0.2s. The phase to ground fault occur at the mid of the distribution line due to which the voltage and current become zero in one of the faults and increase in the rest of two phases. Active and reactive power decrease due to fault incidence. The high spikes occur in the voltage and current THD due to fault occurrence. After unavailability of source, no parameter decreases to zero due to battery system as shown in Figures 4.43 and 4.44.

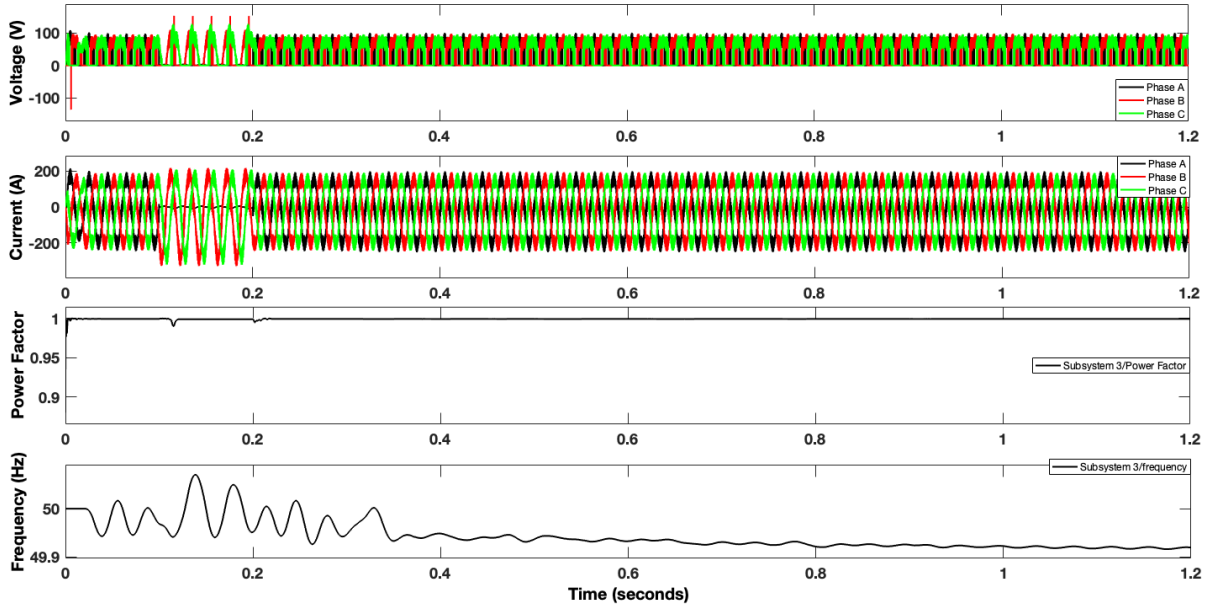

Figure 4.43: Waveforms for voltage, current, power factor and frequency under LG Fault

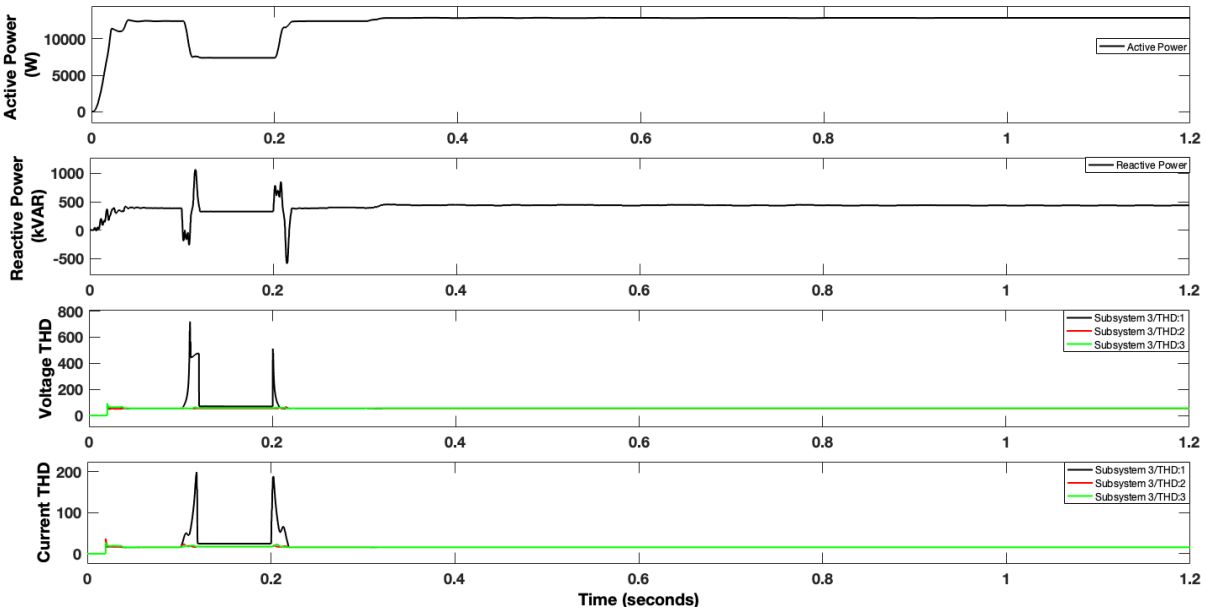

Figure 4.44: Waveforms for active power, reactive power, voltage THD and current THD under LG fault

LL Fault: During line-to-line fault voltage and current decrease instead of becoming zero at 0.1 s and 0.2 s. When there is unavailability of PV source i.e., irradiance becomes zero at 0.3 s, all the power quality parameters are supported by BES which helps in keeping system working which can be seen in Figures 4.45 and 4.46.

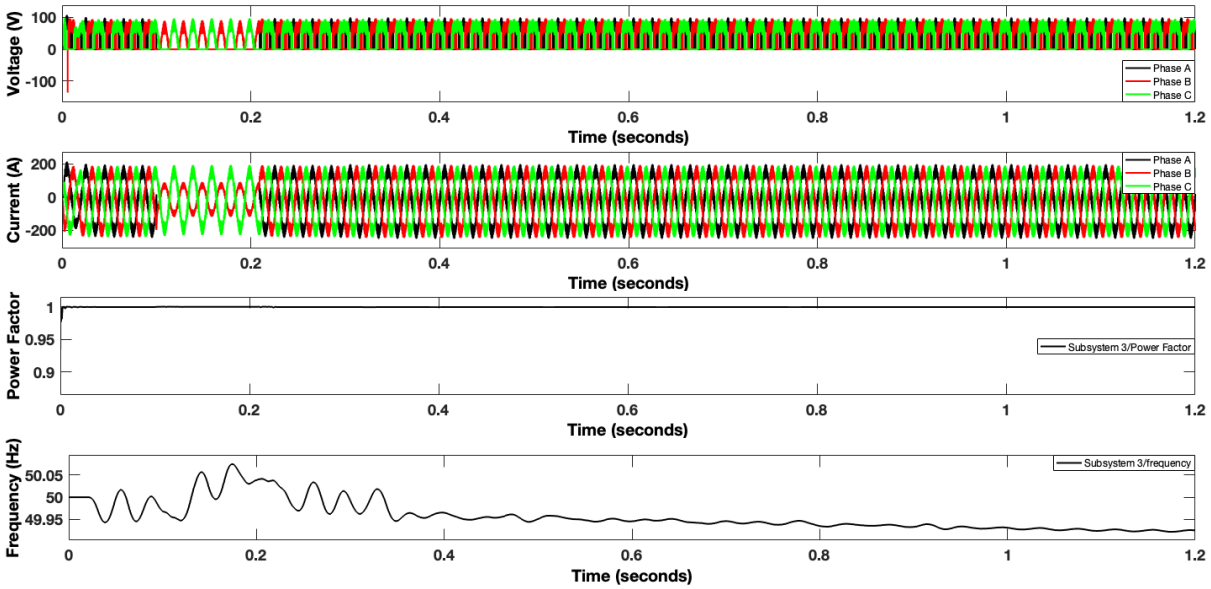

Figure 4.45: Waveforms for voltage, current, power factor and frequency under LL Fault

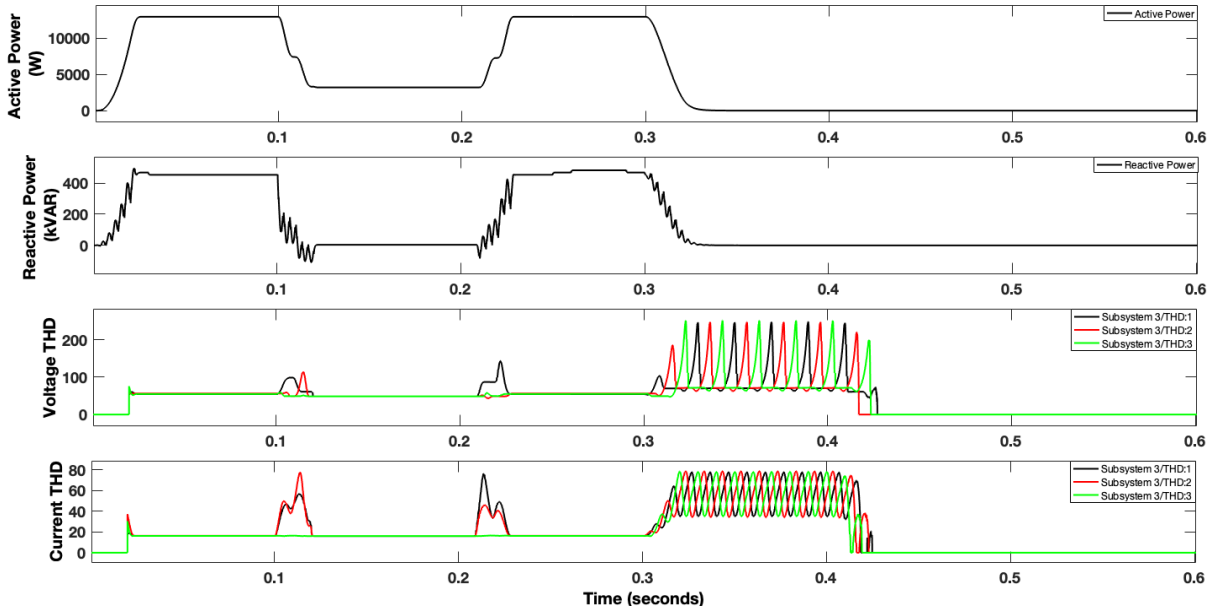

Figure 4.46: Waveforms for active power, reactive power, voltage THD and current THD under LL fault

LLG fault: Due to double line to ground fault the voltage and current become zero in the faulted section while increase in the remaining phase for maintaining a balance in Figure 4.47. There are small disturbances in power factor during the fault conditions. The power and THD waveforms can be seen in Figure 4.48

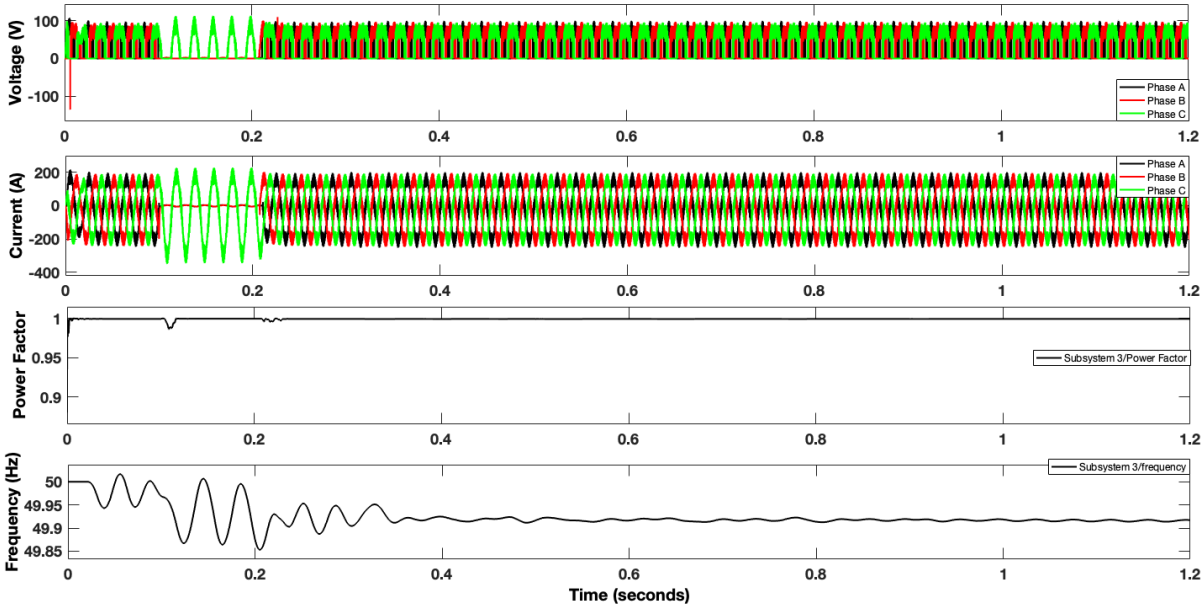

Figure 4.47: Waveforms for voltage, current, power factor and frequency under LLG Fault

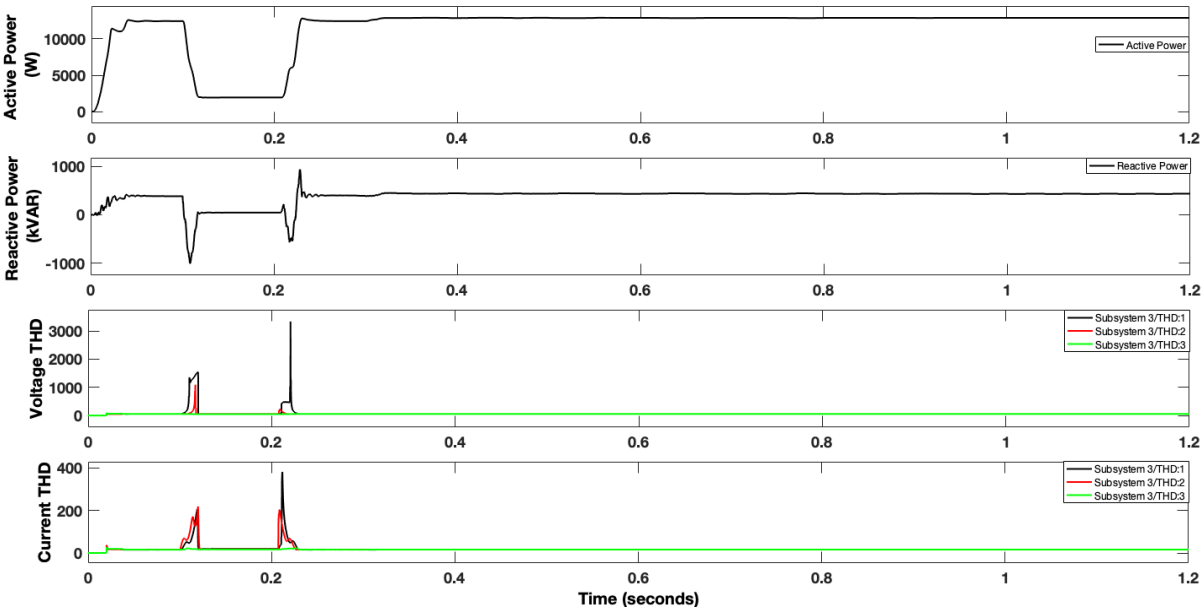

Figure 4.48: Waveforms for active power, reactive power, voltage THD and current THD under LLG fault

Table 4.2 Comparison between the modes of operation under different types of faults for RL load

Types of faults	**Parameters**	**Mode of operation**		
		Isolated mode without BES	**Isolated mode with BES**	**Grid-connected mode**
Normal condition	Voltage	Decreases to 0 after disconnection of PV	Decrease in amplitude after disconnection of PV	Stable

	Current	Decreases to 0 after disconnection of PV	Decrease in amplitude after disconnection of PV	Stable
	Power factor	0.8	0.8	0.8
	Frequency	Moderate variation	Moderate variation	Moderate variation
	Voltage THD	High (≥ 5% limit)	High (≥ 5% limit)	High (≥ 5% limit)
	Current THD	Medium (≥ 5% limit)	Medium (≥ 5% limit)	Medium (≥ 5% limit)
LG fault	Voltage	Decreases to 0 after disconnection of PV	Decrease in amplitude after disconnection of PV	Disturbed during fault period
	Current	Decreases to 0 after disconnection of PV	Decrease in amplitude after disconnection of PV	Disturbed during fault period
	Power factor	0.8	0.8	0.8
	Frequency	Moderate variation	Moderate variation	Moderate variation
	Voltage THD	Extremely high (≥ 5% limit)	Extremely high (≥ 5% limit)	Extremely high (≥ 5% limit)
	Current THD	Very high (≥ 5% limit)	Very high (≥ 5% limit)	Very high (≥ 5% limit)
LL fault	Voltage	Decreases to 0 after disconnection of PV	Decrease in amplitude after disconnection of PV	Disturbed during fault period
	Current	Decreases to 0 after disconnection of PV	Decrease in amplitude after disconnection of PV	Disturbed during fault period
	Power factor	0.8	0.8	0.8
	Frequency	Moderate variation	Moderate variation	Moderate variation
	Voltage THD	Very high(≥ 5% limit)	Very high (≥ 5% limit)	Very high (≥ 5% limit)
	Current THD	High(≥ 5% limit)	High (≥ 5% limit)	High (≥ 5% limit)
LLG fault	Voltage	Decreases to 0 after disconnection of PV	Decrease in amplitude after	High disturbances during fault period

			disconnection of PV	
	Current	Decreases to 0 after disconnection of PV	Decrease in amplitude after disconnection of PV	High disturbances during fault period
	Power factor	0.8	0.8	0.8
	Frequency	Moderate variation	Moderate variation	Moderate variation
	Voltage THD	Extremely high (≥ 5% limit)	Extremely high (≥ 5% limit)	Extremely high (≥ 5% limit)
	Current THD	Extremely high (≥ 5% limit)	Extremely high (≥ 5% limit)	Extremely high (≥ 5% limit)

Table 4.3 Comparison between the modes of operation under different types of faults for Non linear load

Types of faults	**Parameters**	**Mode of operation**		
		Isolated mode without BES	**Isolated mode with BES**	**Grid-connected mode**
Normal condition	Voltage	Decreases to 0 after disconnection of PV	Decrease in amplitude after disconnection of PV	Stable
	Current	Decreases to 0 after disconnection of PV	Decrease in amplitude after disconnection of PV	Stable
	Power factor	Unity (no change in profile)	Unity (no change in profile)	Unity (no change in profile)
	Frequency	Moderate variation	Moderate variation	Moderate variation
	Voltage THD	High (≥ 5% limit)	High (≥ 5% limit)	High (≥ 5% limit)
	Current THD	Medium (≥ 5% limit)	Medium (≥ 5% limit)	Medium (≥ 5% limit)
LG fault	Voltage	Decreases to 0 after disconnection of PV	Decrease in amplitude after disconnection of PV	Disturbed during fault period
	Current	Decreases to 0 after disconnection of PV	Decrease in amplitude after disconnection of PV	Disturbed during fault period

	Power factor	Unity (no change in profile)	Unity (no change in profile)	Unity (no change in profile)
	Frequency	Moderate variation	Moderate variation	Moderate variation
	Voltage THD	Extremely high (≥ 5% limit)	Extremely high (≥ 5% limit)	Extremely high (≥ 5% limit)
	Current THD	Very high (≥ 5% limit)	Very high (≥ 5% limit)	Very high (≥ 5% limit)
LL fault	Voltage	Decreases to 0 after disconnection of PV	Decrease in amplitude after disconnection of PV	Disturbed during fault period
	Current	Decreases to 0 after disconnection of PV	Decrease in amplitude after disconnection of PV	Disturbed during fault period
	Power factor	Unity (no change in profile)	Unity (no change in profile)	Unity (no change in profile)
	Frequency	Moderate variation	Moderate variation	Moderate variation
	Voltage THD	Very high (≥ 5% limit)	Very high (≥ 5% limit)	Very high (≥ 5% limit)
	Current THD	High (≥ 5% limit)	High (≥ 5% limit)	High (≥ 5% limit)
LLG fault	Voltage	Decreases to 0 after disconnection of PV	Decrease in amplitude after disconnection of PV	High disturbances during fault period
	Current	Decreases to 0 after disconnection of PV	Decrease in amplitude after disconnection of PV	High disturbances during fault period
	Power factor	Unity (no change in profile)	Unity (no change in profile)	Unity (no change in profile)
	Frequency	Moderate variation	Moderate variation	Moderate variation
	Voltage THD	Extremely high (≥ 5% limit)	Extremely high (≥ 5% limit)	Extremely high (≥ 5% limit)
	Current THD	Extremely high (≥ 5% limit)	Extremely high (≥ 5% limit)	Extremely high (≥ 5% limit)

4.2 LIGHTNING STRIKE/ HIGH IMPULSE VOLTAGE

The simulation results with lightning strike/ impulse fault with different waveforms are discussed as follows. The complete layout for discussing the results further in this subsection are mentioned in the Table 4.4.

Table 4.4 Microgrid operation under different waveforms with parameters to be calculated

Type of waveform	Parameters to be analyzed	
	Voltage and current impulse waveforms	Voltage and current THD
Standard	1.2/50 µs	1.2/50 µs
Non-standard	1.2/4 µs	1.2/4 µs
Non-standard	1.2/10 µs	1.2/10 µs
Non-standard	3/10 µs	3/10 µs
Non-standard	7.5/30 µs	7.5/30 µs

4.2.1 1.2/50 µs WAVEFORM

Voltage and Current waveforms: The 1.2/50 µs waveform is a standard impulse waveform according to IEEE C62-41.2 2002 and IEEE 1159.1 2009 standards. The impulse fault is provided at 0.15 s. As shown in the Figure 4.49, there is a sudden rise in the voltage and current waveforms. The waveforms come to their original position after a few milliseconds.

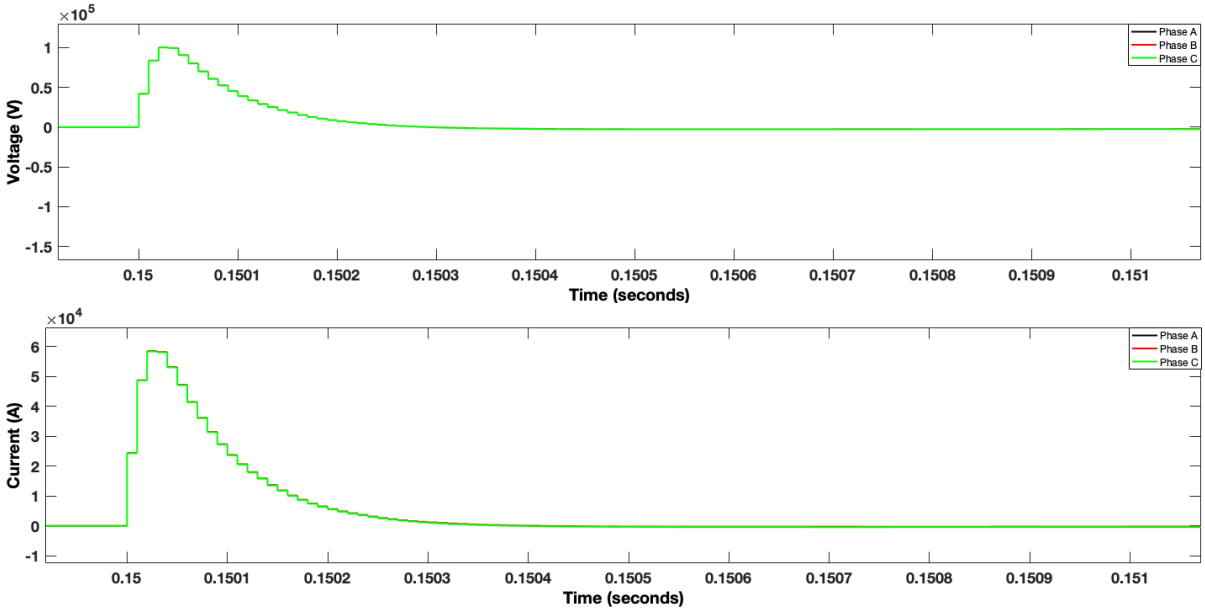

Figure 4.49: Voltage and current impulse waveforms

Voltage and Current THD waveforms: The THD values rise to a few hundred suddenly because of impulsive fault at 0.15 s. The THD comes to its original position after 0.02 s as in Figure 4.50.

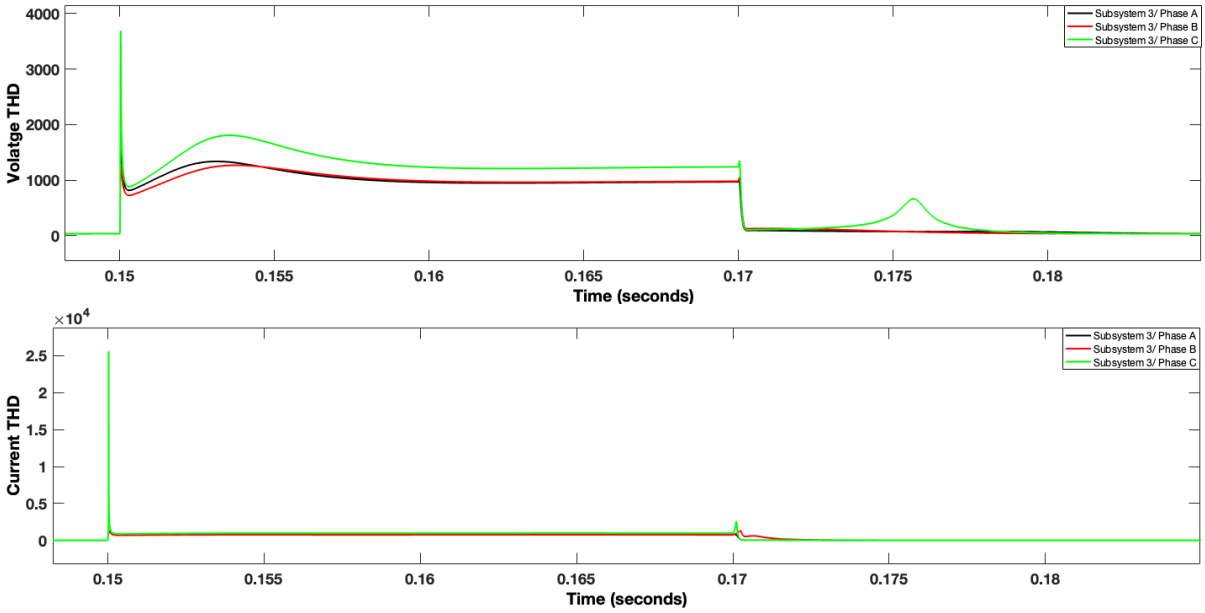

Figure 4.50: Voltage and current THD waveforms

4.2.2 1.2/4 µs WAVEFORM

Voltage and Current waveforms: The impulse fault is provided at 0.15 s. As shown in the Figure 4.51, there is a sudden rise in the voltage and current waveforms. The waveforms come to their original position after a few milliseconds.

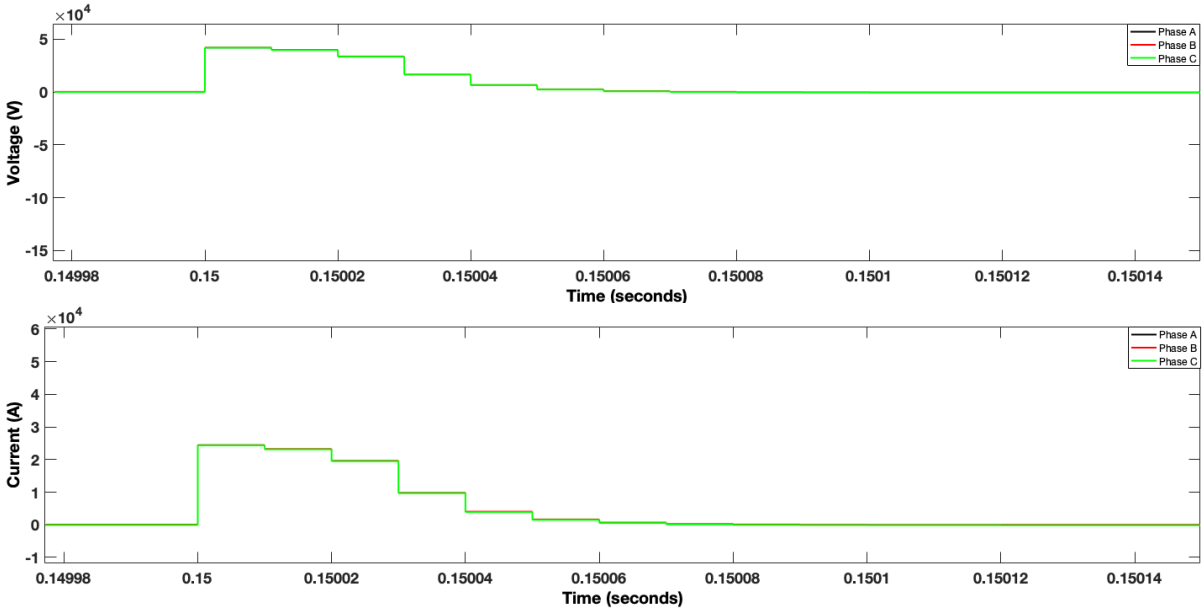

Figure 4.51: Voltage and current impulse waveforms

Voltage and Current THD waveforms: The THD values rise to a few hundred suddenly because of impulsive fault at 0.15 s. The THD comes to its original position after 0.02 s as in Figure 4.52.

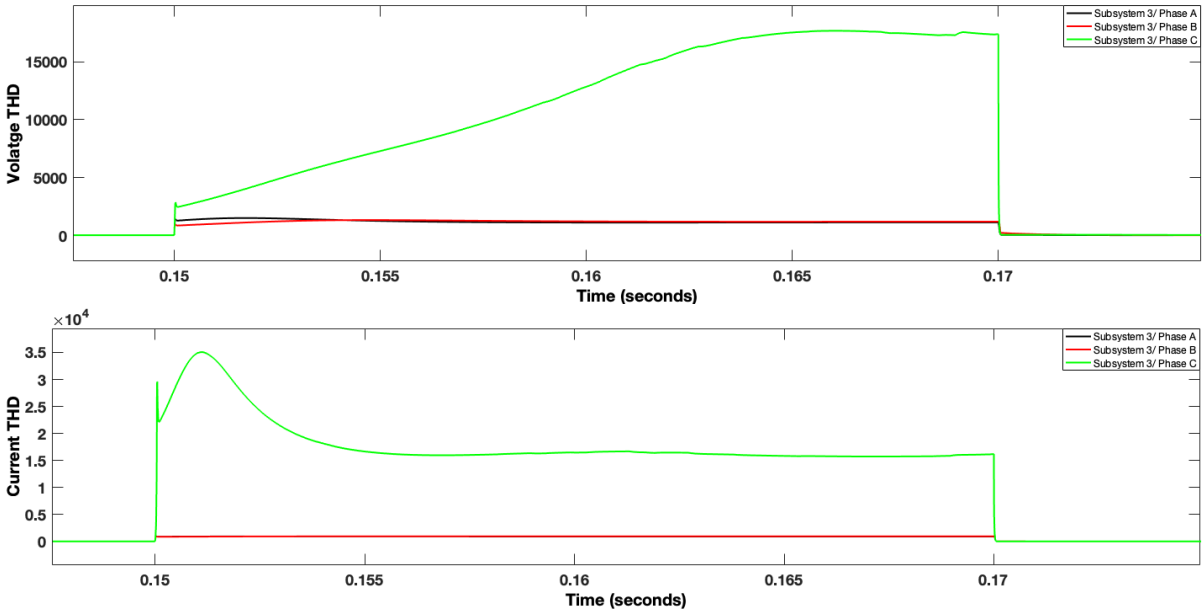

Figure 4.52: Voltage and current THD waveforms

4.2.3 1.2/10 µs WAVEFORM

Voltage and Current waveforms: The impulse fault is provided at 0.15 s. As shown in the Figure 4.53. there is a sudden rise in the voltage and current waveforms. The waveforms come to their original position after a few milliseconds.

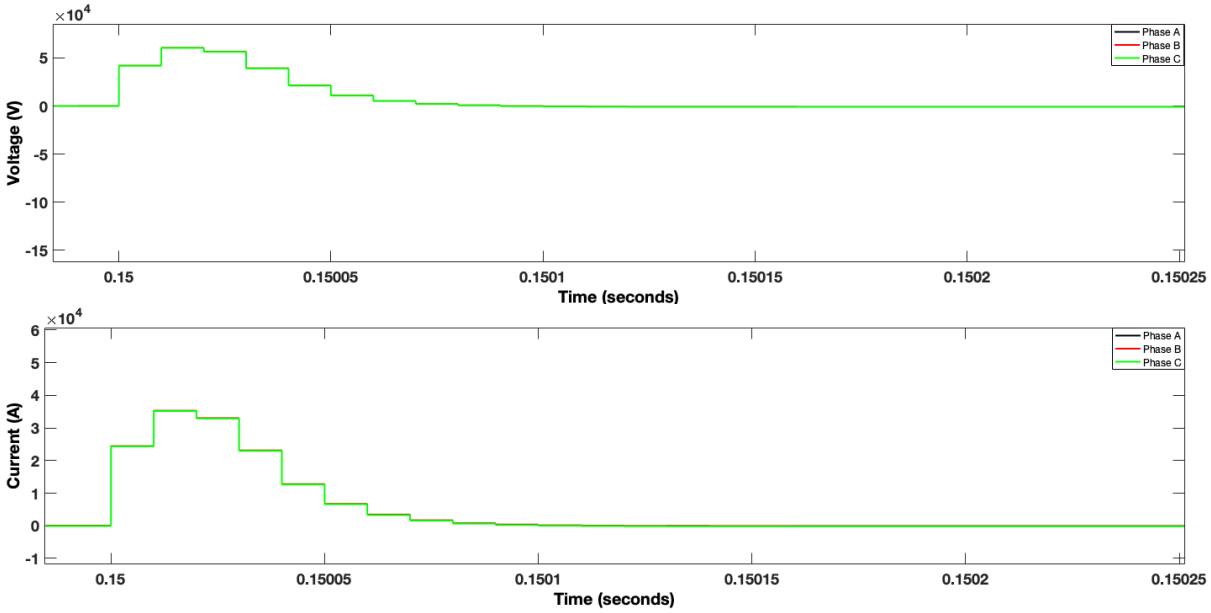

Figure 4.53: Voltage and current impulse waveforms

Voltage and Current THD waveforms: The THD values rise to a few hundred suddenly because of impulsive fault at 0.15 s. The THD comes to its original position after 0.02 s as in Figure 4.54. Due to lightning strike, there is large increase in one of the phases as compared to another two phases.

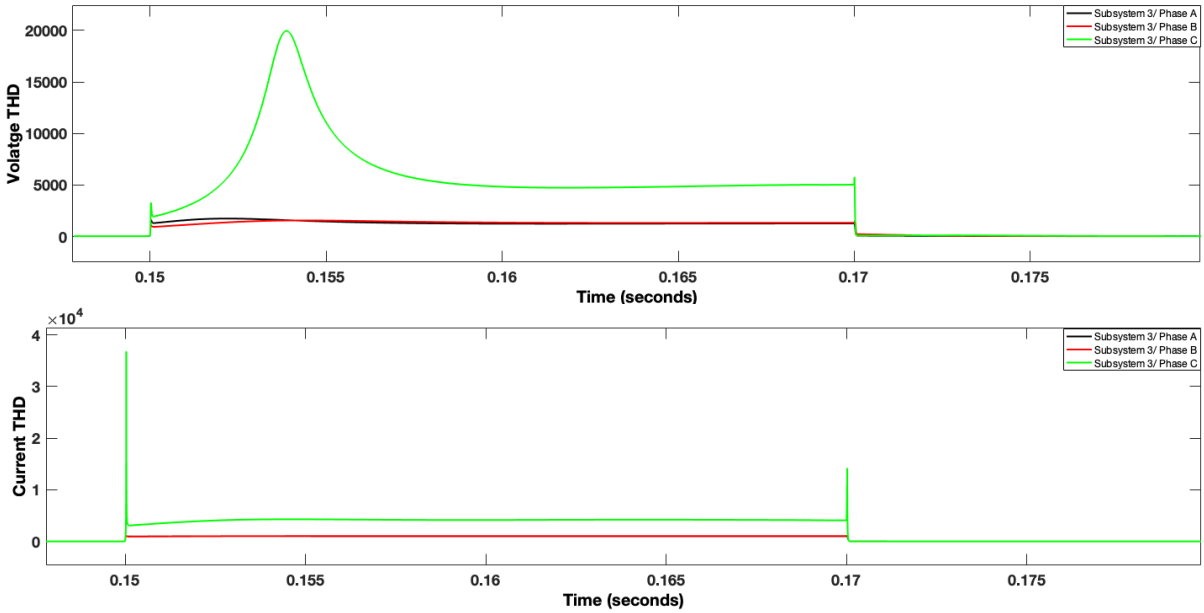

Figure 4.54: Voltage and current THD waveforms

4.2.4 3/10 µs WAVEFORM

Voltage and Current waveforms: The impulse fault is provided at 0.15 s. As shown in the Figure 4.55. there is a sudden rise in the voltage and current waveforms. The waveforms come to their original position after a few milliseconds.

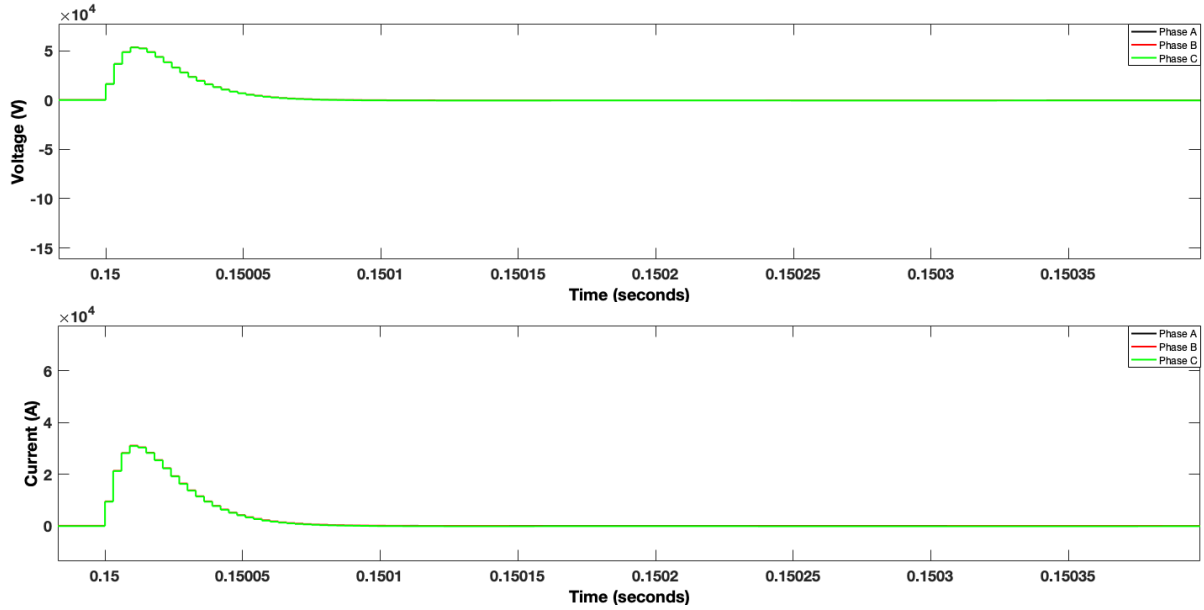

Figure 4.55: Voltage and current impulse waveforms

Voltage and Current THD waveforms: The THD values rise to a few hundred suddenly because of impulsive fault at 0.15 s. The THD comes to its original position after 0.02 s as in Figure 4.56. The voltage THD slowly rises to the value 3×10^4 and suddenly drops at 0.17 s.

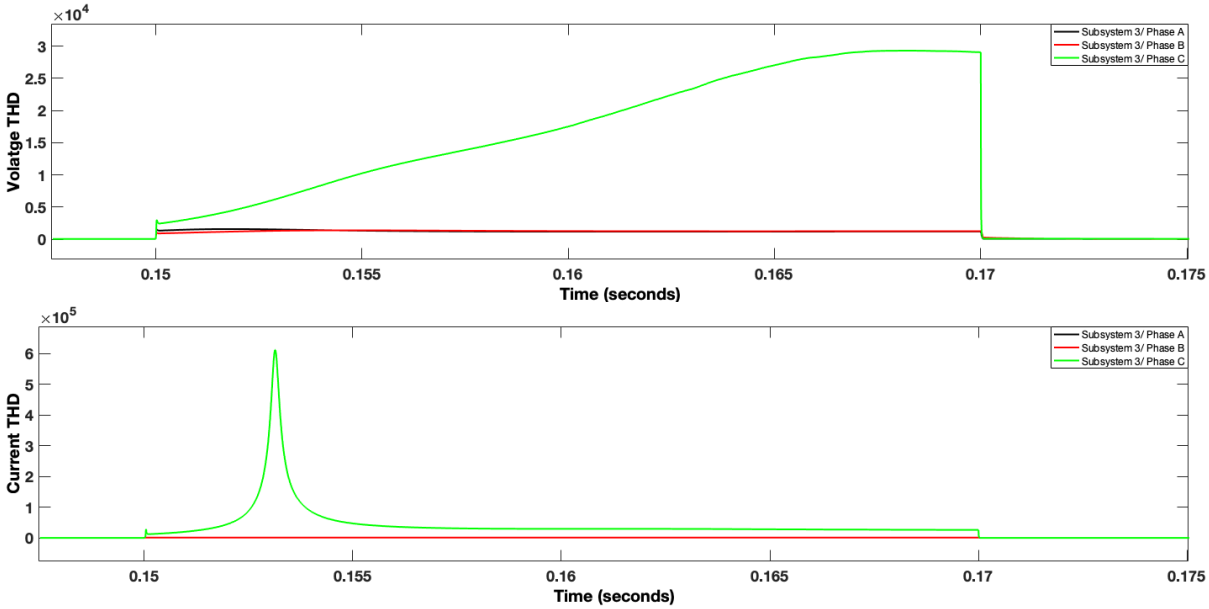

Figure 4.56: Voltage and current THD waveforms

4.2.5 7.5/30 µs WAVEFORM

Voltage and Current waveforms: The impulse fault is provided at 0.15 s. As shown in the Figure 4.57. there is a sudden rise in the voltage and current waveforms. The waveforms come to their original position after a few milliseconds.

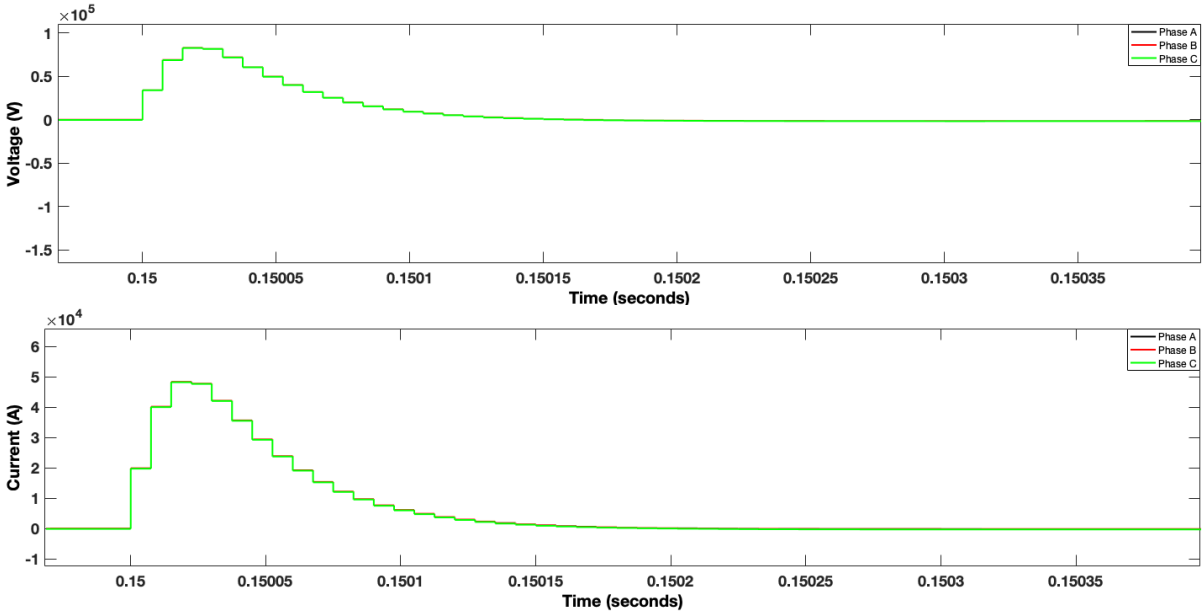

Figure 4.57: Voltage and current impulse waveforms

Voltage and Current THD waveforms: The THD values rise to a few hundred suddenly because of impulsive fault at 0.15 s. The THD comes to its original position after 0.02 s as in Figure 4.58.

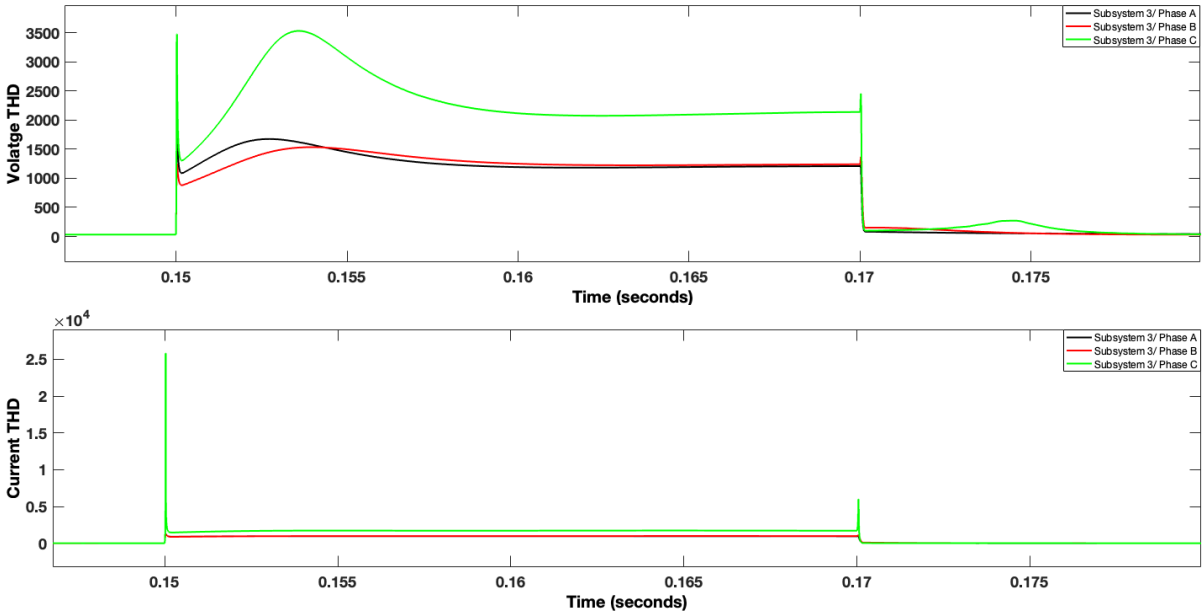

Figure 4.58: Voltage and current THD waveforms

In this chapter, results are analyzed under different fault conditions to fulfill the objectives of the thesis. Due to incidence of faults, transients are created which are temporary and is cleared after fault clearance.

Chapter 5

CONCLUSIONS AND FUTURE SCOPE

The conclusions of the dissertation and future work have been discussed in this chapter.

5.1 CONCLUSIONS

The primary goal of this work is to analyze the reaction of power quality parameters seen under various faults, including L-G, L-L, L-L-G, and impulsive faults with various load situations for the safety of equipment, system dependability, and supply of power to customers or end users. The work on the dissertation was completed in the MATLAB/Simulink software environment. As the interruptions result in equipment damage and poor system performance, the power quality of the supply directly affects electrical systems and equipment. Using the analysis findings from the study as a model, a practical and independent low voltage distribution microgrid power system with improved PQ conditions may be developed. To maintain peak performance, power quality tests should be carried out often on all projects, but especially on those with extremely sensitive machinery.

5.2 FUTURE SCOPE

At the end of the study, some areas can be extended for further studies. These areas are as follows:

- As additional work, the battery backup can be given a control system to manage battery switching in accordance with load needs.
- Another distributed energy supply, such as a wind energy system, might be added.
- The effect of lightning impulse voltage would be analyzed in terms of reflected and refracted coefficients for the existing low voltage microgrid.
- The present scheme will be extended for its verification using OPAL-RT real time simulator.
- The power quality related parameters of the proposed scheme would be controlled and maintained within the allowable limits (as per IEEE/IEC standards) in near future.
- Increased dependability and equipment life can be achieved by researching and implementing various types of relays for power system protection.
- IGBT inverters with two levels can be upgraded to three levels for further benefits and lower THD levels.

REFERENCES

[1] G. Venkataramanan and C. Marnay, "A larger role for microgrids," Power and Energy Magazine, IEEE, Vol. 6, pp. 78-82, 2008.

[2] X. Xufeng, J. Mitra, W. Tingting, and M. Longhua, "Evaluation of Operational Reliability of a Microgrid Using a Short-Term Outage Model," Power Systems, IEEE Transactions on, Vol. 29, pp. 2238-2247, 2014.

[3] "IEEE Recommended Practice for Powering and Grounding Electronic Equipment - Redline," *IEEE Std 1100-2005 (Revision of IEEE Std 1100- 1999) - Redline,* pp. 1-703, 2006.

[4] Ghosh and G. Ledwich, "Power Quality Enhancement Using Custom Power Devices": *Kluwer Academic Publishers*, 2002

[5] B W Kennedy, "Power quality primer": *McGraw-Hill Professional, McGraw-Hill,* 2000

[6] "IEEE Recommended Practice for Interconnecting Distributed Resources with Electric Power Systems Distribution Secondary Networks," *IEEE Std 1547.6-2011,* pp. 1-38, 2011.

[7] L. Xu and D. Chen, "Control and operation of a DC microgrid with variable generation and energy storage," Power Delivery, IEEE Transactions on, Vol. 26, no. 4, pp. 2513–2522, 2011.

[8] R. Zahira, P. Sheshathri, and M. S. Shafiullah, "Technical Investigation on Microgrid and Power Quality Impact", International Journal of Scientific & Engineering Research, Vol. 5, no. 4, pp. 183-187, 2014.

[9] N.S. Srivatchan, P. Rangarajan, S. Rajalakshmi, "Control Scheme for Power Quality Improvement in Islanded Microgrid Operation", Procedia Technology, Volume 21,2015.

[10] Vinayagam, A. Aziz, K. S. V. Swarna, S. Khoo, and A. Stojcevski, "Power quality impacts in a typical microgrid," in *Proccedings of the International Conference on Sustainable Energy and Environmental Engineering (SEEE 2015) Power*, pp. 77–82, Bangkok, Thailand, 2015.

[11] Vinayagam A, Swarna K, Khoo S, Stojcevski A (2016) Power quality analysis in microgrid: an experimental approach. J Power Energy Eng 4:17–34.

[12] K. H. Youssef, "Power Quality Constrained Optimal Management of Unbalanced Smart Microgrids During Scheduled Multiple Transitions Between Grid-Connected and

Islanded Modes," in IEEE Transactions on Smart Grid, Vol. 8, no. 1, pp. 457-464, Jan. 2017.

[13] Daniel L. Gerber, Omkar A. Ghatpande, Moazzam Nazir, Willy G. Bernal Heredia, Wei Feng, Richard E. Brown, Energy and Power Quality measurement for electrical distribution in AC and DC microgrid buildings, Applied Energy, Volume 308,2022, 118308, ISSN 0306-2619.

[14] Jamali, S.Z.; Bukhari, S.B.A.; Khan, M.O.; Mehmood, K.K.; Mehdi, M.; Noh, C.-H.; Kim, C.-H. A High-Speed Fault Detection, Identification, and Isolation Method for a Last Mile Radial LVDC Distribution Network. *Energies* 2018, *11*, 2901, https://doi.org/10.3390/en11112901.

[15] M. T. L. Gayatri and A. M. Parimi, "Power Quality Improvement of PV-WECS Microgrid Using Active Power Filter in Realtime," 2018 53rd International Universities Power Engineering Conference (UPEC), Glasgow, 2018, pp. 1-6.

[16] S. Thakar, A. S. Vijay, and S. Doolla, "Effect of P-Q limits on microgrid reconfiguration: A capability curve perspective," *IEEE Trans. Sustain. Energy*, Vol. 11, no. 3, pp. 2040–2048, Jul. 2020.

[17] José Octávio Cesário Pereira Pinto, Miguel Moreto, Protection strategy for fault detection in inverter-dominated low voltage AC microgrid, Electric Power Systems Research, Volume 190, 2021, 106572,ISSN0378-7796, https://doi.org/10.1016/j.epsr.2020.106572.

[18] M.Devika Rani, P.S.Prakash, M.Venu Gopala Rao, "Power Quality Assessment in Grid connected Mode Hybrid-Microgrid with various loads", Vol.99, No. 18, ISSN:1992-8645, Sept 2021.

[19] S. R. Mohapatra and V. Agarwal, "Enhancement of Line-to-Line Voltage Support During Asymmetrical Microgrid Faults Using a Four-Leg Three-Level Inverter," in *IEEE Transactions on Smart Grid*, Vol. 13, no. 2, pp. 1298-1309, March 2022, doi: 10.1109/TSG.2021.3130745.

[20] Gao Xiaozhi, Li Linchuan, Chen Wenyan, Power Quality Improvement for Microgrid in Islanded Mode, Procedia Engineering, Volume 23,2011,Pages 174-179,ISSN 1877-7058.

[21] F.Nejabatkhah, S.Danyali, S.H.Hosseini, M.Sabahi, and S.M.Niapour, ''Modeling and control of a new three-input DC–DC boost converter for hybrid PV/FC/battery power system,'' *IEEE Trans. Power Electron.*, Vol. 27, no. 5, pp. 2309–2324, May 2012.

[22] D. Debnath, and K. Chatterjee, “Two-stage solar Photovoltaic-based stand-alone scheme having battery as energy storage element for rural deployment,” *IEEE Trans*. *Ind. Electron*., Vol. 62, no. 7, pp. 4148–4157, Jul. 2015.

[23] Laaksonen, Hannu & Kauhaniemi, Kimmo. (2009). Voltage and Frequency Control of Low Voltage Microgrid with Converter Based DG Units. International Journal of Integrated Energy Systems. 1.

[24] M. A. Ravaglio et al., "Evaluation of lightning-related faults that lead to distribution network outages: An experimental case study", *Electr. Power Syst. Res*, Vol. 174, no. November 2018, pp. 105848, 2019.

[25] P. Rajamani, D. Dey, B. Chatterjee and S. Chakravorti, "Classification of Impulse Fault Patterns in Transformers Using Wavelet Network," *2008 Joint International Conference on Power System Technology and IEEE Power India Conference*, 2008, pp. 1-6, doi: 10.1109/ICPST.2008.4745287

[26] K. Bhuyan and S. Chatterjee, "Study of effects of standard and non-standard impulse waves on power transformer," *2010 Joint International Conference on Power Electronics, Drives and Energy Systems & 2010 Power India*, 2010, pp. 1-4, doi: 10.1109/PEDES.2010.5712434

[27] Izadi M, Abd Rahman MS, Ab-Kadir MZ, Gomes C, Jasni J, Hajikhani M. “The influence of lightning induced voltage on the distribution power line polymer insulators”. PLoS One. 2017 Feb 24;12(2):e0172118. doi: 10.1371/journal.pone.0172118. PMID: 28234930; PMCID: PMC5325478

[28] Bhuyan, K., Chatterjee, S., Yadav, A., Bansal, S., Paul, S.K. (2015). Simulation and Analysis of Impulse Faults in Power Transformer. In: Gen, M., Kim, K., Huang, X., Hiroshi, Y. (eds) Industrial Engineering, Management Science and Applications 2015. Lecture Notes in Electrical Engineering, vol 349. Springer, Berlin, Heidelberg. https://doi.org/10.1007/978-3-662-47200-2_15

[29] M. J. V. Vazquez, J. M. A. Marquez, and F. S. Manzano, “A methodology for optimizing stand-alone PV-system size using parallel-connected dc/dc converters,” *IEEE Trans. Ind. Electron.*, Vol. 55, no. 7, pp. 2664–2673, Jul. 2008.

[30] R. H. Tan, and V. K. Ramachandaramurthy, "A Comprehensive Modeling and Simulation of Power Quality Disturbances Using MATLAB/SIMULINK", in Power Quality Issues in Distributed Generation. London, United Kingdom: IntechOpen, 2015 [Online]. Available: https://www.intechopen.com/chapters/48982 doi: 10.5772/61209

[31] OkabeS, TakamiJ, TsuboiT, UetaG (2013) Discussion on Standard Waveform in the Lightning Impulse Voltage Test. IEEE Transactions on Dielectrics and Electrical Installation 20: 147-156.

LIST OF PUBLICATIONS

1. Navneet Kaur, Suman Bhullar, Jitender Kaushal, "Effects of various faults on Power quality parameters in an isolated microgrid", in the 2022 3rd International conference on "Intelligent Computing, Instrumentation and Control Technologies (ICICICT 2022)" held at Vimal Jyothi Engineering College, Kannur (Dt,) Kerala on August 11th and 12th 2022, pp. 1401-1408.

- Declared as a **best paper** under session title Electrical System in offline mode at conference held in Vimal Jyothi Engineering College, Kannur, Kerala.

2. Navneet Kaur, Suman Bhullar, Jitender Kaushal, "Evaluation of lightning impulse voltage for grid-connected and isolated microgrid systems", (under preparation).

Navneet Kaur
Roll No- 802042017

Checked & verified.
30.08.2022

PLAGIARISM REPORT

Report

ORIGINALITY REPORT

13%	7%	8%	6%
SIMILARITY INDEX	INTERNET SOURCES	PUBLICATIONS	STUDENT PAPERS

PRIMARY SOURCES

1	www.intechopen.com Internet Source	2%
2	fr.scribd.com Internet Source	1%
3	Submitted to Universiti Teknikal Malaysia Melaka Student Paper	1%
4	Paul M. Anderson, Charles Henville, Rasheek Rifaat, Brian Johnson, Sakis Meliopoulos. "Power System Protection", Wiley, 2022 Publication	1%
5	Soumya Ranjan Mohapatra, Vivek Agarwal. "Enhancement of Line-to-line Voltage Support during Asymmetrical Microgrid Faults using a Four-leg Three-level Inverter", IEEE Transactions on Smart Grid, 2021 Publication	1%
6	Mahdi Izadi, Muhammad Syahmi Abd Rahman, Mohd Zainal Abidin Ab-Kadir, Chandima Gomes, Jasronita Jasni, Maryam Hajikhani. "The influence of lightning induced	<1%